

**Centrifuge Modeling of Oblique Pipe–Soil Interaction in Dense and Loose Sand**

by

©Pijush Debnath

A Thesis submitted to the

School of Graduate Studies

in partial fulfillment of the requirements for the degree of

**Master of Engineering**

**Faculty of Engineering and Applied Science**

Memorial University of Newfoundland

**May 2016**

St. John's Newfoundland

## **ABSTRACT**

Due to relative ground movement, buried pipelines experience geotechnical loads. The imposed geotechnical loads may initiate pipeline deformations that affect system serviceability and integrity. Engineering guidelines (e.g., ALA, 2005; Honegger and Nyman, 2001) provide the technical framework to develop idealized structural models to analyze pipe–soil interaction events and assess pipe mechanical response. The soil behavior is modeled using discrete springs that represent the geotechnical loads per unit pipe length developed during the interaction event. Soil forces are defined along three orthogonal directions (i.e., axial, lateral and vertical) to analyze the response of pipelines. Nonlinear load-displacement relationships of soil defined by a spring, is independent of neighboring spring elements. However, recent experimental and numerical studies demonstrate significant coupling effects during oblique (i.e., not along one of the orthogonal axes) pipe–soil interaction events. In the present study, physical modeling using a geotechnical centrifuge was conducted to improve the current understanding of soil load coupling effects of buried pipes in loose and dense sand. A section of pipeline, at shallow burial depth, was translated through the soil at different oblique angles in the axial-lateral plane. The force exerted by the soil on pipe is critically examined to assess the significance of load coupling effects and establish a yield envelope. The displacements required to soil yield force are also examined to assess potential coupling in mobilization distance. A set of laboratory tests were conducted on the sand used for centrifuge modeling to find the stress-strain behavior of sand, which was used to examine the possible mechanisms of centrifuge model test. The yield envelope, deformation

patterns, and interpreted failure mechanisms obtained from centrifuge modeling are compared with other physical modeling and numerical simulations available in the literature.

## **ACKNOWLEDGEMENTS**

I would like to express my sincere gratitude and appreciation to all those who gave me their support, assistance and necessary advice to complete my research work and write this thesis.

Above all other, my sincere gratitude is extended to my supervisor Dr. Shawn Kenny for his support, helpful guidance and encouragement throughout the entire research work. His detailed and constructive comments, patience and understanding helped me towards the successful completion of thesis work. I would also like to express my gratitude to Dr. Bipul Hawlader, my co-supervisor, for his comments and encouraging words in difficult days.

Special thanks and appreciation are due to Mr. Gerry Piercey, Centrifuge Manager at C-CORE, who provided significant technical assistance with the testing program. I greatly thanks to Mr. Karl Kuehnemund, Mr. Derry Nicole, and Mr. Karl Tuff for their tirelessly hard work to complete my test set up. I also appreciate the help of Mr. John Barrett and Mr. Anup Fouzder during the testing program. I am must specially thank Mr. David Snook, Machine Shop Supervisor, who machined, fabricated and repaired various parts on short notice to my great relief. I am also grateful to my officemates for the friendly environment of our office.

Finally, I should thanks to Rima, my wife, for her support and patience throughout my research work. I am grateful to my parents' devotion and unconditional love. I would also thank to my sister for her encouragement.

## Table of Contents

ABSTRACT.....	ii
ACKNOWLEDGEMENTS .....	iv
Table of Contents.....	vi
List of Tables.....	viii
List of Figures.....	ix
List of Symbols and Abbreviations.....	xii
List of Appendices.....	xiv
1 INTRODUCTION .....	1
1.1 BACKGROUND.....	1
1.2 PROBLEM STATEMENT .....	2
1.3 OBJECTIVES AND SCOPE .....	5
1.4 ORGANIZATION OF THE THESIS .....	6
2 LITERATURE REVIEW.....	9
2.1 INTRODUCTION.....	9
2.2 CURRENT DESIGN GUIDELINES .....	10
2.3 PIPE-SOIL INTERACTION FOR SAND .....	11
2.3.1 AXIAL PIPE-SOIL INTERACTION .....	11
2.3.2 LATERAL PIPE-SOIL INTERACTION .....	19
2.3.3 AXIAL-LATERAL PIPE-SOIL INTERACTION .....	35
2.4 CLOSURE.....	41
3 CENTRIFUGE PHYSICAL MODELLING .....	42
3.1 CENTRIFUGE MODELLING ASPECTS .....	42
3.1.1 CENTRIFUGE PRINCIPLES AND SCALLING LAWS .....	43
3.1.2 C-CORE CENTRIFUGE FACILITY.....	44
3.2 EXPERIMENTAL SETUP .....	45
3.3 TESTING PROGRAM .....	50
3.4 MATERIAL PROPERTIES.....	51
3.4.1 MATERIALS USED IN PHYSICAL TESTING.....	51
3.4.2 LABORATORY TESTING FOR SHEAR STRENGTH OF SAND.....	52
3.5 TEST BED PREPATION FOR CENTRIFUGE MODELING .....	55

4	AXIAL-LATERAL PIPE–SOIL INTERACTION IN DENSE SAND.....	57
4.1	INTRODUCTION.....	57
4.2	TEST RESULTS, ANALYSIS AND DISCUSSION .....	57
4.2.1	PURE AXIAL TEST .....	59
4.2.2	PURE LATERAL TEST.....	65
4.2.3	OBLIQUE ANGLE TESTS.....	73
4.3	SUMMARY OF THE CHAPTER.....	81
5	AXIAL-LATERAL PIPE–SOIL INTERACTION IN LOOSE SAND.....	84
5.1	INTRODUCTION.....	84
5.2	TEST RESULTS, ANALYSIS AND DISCUSSION .....	84
5.2.1	PURE AXIAL TEST .....	85
5.2.2	PURE LATERAL TEST.....	90
5.2.3	OBLIQUE ANGLE TESTS.....	95
5.3	SUMMARY OF THE CHAPTER.....	101
6	SUMMARY, CONCLUSIONS AND RECOMMENDATIONS.....	104
6.1	SUMMARY .....	104
6.2	FINDINGS FROM THE RESEARCH .....	105
6.3	FUTURE RESEARCH RECOMMENDATIONS.....	108
	REFERENCES.....	110
	APPENDIX A LOAD CELL CALIBRATION.....	118
	APPENDIX B DIRECT SHEAR TEST RESULTS ON DENSE AND LOOSE SAND.....	123
	APPENDIX C INTEGRATED FRAMEWORK IN SUPPORT OF PIPELINE ENGINEERING DESIGN FOR GEOHAZARDS.....	132

## List of Tables

Table 2-1: Friction factors for different type of coatings (ALA, 2005).....	13
Table 2-2: PRCI (2009) recommended chart to calculate $N_h$ .....	34
Table 3-1: Some scaling factors for centrifuge modeling (Taylor, 1995) .....	44
Table 3-2: Key parameters of pipe model.....	45
Table 3-3: Main components in centrifuge model test .....	49
Table 3-4: Test identification, load configuration and soil density .....	51

## List of Figures

Figure 1-1: Definition of angle of movement in horizontal plane (Daiyan, 2013).....	5
Figure 2-1: Pipeline model approach in current guidelines. (ALA, 2005; Honegger and Nyman, 2001) .....	12
Figure 2-2: Load–displacement relationship of axial pullout test, after Karimian (2006) 16	
Figure 2-3: Effect of dilation on soil loads on pipe during axial pullout test, after Wijewickreme et al. (2009).....	18
Figure 2-4: Comparison of assumption between vertical restraints.....	21
Figure 2-5 : Failure mechanisms for different depth (Audibert and Nyman, 1977).....	23
Figure 2-6: Horizontal bearing capacity factor on buried pipelines (Audibert and Nyman, 1977) .....	25
Figure 2-7: $N_h$ versus H/D for pipeline design (Trautmann 1983). .....	27
Figure 2-8: Lateral bearing force of different experimental works (Guo and Stolle 2005) .....	29
Figure 2-9: Comparison of the proposed equation and experimental works (Guo and Stolle 2005).....	30
Figure 2-10: Proposed design chart for lateral and upward pipe movement .....	31
Figure 2-11: Schematic diagram of log spiral model (O’Rourke et al., 2008). .....	33
Figure 2-12: Axial-lateral oblique angle (Hsu et al. 2001, 2006).....	37
Figure 2-13: Oblique pipe–soil interaction in loose sand (a) lateral loads, (b) axial loads (Hsu et al. 2001).....	38
Figure 2-14: Oblique pipe–soil interaction in dense sand (a) lateral loads, (b) axial loads (Hsu et al. 2006).....	38
Figure 2-15: Axial-lateral pipe–soil interaction envelope (C-CORE 2008).....	40
Figure 3-1: Basic concept of centrifuge physical modeling. ....	43
Figure 3-2: Pipe setup in the strongbox for centrifuge tests .....	47
Figure 3-3: Model pipe (#1) with load cell (#2, #3), stanchions (#4, #5) and dogbone (#6) .....	47
Figure 3-4: Test setup for Test 3 .....	48
Figure 3-5: Test setup for Test 5 .....	48
Figure 3-6: Load cell configuration, after Stroud (1971).....	49
Figure 3-7: Particle size distribution of silica sand used in experiments.....	52
Figure 3-8: Direct shear test results on dense sand (average density = 1577 kg/m <sup>3</sup> ). .....	54
Figure 3-9: Direct shear test results on loose sand (average density = 1493 kg/m <sup>3</sup> ). .....	55
Figure 3-10: Density trial test results for sand raining.....	56
Figure 4-1: Schematic illustration of how the peak force was defined to define ultimate load (after Pike et al., 2011).....	59
Figure 4-2: Load–displacement relationship for test TD0 .....	60
Figure 4-3: Normalized load–displacement relationship for test TD0. ....	61
Figure 4-4: Comparing the normalized axial force for axial pipe–soil interaction with some other test results .....	62
Figure 4-5: Comparison of the axial test results (TD0) with ALA (2005) and Karimian (2006) .....	64

Figure 4-6: Load–displacement relationship for pure lateral test (TD90). .....	66
Figure 4-7: Normalized load–displacement relationship for pure lateral test (TD90).....	67
Figure 4-8: Comparison of the test results with Audibert and Nyman (1977) and Guo and Stoll (2005). .....	68
Figure 4-9: Comparison of the normalized peak loads with several published test results. ....	70
Figure 4-10: Effects on normalized yield load and displacement for lateral pipe–soil interaction .....	73
Figure 4-11: Normalized load–displacement relationship for oblique angle test (TD70). 74	
Figure 4-12: Normalized load–displacement relationship for oblique angle test (TD50). 74	
Figure 4-13: Normalized load–displacement relationship for oblique angle test (TD40). 75	
Figure 4-14: Normalized load–displacement relationship for oblique angle test (TD20). 75	
Figure 4-15: Variation of axial and lateral interaction factor using Method (1) and Method (2). ....	76
Figure 4-16: Deformed colored soil layers for the oblique loading test (TD50) after centrifuge test. ....	78
Figure 4-17: Axial-lateral interaction curve for dense sand. ....	81
Figure 5-1: Load–displacement relationship for test TL0. ....	86
Figure 5-2: Normalized load–displacement relationship for test TL0. ....	86
Figure 5-3: Comparison of the axial test results (TL0) with ASCE (1984) and Karimian (2006). ....	89
Figure 5-4: Load–displacement relationship for pure lateral test (TL90).....	90
Figure 5-5: Normalized load–displacement relationship for pure lateral test (TL90). ....	91
Figure 5-6: Comparison of the test results for loose sand with Audibert and Nyman (1977) and Guo and Stoll (2005). ....	92
Figure 5-7: Comparison of the normalized peak loads with several published test results for loose sand. ....	93
Figure 5-8: Normalized load–displacement relationship for oblique angle test in loose sand (TL40).....	95
Figure 5-9: Normalized load–displacement relationship for oblique angle test in loose sand (TL70).....	96
Figure 5-10: Variation of axial and lateral interaction factor for loose sand.....	98
Figure 5-11: Deformed colored soil layers for the oblique loading test (TL40) after centrifuge test. ....	99
Figure 5-12: Axial-lateral interaction curve for loose sand. ....	101
Figure A-1: Axial response during axial load in load cell -1 .....	119
Figure A-2: Load cell response during lateral load applied for the level arm 35 mm in load cell - 1.....	119
Figure A-3: Load cell response during lateral load applied for the level arm 40 mm in load cell -1.....	120
Figure A-4: Load cell response after calibrating for applying lateral load for 35 mm and 40 mm level arm in load cell - 1 .....	120
Figure A-5: Load cell response during axial load applied in load cell - 2.....	121
Figure A-6: Load cell response during lateral load applied for the level arm 35 mm in load cell - 2.....	121

Figure A-7: Load cell response during lateral load applied for the level arm 40 mm in load cell - 2.....	122
Figure A-8: Load cell response after calibrating for applying lateral load for 35 mm and 40 mm level arm in load cell - 2 .....	122
Figure B-1: Variation of shear stress with displacement for dense sand; Density = 1578.5 Kg/m <sup>3</sup> (Dr= 75.3%) and normal stress =8 kPa. ....	124
Figure B-2: Vertical displacement vs shear displacement for dense sand; Density = 1578.5 Kg/m <sup>3</sup> (Dr = 75.3%) and normal stress = 8 kPa. ....	124
Figure B-3: Variation of shear stress with displacement for dense sand; Density = 1576.7 Kg/m <sup>3</sup> (Dr = 74.5%) and normal stress = 16 kPa. ....	125
Figure B-4: Vertical displacement vs shear displacement for dense sand; Density = 1576.7 Kg/m <sup>3</sup> (Dr = 74.5%) and normal stress = 16 kPa. ....	125
Figure B-5: Variation of shear stress with displacement for dense sand; Density = 1576.7 Kg/m <sup>3</sup> (Dr = 74.5%) and normal stress = 32 kPa. ....	126
Figure B-6: Vertical displacement vs shear displacement for dense sand; Density = 1576.7 Kg/m <sup>3</sup> (Dr = 74.5%) and normal stress = 32 kPa. ....	126
Figure B-7: Variation of shear stress with displacement for dense sand; Density = 1578 Kg/m <sup>3</sup> (Dr = 75%) and normal stress = 64 kPa. ....	127
Figure B-8: Vertical displacement vs shear displacement for dense sand; Density = 1578 Kg/m <sup>3</sup> (Dr = 75%) and normal stress = 64 kPa. ....	127
Figure B-9: Variation of shear stress with displacement for loose sand; Density = 1493.8 Kg/m <sup>3</sup> (Dr = 33.6%) and normal stress = 8 kPa. ....	128
Figure B-10: Vertical displacement vs shear displacement for loose sand; Density = 1493.8 Kg/m <sup>3</sup> (Dr = 33.6%) and normal stress = 8 kPa.....	128
Figure B-11: Variation of shear stress with displacement for loose sand; Density = 1491 Kg/m <sup>3</sup> (Dr = 32.2%) and normal stress = 16 kPa. ....	129
Figure B-12: Vertical displacement vs shear displacement for loose sand; Density = 1491 Kg/m <sup>3</sup> (Dr = 32%) and normal stress =16 kPa. ....	129
Figure B-13: Variation of shear stress with displacement for loose sand; Density = 1493.8 Kg/m <sup>3</sup> (Dr = 33.6%) and normal stress = 32 kPa. ....	130
Figure B-14: Vertical displacement vs shear displacement for loose sand; Density = 1493.8 Kg/m <sup>3</sup> (Dr = 33.6%) and normal stress = 32 kPa. ....	130
Figure B-15: Variation of shear stress with displacement for loose sand; Density = 1493.8 Kg/m <sup>3</sup> (Dr = 33.6%) and normal stress =64 kPa. ....	131
Figure B-16: Vertical displacement vs shear displacement for loose sand; Density = 1493.8 Kg/m <sup>3</sup> (Dr = 33.6%) and normal stress = 64 kPa. ....	131

## List of Symbols and Abbreviations

$c'$	cohesion of soil
$c_u$	undrained shear strength of soil
$D$	pipe external diameter
$Dr$	relative density
$D_{ref}$	reference diameter
$E$	soil elastic modulus
$f$	pipe external surface friction factor
$H$	soil cover depth to the pipe centerline
$K_0$	coefficient of lateral earth pressure at rest
$K_a$	coefficient of active lateral earth pressure
$L$	pipe length
$N_{ch}, N_{qh}$	lateral interaction (bearing capacity) factors for cohesive and frictional effects respectively
$N_{cv}, N_{qv}$	vertical interaction (bearing capacity) factors for cohesive and frictional effects respectively
$N_{qh(90)}$	lateral interaction factor for pure lateral pipe-soil interaction
$N_t$	axial interaction factor
$N_c, N_q, N_\gamma$	bearing capacity factors for horizontal strip footings, vertically loaded in downward direction
$p$	mean effective stress
$p_0$	atmospheric (reference) pressure
$q$	deviatoric stress
$T, P, Q$	soil forces applied to unit length of pipeline in axial, lateral and vertical directions respectively
$T_u, P_u, Q_u, Q_{ud}$	ultimate soil forces applied to unit length of pipeline in axial, lateral, vertical upward and vertical downward directions respectively
$t$	pipe wall thickness
$W_p$	pipe self-weight
$x, y, z$	relative pipe-soil displacements in axial, lateral and vertical directions respectively

$x_u, y_u, z_u, z_{ud}$ vertical	ultimate relative displacements in axial, lateral, vertical upward and downward directions respectively
$X_u, Y_u$	ratio of ultimate relative displacements in axial and lateral directions over pipe diameter
$\alpha$	lateral-vertical oblique angle of movement
$g'$	effective unit weight of soil
$\delta$	interface friction angle between pipeline and soil
$\theta$	axial-lateral oblique angle of movement
$\mu$	pipe-soil interface friction coefficient
$\rho$	density of soil
$\psi$	dilation angle of soil

## **List of Appendices**

Appendix A: LOAD CELL CALIBRATION

Appendix B: DIRECT SHEAR TEST RESULTS ON DENSE AND LOOSE SAND

Appendix C: INTEGRATED FRAMEWORK IN SUPPORT OF PIPELINE

ENGINEERING DESIGN FOR GEOHAZARDS

# 1 INTRODUCTION

## 1.1 BACKGROUND

Pipelines are energy lifelines for the transport of hydrocarbon products, such as oil and natural gas, over long distances that may cross national or international boundaries. In Canada, more than 200,000 kilometers of flow lines and gathering systems deliver oil and gas (<http://www.psac.ca/>).

As a means of protection from external forces (e.g., wind waves, current) and interference (e.g., impact from vehicles, mobile fishing gear), both offshore and onshore energy pipelines are typically buried. Buried pipelines, however, can be subject to large deformations and geotechnical loads due to relative ground movements that may be associated with geohazards (e.g., subsidence, fault movements, liquefaction, thaw settlement, slope instabilities, etc.). These geotechnical loads may initiate pipeline deformations that can affect operations and serviceability (e.g., section ovalization, coating damage), as well as pipe strength, stability and mechanical integrity (e.g., local buckling, rupture). The consequences may have a significant impact on pipe operations that may also adversely affect the economy, society and environment with economic losses in the tens to hundreds of millions of dollars.

During pipe–soil interaction events, a complex relationship exists between the geotechnical loads and failure mechanisms (i.e., loads or hazards), load transfer and pipe–

soil interaction mechanisms, pipeline mechanical response and performance (i.e., load effects). An improved understanding is required to advance more effective, practical and economical engineering design solutions, and operational practices for pipelines subject to geohazards. This will result in improved performances, higher safety and greater confidence in the integrity of buried pipelines for the benefit of all stakeholders (e.g., engineering consultants, operators, regulator, and public).

## **1.2 PROBLEM STATEMENT**

Current engineering guidelines (e.g., ALA, 2005; Honegger and Nyman, 2004) provide the technical basis for developing an engineering model, known as a Winkler-type model, to analyze pipe–soil interaction events. The pipeline is modeled using structural elements based on beam theory that account for the effects of internal pressure and thermal expansion. Spring elements are used to characterize the soil continuum response and represent the distributed geotechnical load acting on a unit pipe length segment along one of the three mutually orthogonal axes relative to the pipe cross-section (i.e., axial, lateral and vertical directions). The spring elements represents the soil force displacement relationship and are independent (i.e., uncoupled) with adjacent soil spring elements. In general, bilinear or hyperbolic functions are used to characterize the soil spring the load displacement relationship that are defined using the soil yield load and yield displacement parameters.

A number of experimental (e.g., Trautmann, 1983; White et al., 2000; Karimian et al., 2006; Wijewickreme et al., 2009), numerical (e.g., Guo and Stolle, 2005; Jung and Zhang, 2011), and theoretical (e.g., Nyman, 1984) studies have been conducted in the past to establish the soil yield load, mobilization distance to yield and soil failure mechanisms during pipe–soil interaction events. In these studies, the pipeline has assumed to be a rigid body, and the relative pipe translation was along one of the three mutually perpendicular axes (i.e., axial, lateral and vertical directions). Recent studies (e.g., Hsu et al., 2001; 2006; Cocchetti et al., 2009a; 2009b; Daiyan et al. 2010a; 2010b; 2011) have demonstrated the effects of oblique attack angles (i.e., not along one of the three mutually perpendicular axes) during pipe–soil interaction events on soil load coupling response. An oblique pipe–soil interaction event in the axial-lateral plane is illustrated in Figure 1-1. Small oblique attack angles, which deviate from pure axial translation, can significantly increase the magnitude of axial soil loads imposed on the pipe (Hsu et al., 2001; 2006; Daiyan et al. 2010a; 2010b; 2011). For axial-lateral oblique interaction events, the axial soil restraint or load increases with the attack angle until the soil failure mechanism is governed by lateral bearing failure (e.g., Phillips et al., 2004b). The interaction is also a function of other parameters including the pipe diameter and weight, pipe–soil interface condition, and soil density. In addition, Daiyan et al. (2009) and Pike et al. (2011) have shown the method for selecting the ultimate load and mobilization distance to yield can influence characterization of the soil failure envelope for oblique load events. This would impact the mathematical relationships defining the coupled, force–displacement response of the soil springs used in the structural pipe–soil interaction model. The significance of oblique loading on the soil yield load or

mobilization has not been considered in the current design guidelines. Thus, these research outcomes have demonstrated for the oblique pipe–soil interaction events that the assumption of independent soil spring behavior was not valid and has highlighted the limitations and uncertainty of current engineering practice to address practical engineering solutions for the design and operations of buried pipelines.

While these studies have demonstrated on the importance of coupling on oblique pipe–soil interaction events, limited studies on physical modeling of this event are available in the literature. As full-scale tests are expensive, the geotechnical centrifuge can be used to assess soil load coupling effects during pipe–soil interaction events.

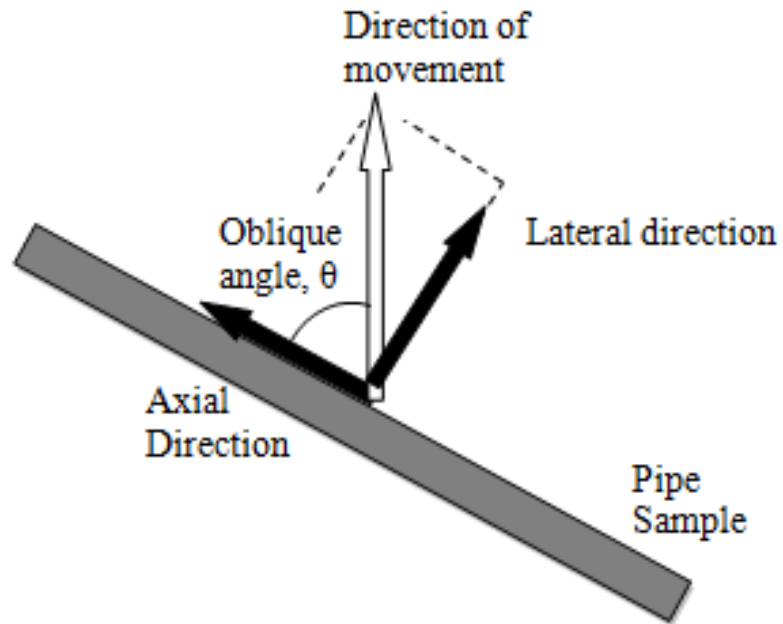


**Figure 1-1: Definition of angle of movement in horizontal plane (Daiyan, 2013)**

### **1.3 OBJECTIVES AND SCOPE**

The main objective of this study is to advance the knowledge on soil load coupling effects during oblique pipe–soil interaction events in the axial-lateral plane for loose and dense sand (i.e., cohesionless soil) conditions. Reducing some of the limitations of previous centrifuge physical modeling, a set of tests were conducted in this study to provide additional new data and further insight into the effects of soil load coupling. Laboratory tests were conducted for a critical examination of the response of pipe in centrifuge tests based on stress-strain behavior of the sand. The outcomes of this study could be used for

further advancement of the current engineering design guidelines for modeling pipe–soil interaction events. The following are the work scope of this study:

- i. Conduct a series of reduced-scale centrifuge tests to examine soil load coupling effects during oblique pipe–soil interaction events in dry loose and dry dense sand test beds. A rigid pipe was translated through the test bed in the axial-lateral plane.
- ii. Examine the physical modeling data with an emphasis on soil yield, mobilization distance to yield, deformation patterns and failure mechanisms. Compare experimental results with existing data on pipe–soil interaction events and current engineering design guidelines. Establish the failure envelope characterizing the coupled load effects during axial-lateral pipe–soil interaction events.
- iii. Examine the significance of scale effects on soil yield, mobilization distance to yield, deformation patterns and failure mechanisms.

#### **1.4 ORGANIZATION OF THE THESIS**

This thesis is organized into six main chapters and three appendices.

**Chapter 1** provides an introduction to the topic of this research through the background and problem statement. Importance of the research including the objectives and work scope are also provided.

**Chapter 2** is the literature review that covers analytical, physical modeling and numerical simulations on pipe–soil interaction events that form the basis of the current engineering guidelines. The emergence of studies on oblique axial-lateral pipe–soil interaction events and the significance of soil load coupling are also discussed.

**Chapter 3** provides a discussion on the reduced-scale centrifuge tests conducted in this study. Discussions on test setup, apparatus and measurement devices, pipe and soil properties are provided in this chapter.

**Chapter 4** presents the centrifuge test results for axial, lateral and oblique pipe–soil interaction events in dense sand test bed. The results are compared with the available literature and current engineering design guidelines for analyzing pipe–soil interaction events. The failure envelope characterizing soil load coupling is developed, the effects of scale are examined, and the deformation patterns and failure mechanisms are assessed.

**Chapter 5** presents the centrifuge test results for axial, lateral and oblique pipe–soil interaction events in loose sand test bed. The results are compared with the available literature and current engineering design guidelines for analyzing pipe–soil interaction events. The failure envelope characterizing soil load coupling is developed, the effects of scale are examined, and the deformation patterns and failure mechanisms are assessed.

**Chapter 6** presents a summary and conclusions of the research. Some recommendations for future studies are also provided in this chapter.

**Appendix A** presents the calibration results of load cells used in centrifuge tests.

**Appendix B** presents the direct shear test results on sand used in centrifuge modeling.

**Appendix C** presents a technical paper where the research work of this study is addressed through examination of recent studies that have included laboratory testing, centrifuge and full-scale modelling, and numerical simulation to address pipe–soil interaction events. The potential improvement of current pipeline engineering practice is also explored.

## 2 LITERATURE REVIEW

### 2.1 INTRODUCTION

A significant level of work has been undertaken regarding the pipe–soil interaction event to investigate the axial and lateral loading on buried pipelines. A comprehensive literature review of current state of practice and recommended guidelines for the analysis of pipe–soil interaction events is presented in this chapter. Previous empirical, analytical, numerical and as well as full- and reduced-scale experimental studies on pipe–soil interactions subject to ground deformation are discussed. Studies on the more complex oblique pipe–soil interaction event, which is the focus of this thesis, are also reviewed.

Buried pipelines are subjected to geotechnical loads due to relative ground movement generally associated with geohazards. These imposed geotechnical loads may initiate pipeline deformations that affect system serviceability (e.g., ovalization) and mechanical integrity (e.g., local wrinkling, rupture). The majority of research studies conducted and the formation of current industry practice guidelines for pipe–soil interaction analysis has focused on the unidirectional soil load–displacement response (e.g., pure lateral bearing) with monotonic loading conditions. In the past decade, there have been a limited number of studies examining the coupled load response (i.e., combined axial-lateral pipe–soil interaction) for oblique load events. Literature review mainly on pipelines buried in sand is provided because pipe-soil interaction in sand is the focus of this study.

## 2.2 CURRENT DESIGN GUIDELINES

Current engineering guidelines (i.g., ALA, 2005; Honegger and Nyman, 2001) provide an engineering model to analyze the pipe–soil interaction system which is represented by nonlinear load–displacement relationships. The pipeline is modeled using beam elements while the soil behavior is modeled using discrete springs in three perpendicular directions (axial, lateral and vertical) as shown in Figure 2-1. This simplification is derived from the concept of sub-grade reaction originally proposed by Winkler (1867). The nonlinear, stress-dependent load–deformation characteristics of the springs are denoted as  $t$ – $x$ ,  $p$ – $y$  and  $q$ – $z$  curves, representing the behavior of the soil in the axial, transverse horizontal and transverse vertical directions respectively. Load–displacement relationships for springs are generally defined by bilinear or hyperbolic functions.

The general forms of the resistant forces can be expressed as:

$$\text{Eq. 2-1} \quad t = f(x), p = f(y), q = f(z)$$

where  $(t, x; p, y; q, z)$  are soil forces per unit length and pipeline displacement in the axial, horizontal, vertical directions respectively. Usually, the force–displacement relationships of soil are nonlinear and there exist upper limits for  $t$ ,  $p$  and  $q$ . Furthermore, all soil springs are independent and the effect of coupling between two adjacent soil springs is not considered. As shown in Figure 2-1, three frequently used notations to define the location of pipelines are: pipe cover depth  $C$ , burial depth  $H$  and embedment depth  $h$ . In

this section, the discussion will focus only on the research and current engineering practice guidelines for non-cohesive soil.

## 2.3 PIPE–SOIL INTERACTION FOR SAND

### 2.3.1 AXIAL PIPE–SOIL INTERACTION

To evaluate the loads on pipeline buried in sand during axial ground movement Equation 2-2 is used (ALA, 2005; Honegger and Nyman, 2001; PRCI, 2004).

$$\text{Eq.2-2 } T_u = \pi D H \gamma \frac{1+K_o}{2} \tan \delta$$

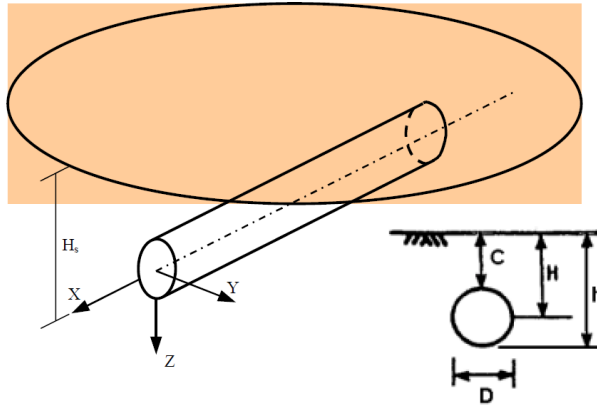
Where,

$T_u$  = ultimate axial soil loads on pipe per unit length (N);  $D$  = pipe diameter (m);  $H$  = depth to pipe centerline (m);  $\gamma$  = dry unit weight of soil ( $\text{N}/\text{m}^3$ );  $K_o$  = coefficient of earth pressure at rest;  $\delta$  = interface angle of friction between pipe and soil =  $f(\phi')$ ;  $\phi'$  = internal angle of friction of soil.

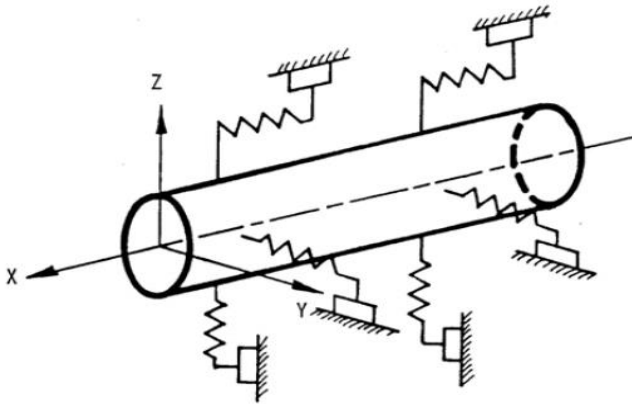
The relative displacement required to mobilize the above force ( $T_u$ ) typically varies between 3 mm and 5 mm with lower values for dense sand. Generally, the load–displacement relationship for the axial loading condition is defined by a bilinear elastic perfectly plastic curve.

The normalized axial soil resistance per unit length,  $N_t$ , can be expressed as

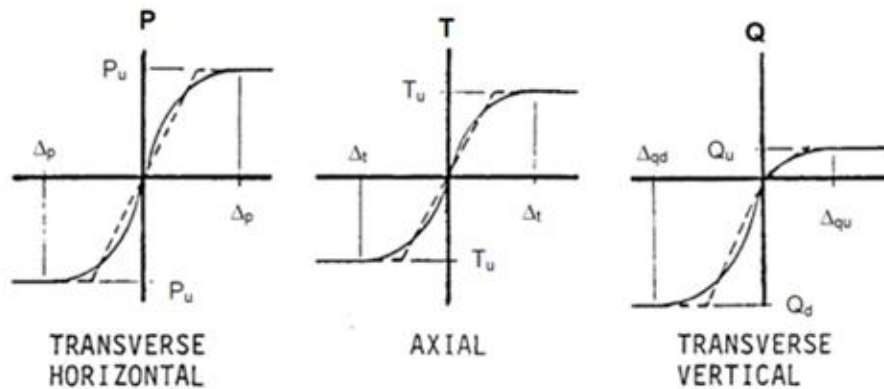
$$\text{Eq. 2-3 } N_t = \frac{T_u}{\gamma D H}$$



a) Schematic illustration of continuum pipe-soil interaction



b) Idealized representation of soil with discrete springs



c) Bi-linear soil springs used to represent soil force on pipe

**Figure 2-1: Pipeline model approach in current guidelines. (ALA, 2005; Honegger and Nyman, 2001)**

ALA (2005) suggested the range of  $\delta$  between  $0.5\phi'$  to  $1.0\phi'$ . The recommended values of the coating dependent friction factor,  $f$ , for various external pipe coatings are summarized in Table 2-1. Kulhawy et al. (1983) suggested that the interface friction angle between sand and smooth steel varies from  $0.5\phi'$  to  $0.7\phi'$ , whereas  $\delta$  between sand and rough steel varies from  $0.7\phi'$  to  $1.0\phi'$ .

**Table 2-1: Friction factors for different type of coatings (ALA, 2005).**

<b>Pipe Coating</b>	<b><math>f</math></b>
Concrete	1.0
Coal Tar	0.9
Rough Steel	0.8
Smooth Steel	0.7
Fusion Bonded Epoxy	0.6
Polyethylene	0.6

The current guidelines do not provide any recommendation for the co-efficient of lateral earth pressure at rest,  $K_0$ , in Equation 2-2. However, the empirical relation proposed by Jacky (1944) could be used for loose sand.

$$\text{Eq. 2-4 } K_0 \approx 1 - \sin\phi'$$

For dense sand, Sherif et al. (1984) proposed the following empirical relation.

$$\text{Eq. 2-5 } K_0 \approx 1 - \sin\phi' + 5.5(\gamma_d/\gamma_{dmin} - 1)$$

Karimian (2006) also provided recommendations for estimating  $K_0$  based on data obtained from full-scale axial pullout tests and concluded that the conventional approach for defining  $K_0$  using Equation 2-2 does not adequately represent the actual normal stress on the pipe. Wijewickreme et al. (2009) and Karimian (2006) suggested larger values of  $K$  equal to 2.5 based on model tests, instead of conventional  $K_0$  values of approximately 0.5, provide better correlation with observed peak frictional resistance for a 457 mm diameter steel pipe with a H/D ratio of 2.5 buried in dense sand.

Other expressions have been also developed to estimate the axial soil loads on pipe.

McAllister (2001) suggested Equation 2-6 for calculating the axial resistance, which includes the weight of the pipe ( $W_p$ ).

$$\text{Eq. 2-6 } T_u = \{ 2D\bar{\gamma} (H - D/2) + W_p \} \tan\delta$$

Danish Submarine Pipeline Guidelines (1985) proposed Equation 2-7 to estimate the frictional force per unit length of pipe which is based on the integration of shear stress around the pipe.

$$\text{Eq. 2-7 } T_u = \left[ \frac{\bar{\gamma}D}{2} \tan\phi \left( H + \frac{D}{2} \right) \pi (1 + K_0) + \frac{4}{3} \frac{W_p}{\pi} (2 + K_0) - \frac{\bar{\gamma}D}{3} (2 + K_0) \right] \tan\delta$$

Hsu et al. (2001, 2006) conducted a series of experiments in a prefabricated large-scale drag box using pipes of three diameters (i.e., 152.4, 228.6 and 304.8 mm) buried in loose and dense sand. The ultimate normalized axial soil resistance,  $N_t$ , was 0.9 for a 229 mm diameter pipe buried in loose sand with a peak friction angle of 33°, pipe–soil friction

angle of  $21^\circ$  and H/D of 2, which is very close to the value that obtained from Equation 2-3 (Hsu et al. 2001). In dense sand conditions, with the peak friction angle of  $42^\circ$ , pipe–soil friction angle of  $26^\circ$  and for H/D of 2, Hsu et al. (2006) reported a value of 1.1 which is also consistent with Equation 2-3.

Karimian (2006) and Wijewickreme et al. (2009) presented the results of a series of axial pullout tests on sand with bare pipe and showed that the axial soil loads is in good agreement with the predicted loads using the PRCI (2004) guidelines for loose sand. For dense sand, axial pullout tests give approximately three times higher values than that predicted by ACSE (1984) and PRCI (2004) as shown in Figure 2-2. The difference is attributed due to the constrained dilation of the dense sand during shear deformation that occurred within a thin annular shear zone around the pipe.

Karimian (2006) and Wijewickreme et al. (2009) mounted 5 pressure transducers on the pipe surface during axial pullout tests, and showed that the normal stress increases during pullout. Karimian (2006) attributed the increase in normal stress with soil pressure due to dilation and stated the conventional earth pressure co-efficient “at rest” ( $K_o$ ), as defined in Equation 2-2, does not adequately represent the mechanisms for the dense sand conditions. The physical tests were also compared with plane strain, numerical simulations developed using FLAC 4.0. Sand dilation at the pipe–soil interface has been simulated by numerically “expanding” the circumferential pipe surface (i.e., diameter) to match the measured pressure as shown in Figure 2-3. Wijewickreme et al. (2009) suggested using higher  $K$  values rather than conventional  $K_o$  for the axial pullout

resistance of buried pipes in dense sand. Note that, Karimian (2006) back calculated  $K$  of 2.5 from the measured peak axial frictional resistance, which is again significantly higher than conventional  $K_0$  obtained from Equations 2.4 and 2.5.

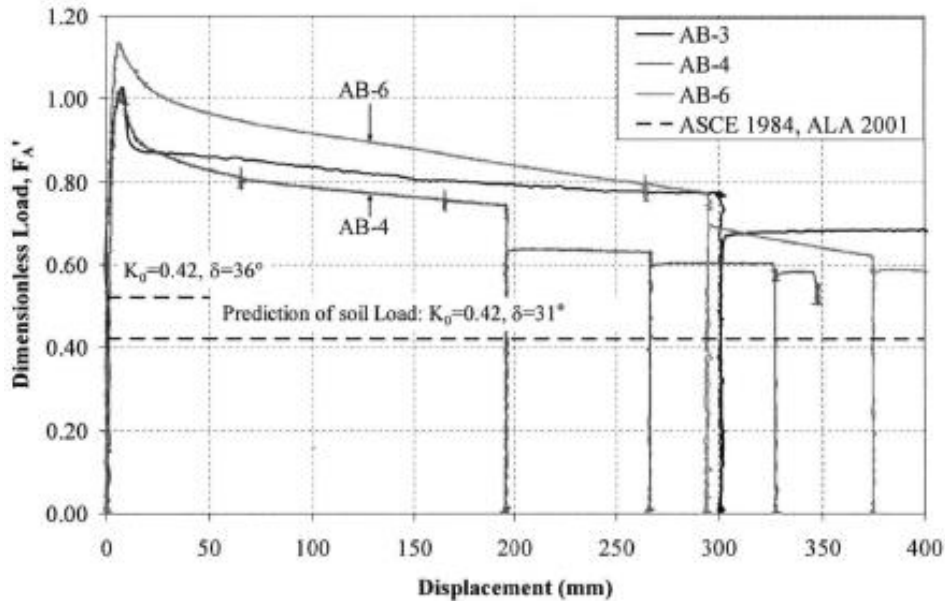


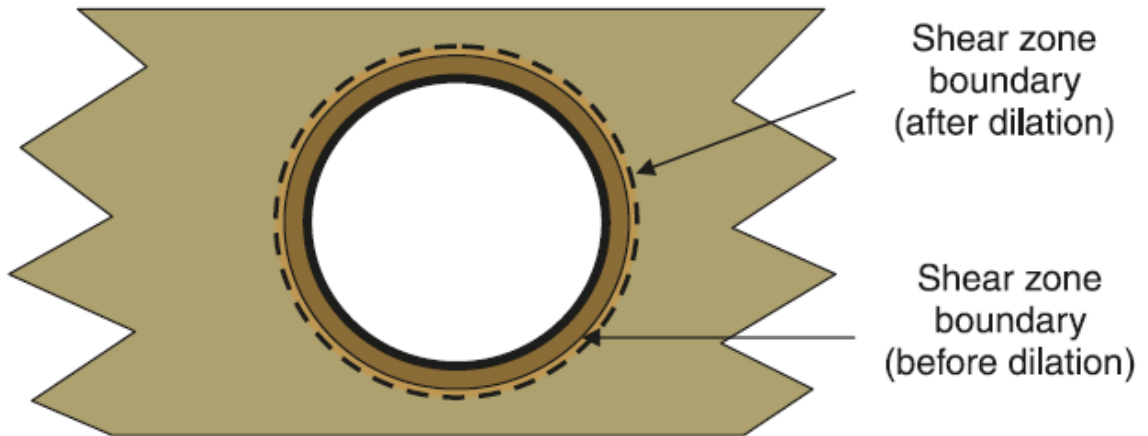
**Figure 2-2: Load–displacement relationship of axial pullout test, after Karimian (2006)**

Daiyan et al. (2010, 2011) reported the maximum normalized axial soil resistance of 3.75 from centrifuge tests on rigid pipe buried in dense sand at the depth of  $2D$ . Daiyan et al. (2010) attributed the higher axial resistance, in comparison with Equation 2-2, with the normal stress on the pipe surface due to the end bearing of the pipe loading system. Daiyan et al. (2011) also suggested that small amount of pipe misalignment in the vertical plane and a confined dilation of sand near the pipe–soil interface may have caused increased normal stress on the pipe surface. The weight of pipe loading system was also

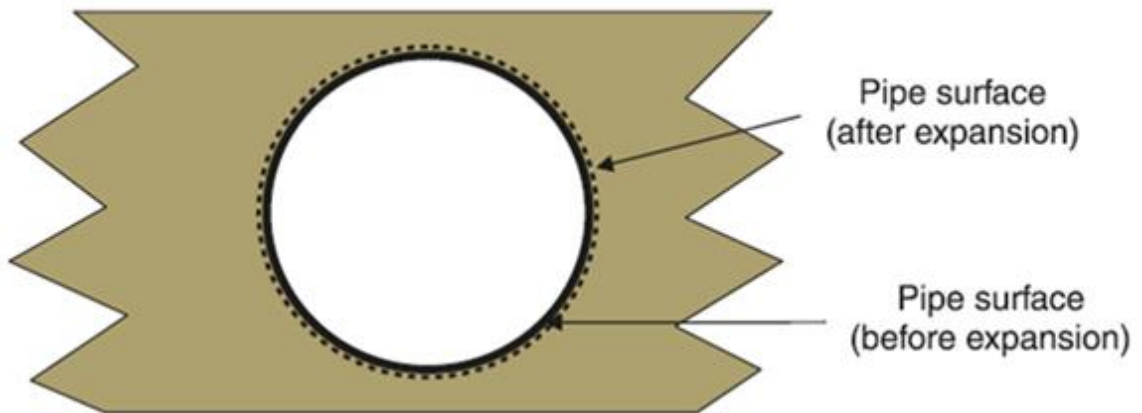
thought to have caused higher values of axial resistance, which is not accounted for in Equation 2-2. Daiyan et al. (2011) carried out a numerical simulation to verify the centrifuge test results where the weight of pipe loading system was considered and found that the maximum axial resistance was about 2. This numerical result was consistent with the value of 1.94 from the Equation 2-8 used by Schaminee et al. (1990) where the pipe's self-weight is considered.

$$\text{Eq.2-8} \quad T_u = 0.25 \left[ \gamma' H + 2K_a \gamma' \left( H + \frac{D}{2} \right) + \gamma' H + \frac{W_p}{D} \right] \mu \pi D$$

where  $K_a$  is the active lateral pressure coefficient and  $W_p$  is the pipe's self-weight.



a) Size of shear zone before and after dilation



b) Expansion of pipe to mimic dilation effects in numerical modeling

**Figure 2-3: Effect of dilation on soil loads on pipe during axial pullout test, after Wijewickreme et al. (2009)**

Daiyan et al. (2010) also reported the large pipe displacement to mobilize the maximum axial resistance as compared to other full-scale tests 14 mm in model scale in centrifuge tests ( $0.34D$  in prototype scale) while the current design guidelines recommend 2.5 - 3 mm. The higher mobilized displacement might be resulted from pipe setup with loading

system, the crushable foam used in front of the stanchions to reduce the effect of end bearing, and variation of sand density around the pipe.

### **2.3.2 LATERAL PIPE–SOIL INTERACTION**

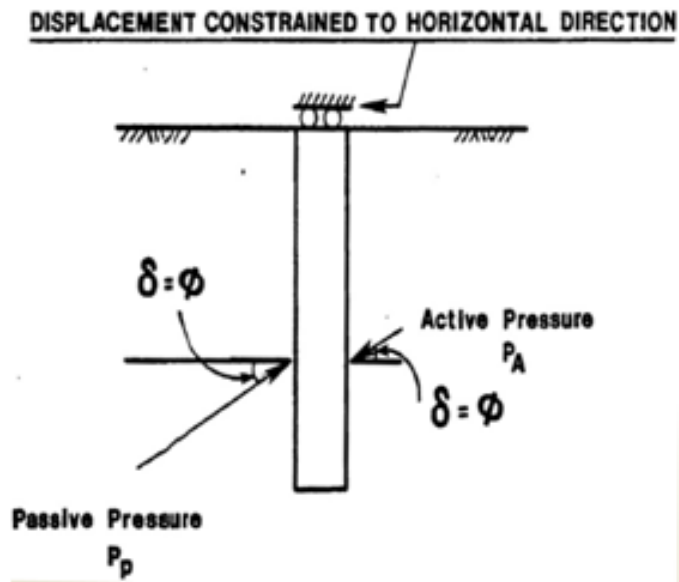
A number of analytical, numerical and experimental studies have been performed in the past for lateral structure–soil interaction. Experience from analogue infrastructure such as vertical anchors and piles have been also brought for further clarification.

Hansen (1961) developed a design method for buried vertical anchors which is considered the first well known analytical solution used for predicting lateral forces on buried pipelines. The model examined the soil response interacting with rigid piles for shallow failure mechanism, a deep failure mechanism and an empirical interpolation function to compute at intermediate depth. For a shallow rigid pile, the laterally loaded pile was assumed to behave similar to the response of retaining walls. For deep piles, the response was assumed to behave similar to a deep strip footing. At intermediate depths an empirical interpolation function was developed based on the frictional resistance along the sides of a failure wedge having dimensions defined by Rankine passive earth pressure theory.

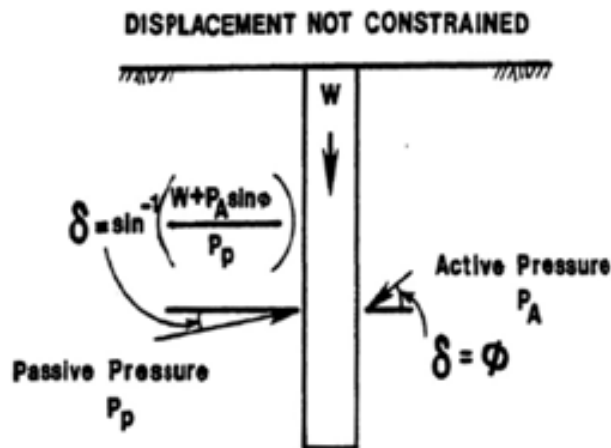
According to Hansen (1961), the model would yield good results for buried anchors at shallow depth (i.e., burial depth/width of anchor plate up to 2). Comparing Hansen (1961)

model with other studies (e.g., Ovesen 1964; Trautmann and O'Rourke 1983; 1985), the Hansen (1961) model leads to higher soil resistance on the buried pipe as it was assumed that the pipe is restrained from vertical movement as shown in Figure 2-4. This assumption does not represent the actual pipe–soil interaction events as pipe–soil interaction events are independent of unidirectional movement. However, the current design guidelines (PRCI 2004) still recommend to use the Hansen (1961) model.

To develop the method to calculate the soil resistance, Ovesen (1964) conducted a series of experimental tests on 15 cm high vertical plate anchors with overburden ratios (i.e., ratio between burial depth to height of the anchor plate) from 1 to 10 that were subjected to lateral displacement in loose and dense sand test beds in a plane strain condition. Based on the test results, Ovesen (1964) developed an analytical model to estimate passive soil loads on anchors considering the curvature in the active soil edge and the upward movement of the anchor plate. This model predicts lower lateral soil resistance in comparison with the Hansen (1961) model. Ovesen (1964) used vertical anchor plate in plane strain conditions, which may not fully reflect the characteristics of pipe–soil interaction events particularly the effect of stress around the anchor and the pipe. Hansen (1961) used rigid piles to develop the model where stress distribution around the pile can be accounted for the pipe of the pipe–soil interaction events though the model has some limitations for its assumptions.



a) Hansen method (1961)

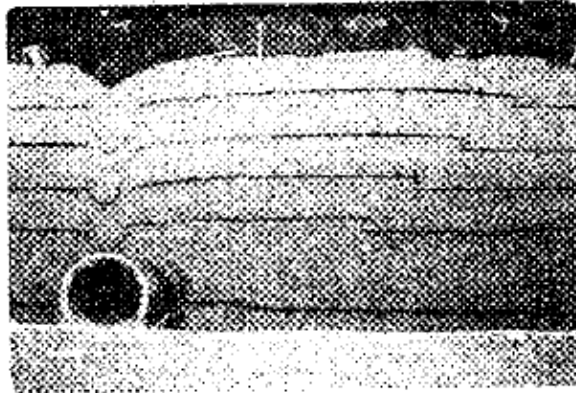


b) Ovesen method (1964)

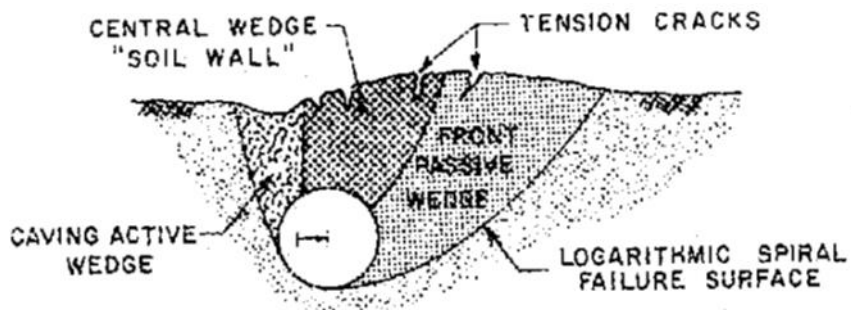
Figure 2-4: Comparison of assumption between vertical restraints  
(Trautmann, 1983)

A similar study was conducted, by Das and Seeley (1975), to investigate the effects of aspect ratio (i.e., ratio between width and height of the anchor) on soil resistance for shallow-vertical anchor plates. The soil resistance was observed to decrease with the increasing aspect ratio. This finding is of relevance to buried pipes because it shows the importance of geometry in determining lateral soil resistance.

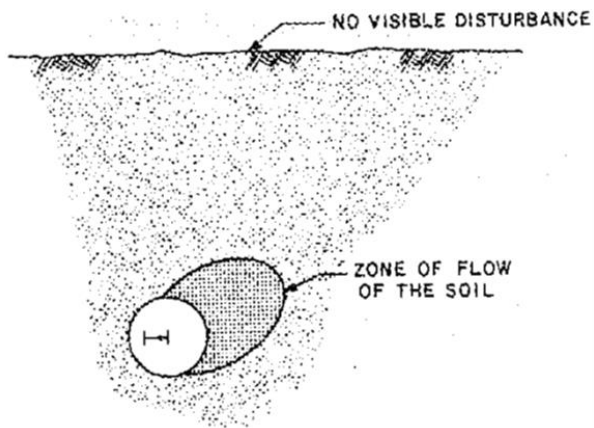
Audibert and Nyman (1977) conducted a series of small-scale tests on pipelines, buried in loose and dense sand, to investigate the lateral pipe-soil interactions. The mobilization of soil restraint was found to be dependent on soil density, depth embedment and pipe diameter. They demonstrated the failure mechanism for different burial depths. For shallow burial depths, a passive wedge was formed bounded by a logarithmic spiral in front of the pipe, along with the nearly vertical active zone in the back of the pipe. For intermediate depths, a funnel shaped passive wedge was observed (see Figure 2-5b). For deep burial depths, a confined zone of soil flow was developed around the pipe (see Figure 2-5c) and a punching type failure mechanism was observed for cover ratios from 12 to 24.



a) Shallow burial depth



b) Intermediate burial depth.



c) Deep burial depth

**Figure 2-5 : Failure mechanisms for different depth (Audibert and Nyman, 1977)**

Based on the experimental test results, Audibert and Nyman (1977) showed that the load–displacement relationship is non-linear and the soil resistance reaches a maximum value at a certain level of pipe displacement. The soil load–displacement relationship can be approximated by a rectangular hyperbolic curve and can be related to a set of non-dimensional parameters relating a normalized force ( $\bar{p}$ ) with normalized displacement ( $\bar{y}$ ) as shown in Equation 2-9.

$$\text{Eq. 2-9} \quad \bar{p} = \frac{\bar{y}}{0.145 + 0.855 \bar{y}}$$

Where

$$\text{Eq. 2-10} \quad \bar{p} = \frac{p}{p_u} \quad \text{and} \quad \bar{y} = \frac{u}{Y}$$

in which  $p_u$  is the maximum lateral soil resistance at displacement  $Y$ .

Audibert and Nyman (1977) proposed to use the Hansen (1961) capacity factor  $N_{qh}$  to predict the maximum soil resistance  $p_u$ . The variation of  $N_{qh}$  with burial depth is shown in Figure 2-6. Audibert and Nyman (1977) recommended the value of approximately 1.5% – 2% of the embedment depth for defining the ultimate displacement  $Y$ .

Rowe and Davis (1982) numerically investigated the behavior of anchor plates buried in sand using FE method for  $H/D$  ranging from 1 to 8. The effects of burial depth, friction angle, dilation angle, initial soil stress condition and the surface roughness of the vertical anchor plates were examined. The soil dilatancy was found to have a significant effect on anchor capacity for deep embedments ( $H/D > 3$ ) in medium to dense sand ( $\phi' > 30^\circ$ ). The

anchor roughness was also a significant factor on ultimate strength for shallow burial depths ( $H/D < 3$ ). A series of charts were developed to estimate the lateral soil resistance of anchor plates for different conditions. Several correction factors were also introduced to modify the anchor capacity based on the surface roughness, soil dilatancy and initial stress condition.

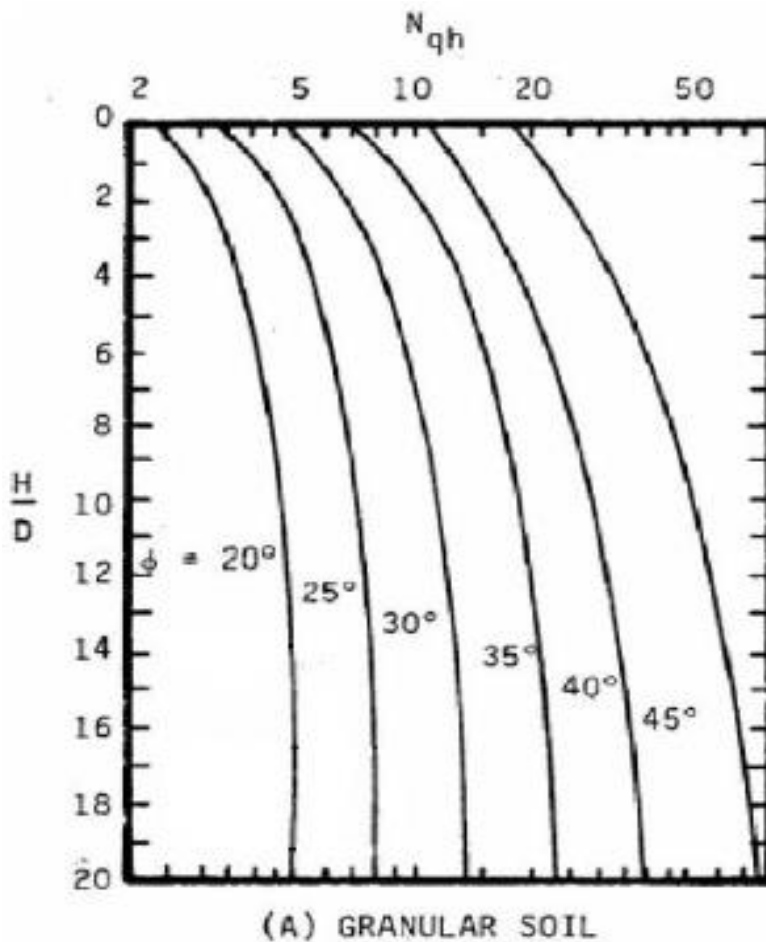


**Figure 2-6: Horizontal bearing capacity factor on buried pipelines (Audibert and Nyman, 1977)**

Trautmann (1983) and Trautmann and O'Rourke (1985) performed a series of lateral pipe pullout tests using buried steel pipes of diameter 102 mm and 324 mm for burial depth ratios of 1.5, 3.5, 5.5, 8 and 11. The tests were conducted at soil densities of 14.8 kN/m<sup>3</sup>, 16.4 kN/m<sup>3</sup> and 17.7 kN/m<sup>3</sup> with peak friction angles of 31°, 36° and 44°. Equation 2-11 defines the measured lateral force expressed as a dimensionless force.

$$\text{Eq.2-11 } N_h = \frac{P_u}{\gamma HDL}$$

where  $\gamma$  is the unit weight (N/m<sup>3</sup>) of the sand,  $L$  is the length of the pipe (m),  $D$  is the diameter of the pipe (m) and  $H$  is the cover depth from the center of pipe to the surface of soil (m). Lateral pipe displacements are also defined as the dimensionless coefficient  $u/D$  where  $u$  is the lateral displacement of the pipe.

The lateral soil resistance values of Trautmann's (1983) pullout tests were in good agreement with Ovesen (1964) and Rowe and Davis (1982) for the anchor plates; however, much lower than that predicted by the Hansen (1961) model. Hansen (1961) assumed a fully vertical restraint condition that leads to a conservative estimation of the ultimate strength by 150% to 200%. Trautmann (1983) also stated that a heavy model pipe, including contents, could form a larger soil passive wedge in front of the pipe resulting in higher lateral loads as compared to light pipes. Trautmann (1983) and Trautmann and O'Rourke (1985) also developed the following chart (Figure 2-7) for estimation of the lateral force depending upon the soil condition and pipe burial depth.

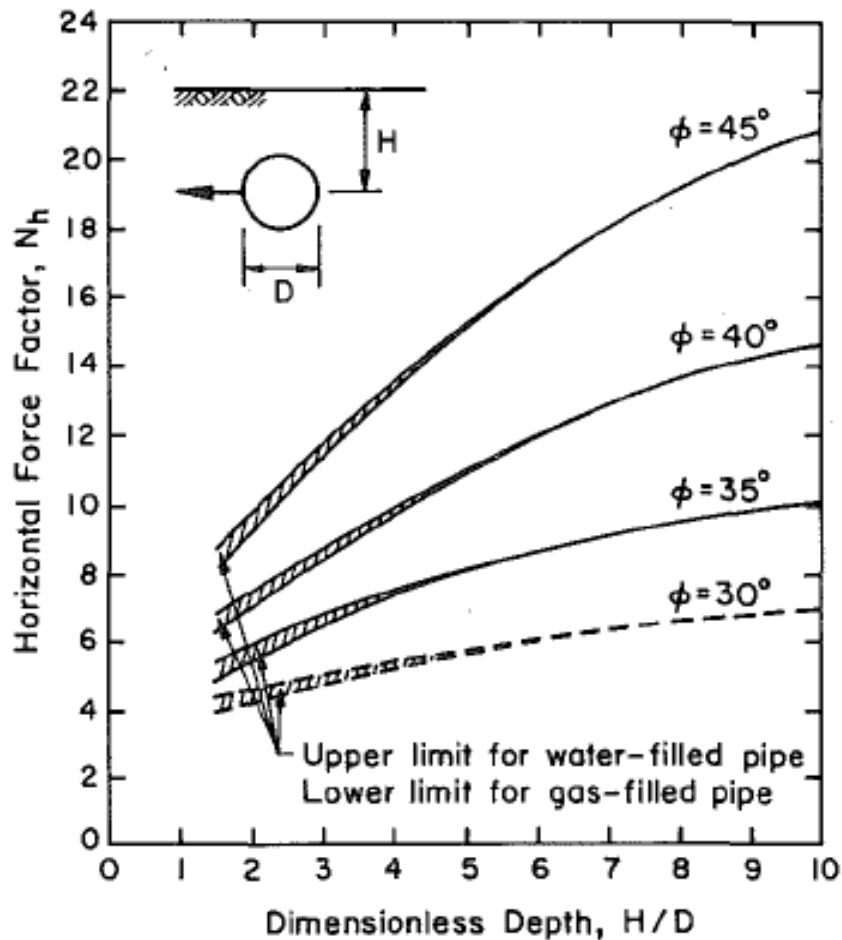
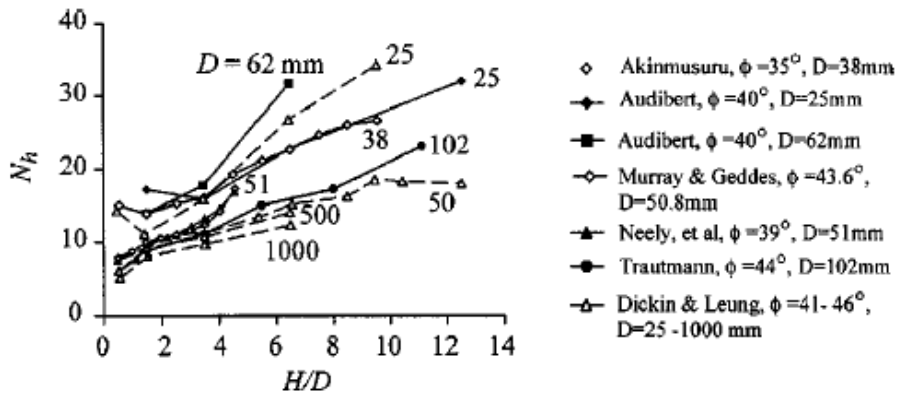


Figure 2-7:  $N_h$  versus  $H/D$  for pipeline design (Trautmann 1983).

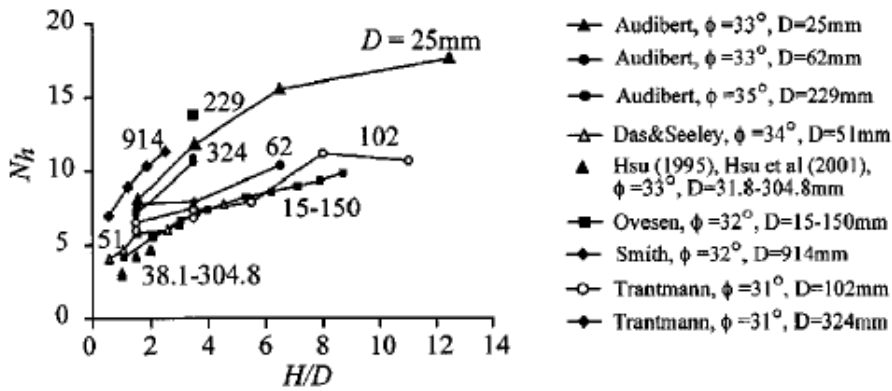
Trautmann (1983) also observed a similar pattern of failure that was described by Audibert and Nyman (1977). For shallow burial depth, with displacement, a shear failure surface in front of the pipe develops and propagates to the soil surface. The transition between shallow and deep failure mechanism takes place at  $H/D$  of 8.5 to 11.5 for loose and medium sand. For dense sand, the transition takes place at  $H/D$  greater than 11.5. Trautmann (1983) stated that the displacement at maximum lateral force depends on the soil density. Their results show the maximum lateral force occurred at  $u/D$  of 16% and

7% for loose and medium sand, respectively, whereas for dense sand the peak force mobilized at  $u/D$  of 2%.

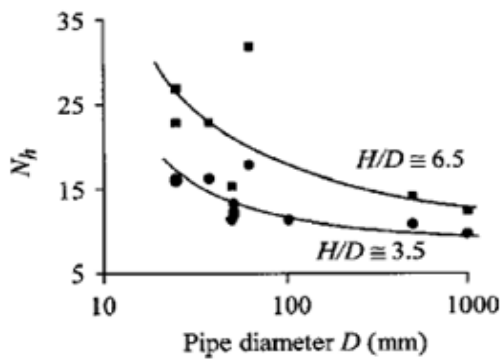
Guo and Stolle (2005) reviewed a number of experimental studies on lateral pipe–soil interaction for non-cohesive test beds. A parametric study, using FE methods, was conducted to assess the effects of burial depth, overburden ratio, soil dilatancy, strain hardening and scale effect on the peak load and ultimate displacement. The wide variability observed in the  $N_h$  versus  $H/D$  relationship was explained using the scale effect (ratio between pipe diameter with respect to reference pipe diameter), pipe size and burial depth (see Figure 2-8). An empirical equation was developed that accounts for the scale and burial depth effects (see Figure 2-9).



a) Dense sand ( $\phi' > 35^\circ$ )



b) Loose sand ( $\phi' < 35^\circ$ )



c) Effect of pipe diameter

**Figure 2-8: Lateral bearing force of different experimental works (Guo and Stolle 2005)**

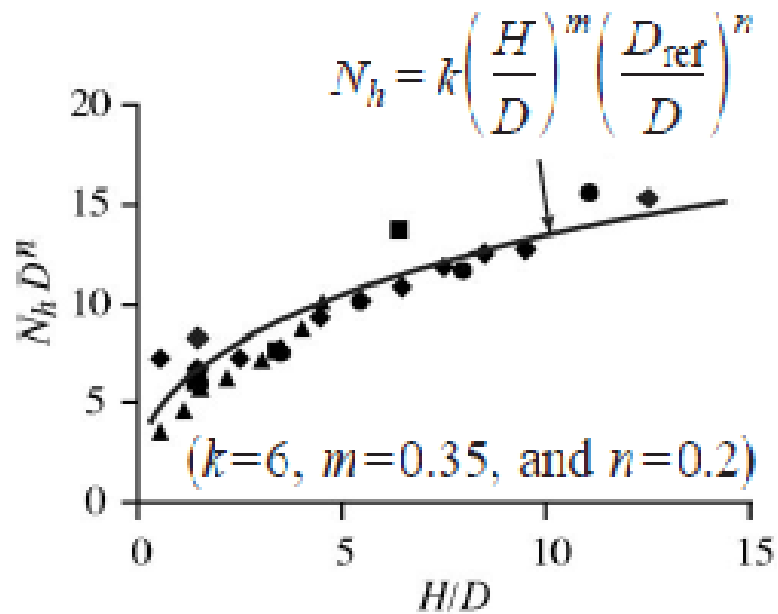


**Figure 2-9: Comparison of the proposed equation and experimental works (Guo and Stolle 2005)**

Yimsiri et al. (2004) also conducted a FE analysis for a wide range of embedments to investigate the peak forces for lateral and upward pipe movements. The experimental results of Trautmann and O'Rourke (1983) with overburden ratios of 2 to 11 were used to calibrate the numerical modeling procedures. Two soil constitutive models (Mohr-Coulomb and Nor-Sand models) were used in the simulation. A design chart was proposed (see Figure 2-10) to calculate the peak force for lateral and upward pipe movement with different friction angles.

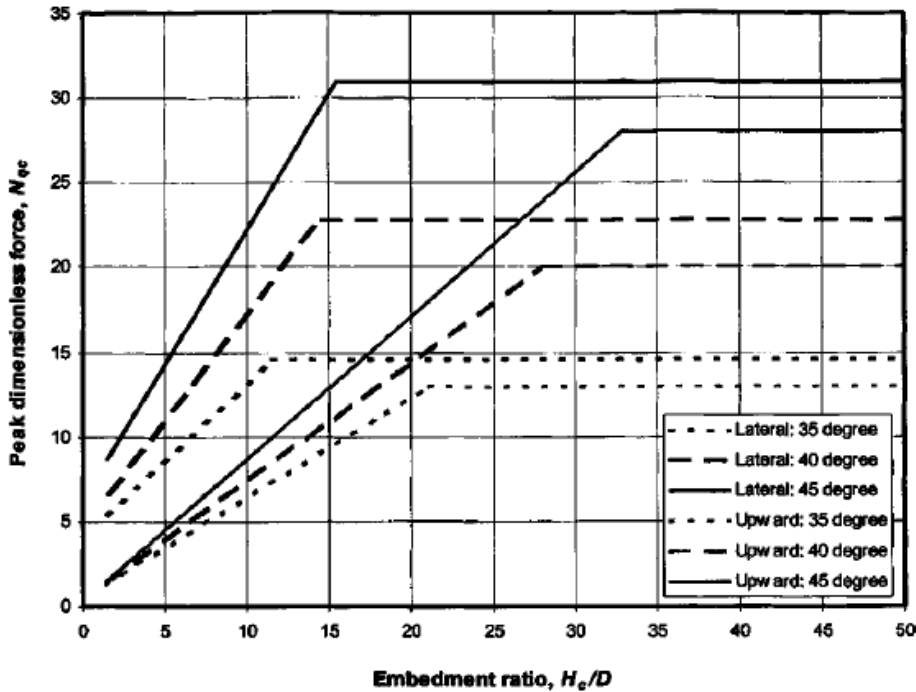


**Figure 2-10: Proposed design chart for lateral and upward pipe movement (Yimsiri et al. 2004)**

Karimian (2006) performed a series of full scale tests on rigid steel pipe to determine longitudinal and horizontal soil restraint for three different diameter pipes in loose and dense sand test beds. In comparison with this study, the investigations by Trautmann and O'Rourke (1983) and Turner (2004) were observed to slightly over predict the soil load than these observed values. Moreover, the horizontal bearing factor from Hansen (1961) over predicts the measured horizontal peak loads obtained in these tests. Karimian (2006) also developed a numerical model using a modified hyperbolic model to investigate the effect of different parameters (i.e., pipe diameter, surface roughness and pipe and its content weight) on soil loads during horizontal ground movement. The results were in agreement with the scale effect model proposed by Guo and Stolle (2005).

O'Rourke et al. (2008) conducted large-scale and reduced-scale centrifuge tests on high density polyethylene (HDPE) and steel pipelines to investigate the pipeline system response to earthquake by observing the horizontal load–displacement relationship for both dry and partially saturated sand. The results for the measured maximum lateral soil forces during pipeline horizontal movement, for both the large-scale and reduced-scale centrifuge tests, were in good agreement for dry and partially saturated sand across the range of  $H/D$  ratios and peak soil friction angle.

O'Rourke et al. (2008) also proposed an analytical model, called log spiral model, for the cohesionless soils that was validated by comparing the values from this model with the values from the full-scale experimental test data and those given by ASCE (1984). The model was developed for the maximum horizontal pipe force as a function of depth to pipe diameter ratio and peak soil friction angle. The lateral soil resistance ( $P_H$ ) (Figure 2-11) can be found by satisfying the moment equilibrium about the center of rotation as:

$$\text{Eq. 2-12 } P_H = \frac{W_s L_2 + W_P L_3}{L_1}$$

Where,

$P_H$  = horizontal soil force per unit distance;

$W_s$  = weight of soil mass;

$W_P$  = pipe weight (including contents);

$L_1$  = moment arm between  $P_H$  and center of rotation;

$L_2$  = moment arm between  $W_s$  and center of rotation;

$L_3$  = moment arm between  $W_P$  and center of rotation;

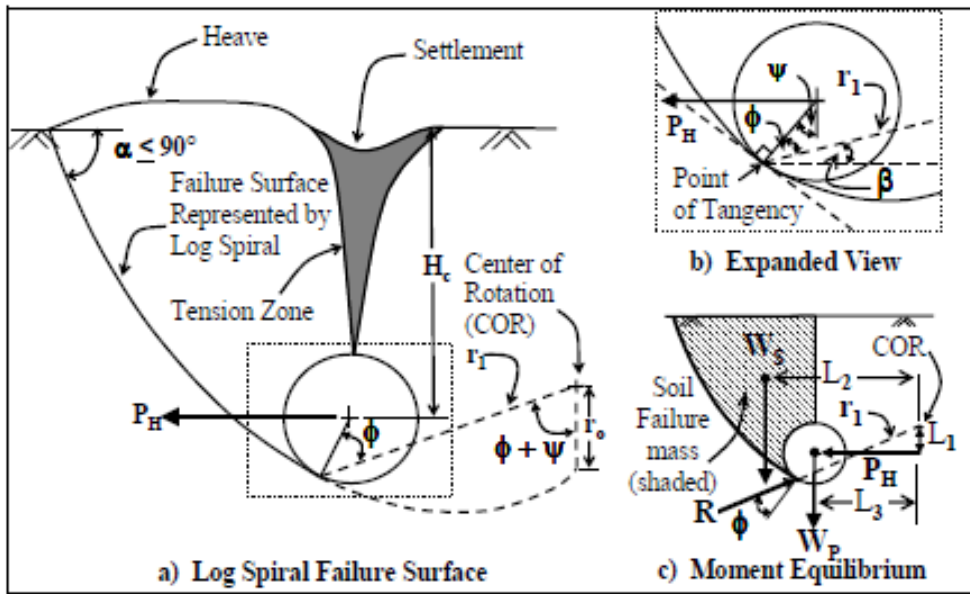


**Figure 2-11: Schematic diagram of log spiral model (O'Rourke et al., 2008).**

Daiyan et al. (2010, 2011) performed a series of centrifuge tests to investigate the coupling mechanism during the pipe–soil interaction event. In the pure lateral test, they found higher lateral interaction factors as compared to Trautmann (1983) and Guo and Stolle (2005), which might be due to the use of a heavy model pipe and loading system in centrifuge tests. Daiyan et al. (2010, 2011) also confirmed the increase in lateral resistance with self-weight of the pipe through FE simulation. They also obtained higher lateral displacements to mobilize the peak load, which might be due to the variation in soil properties in the test bed preparation especially near the pipe.

In the current guidelines, such as PRCI (2004; 2009) and ALA (2005), the ultimate lateral soil resistance,  $P_u$  per unit length of the pipe buried in sand can be calculated using the following equation:

$$\text{Eq. 2-13 } P_u = N_h \gamma H D$$

where  $N_h$  is the dimensionless horizontal bearing capacity factor. ALA (2005) and PRCI (2004) recommends the Hansen (1961) analytical model to calculate  $N_h$  which is in agreement with the experimental finding from Audibert and Nyman (1977) (see Figure 2-6) whereas PRCI (2009) recommends a chart to calculate  $N_h$  as below.

**Table 2-2: PRCI (2009) recommended chart to calculate  $N_h$**

$\phi'$	H/D Range	a	b	Maximum $N_h = a + b \frac{H}{D}$
35°	0.5 to 12	4	0.92	15
40°	0.5 to 6	5	1.43	23
	6 to 15	8	1.00	
45°	0.5 to 7	5	2.17	30
	7 to 15	10	1.33	

$N_h$  for other value of  $\phi'$  between 35° and 45° could be obtained by interpolation.

Moreover,  $\phi'$  should not be taken less than 35° even if soil tests indicate lower  $\phi'$  values.

For the displacement at  $P_u$ , ALA (2005) and PRCI (2004, 2009) recommends the

Equation 2-15 as follows:

$$\text{Eq. 2-15 } y_u = 0.04 \left( H + \frac{D}{2} \right) \leq 0.10D \text{ to } 0.15D$$

where as in ASCE (1984), the following relationship is recommended.

$$\text{Eq. 2-16} \quad y_u = \begin{cases} 0.07 \text{ to } 0.10 (H+D/2) & \text{for loose sand} \\ 0.03 \text{ to } 0.05 (H+D/2) & \text{for medium sand} \\ 0.02 \text{ to } 0.03 (H+D/2) & \text{for dense sand} \end{cases}$$

Depending upon soil density and embedment, the lateral force–displacement relationship curves might show strain hardening or strain softening behavior (Trautmann and O’Rourke 1983; Roy et al. 2015). Bilinear, elastic perfectly plastic or a hyperbolic function can be used to define the soil spring force–displacement relationship.

In summary, the lateral pipe–soil interaction response, more specially the peak force and its mobilized displacement, depends on a number of factors, such as soil strength, burial depth, loading rate, large deformation soil behavior (e.g., strain hardening, strain softening), interaction and contact process, trench effects (e.g., backfill properties, trench geometry), and failure mechanisms (e.g., plastic wedge formation at shallow burial conditions, local punching failure with flow around mechanisms in deep burial conditions).

### 2.3.3 AXIAL-LATERAL PIPE–SOIL INTERACTION

In the current guidelines, it is recommended to analyze the pipe–soil interactions within a simplified independent analytical model that does not account for the complex interaction

between the pipeline and soil during ground movement. There are a limited number of studies (Hsu et al., 2001; 2006; Phillips et al., 2004; C-CORE, 2008 and Daiyan et al., 2010; 2011) that address the coupled or oblique loading response during axial-lateral pipe–soil interaction events.

Kennedy et al. (1977) recognized the effect of lateral soil pressure on the increasing maximum axial resistance around the curved pipe lengths in moderately dense sand. The axial soil restraint in regions with relative ground displacement was calculated by multiplying the pipe–soil interface friction angle,  $\delta$ , and the maximum lateral soil restraint.

After that, Hsu et al. (2001, 2006) conducted large–scale laboratory tests to investigate the effect of oblique pipe movement in a horizontal plane (axial-lateral) for shallow buried pipes in loose and dense sand respectively. They performed tests for 10 different angles of movement ( $\alpha$ ) between  $0^\circ$  (represents axial loading) and  $90^\circ$  (represents lateral loading) with three different diameters and H/D ratios where Hsu et al. (2001, 2006) defined the angle of movement using Figure 2-12.

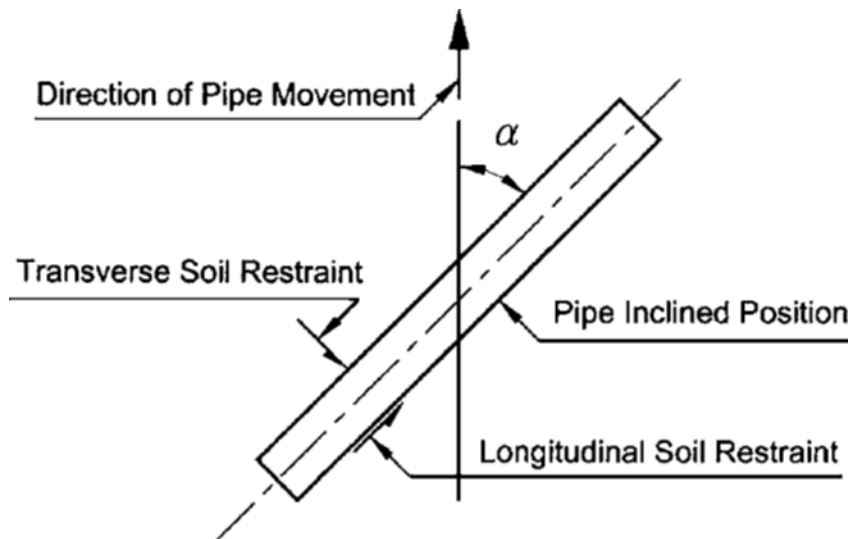


**Figure 2-12: Axial-lateral oblique angle (Hsu et al. 2001, 2006).**

The laboratory test results are shown in Figures 2-13 and 2-14 from where the longitudinal and transverse soil resistance for an oblique movement of the pipes can be obtained geometrically by multiplying the corresponding cosine and sine value of the oblique angle, respectively. Minor scale effects on the soil resistance were observed for pipe diameters up to 304.8 mm.

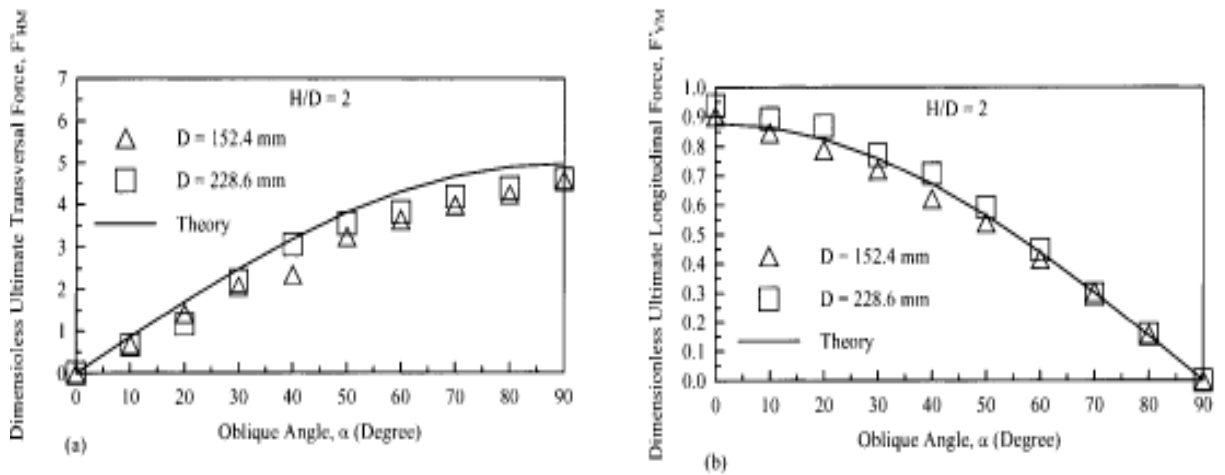


**Figure 2-13: Oblique pipe-soil interaction in loose sand (a) lateral loads, (b) axial loads (Hsu et al. 2001)**

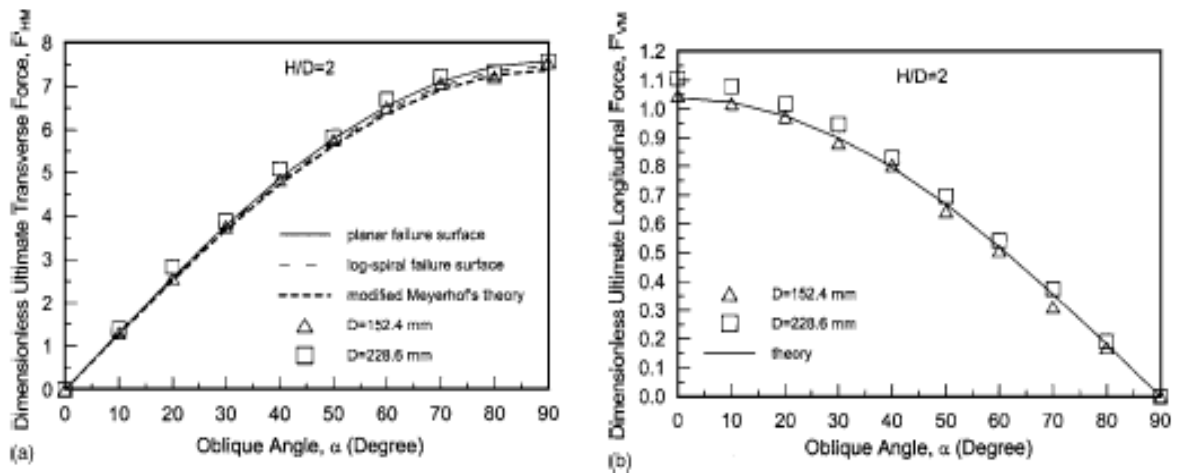


**Figure 2-14: Oblique pipe-soil interaction in dense sand (a) lateral loads, (b) axial loads (Hsu et al. 2006)**

C-CORE (2008) and Daiyan et al. (2010, 2011) conducted centrifuge tests to investigate the coupled lateral-axial pipe-soil interaction during the pipe movement in the horizontal plane for a pipe specimen of diameter 41 mm at 12.3g. Although vertical movement of

the pipe was allowed during the test, the heavy weight pipe and loading system lead to vertical restraint that resulted in higher lateral resistance than Trautmann (1983).

C-CORE (2008), Phillips et al. (2004) and Daiyan et al. (2010, 2011) observed a higher maximum axial soil restraint during the oblique axial-lateral pipe–soil interaction than the pure axial condition, with a factor of even 2.5 for oblique angles less than 40°. The observed higher axial soil restraint was associated with increased normal soil pressure due to the lateral component of oblique relative displacement. Daiyan et al. (2011) simulated the centrifuge test using 3D continuum finite element methods where the axial soil restraint increased for low oblique angles of 1° (pipe misalignment).

Phillips et al. (2004) proposed the following equation based on reduced–scale centrifuge test results and numerical simulation to define the lateral-axial yield envelop.

$$\text{Eq. 2-17} \quad N_{qh\theta}^2 + 3 N_{t\theta}^2 = N_{qh90}^2$$

where  $N_{qh90}^2$  is the interaction factor for the pure lateral loading.

C-CORE (2008) also recommended a pipeline–soil interaction envelop as shown in Figure 2-15. Daiyan et al. (2010) also proposed a similar interaction envelope for sand.

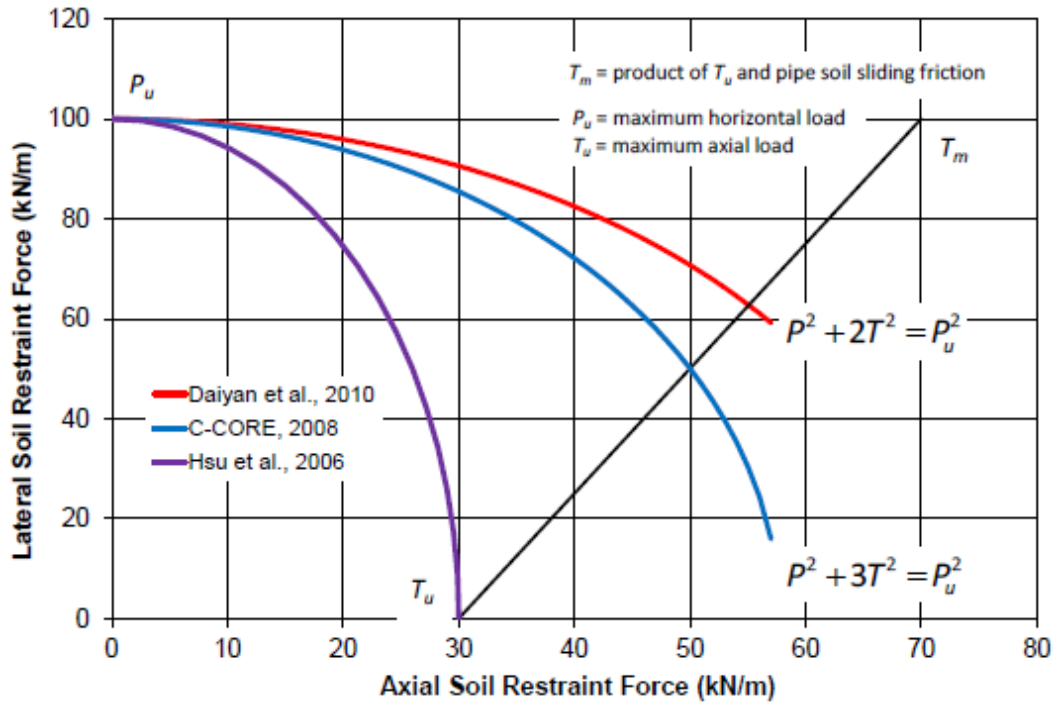


**Figure 2-15: Axial-lateral pipe-soil interaction envelope (C-CORE 2008)**

The above interaction diagram (Figure 2-15) has two segments: (i) the linear portion of the diagram, represents the lower angle of attack (less than  $10^\circ$ ), which is mainly controlled by the shear resistance at the pipe-soil interface, and (ii) the non-linear portion for larger attack angles ( $>30^\circ$ ), which are mainly associated with the shear failure in the soil mass in front of the pipe.

## 2.4 CLOSURE

A comprehensive literature review on analytical, experimental and numerical studies on pipe–soil interaction is presented in this chapter. Most of the previous studies available in the literature are on purely axial (i.e., longitudinal), or purely lateral (i.e., bearing) loading conditions. A limited number of studies on oblique axial-lateral interaction are available. Most of the available studies are primarily focused on the maximum soil force and the displacement required to mobilize the maximum force. A wide range of discrepancies is observed both in numerical and experimental studies. Moreover, although limited, a significant variation is observed in experimental results for axial-lateral pipe–soil interaction (e.g., Hsu et al., 2001, 2006; Daiyan et al., 2010). Potential underlying factors associated with this discrepancy might be explained by conducting additional centrifuge tests, which are relatively cheaper than full-scale tests. It is also expected that the finding of this research might help improve the guidelines for modelling coupling effects of axial-lateral displacements of pipe–soil interaction. With these considerations in mind, a series of reduced–scale centrifuge tests were conducted in this study for pipelines buried in loose and dense sand using the geotechnical centrifuge at C-CORE.

### **3 CENTRIFUGE PHYSICAL MODELLING**

#### **3.1 CENTRIFUGE MODELLING ASPECTS**

Physical modeling is widely used in geotechnical engineering to examine many complex boundary value problems, including soil–structure interaction systems at large strains and failure, which cannot be modeled using analytical techniques.

Among the different types of physical modeling, centrifuge modeling is an efficient and cost-effective method. The stress-strain behavior of soils are highly stress dependent and the centrifuge applies an increased gravitational acceleration to physical models in order to produce equal confining stresses in model and prototype. The one to one scaling of stresses enhances the similarity of geotechnical models and makes it possible to obtain accurate stress-strain behavior of soil elements in the whole domain of complex problems like pipe–soil interactions. Centrifuge model tests have been also used in many applications to calibrate numerical modeling techniques.

### 3.1.1 CENTRIFUGE PRINCIPLES AND SCALLING LAWS

The basic concept of centrifuge modeling is accelerating a reduced-scale geotechnical model to simulate the behavior in the prototype scale by increasing stresses through centrifuge acceleration. If a model is made on a reduced scale of 1:  $N$  and, centrifugally accelerated at  $N$  times of Earth's gravity ( $g$ ), soil behavior in the model and prototype is expected to be the same, because the stress level at any point of the model is similar to the corresponding level in the prototype as shown in Figure 3-1.

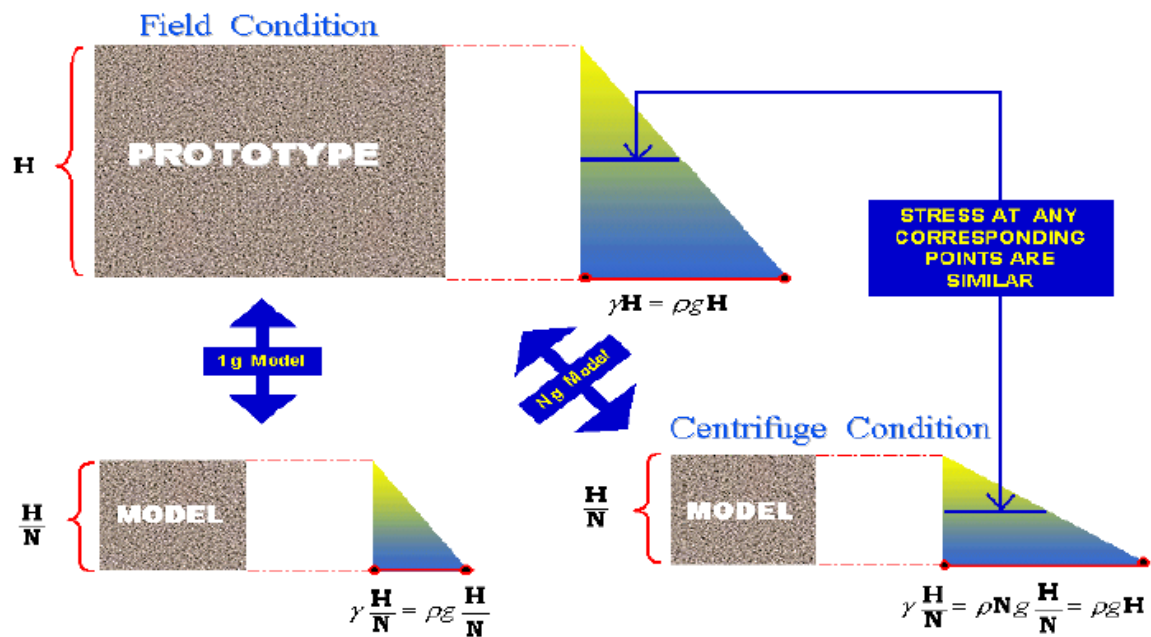


**Figure 3-1: Basic concept of centrifuge physical modeling.**

To ensure the stress similarity between the model and corresponding prototype, some basic scaling laws are introduced in geotechnical centrifuge testing. These scaling factors for physical quantities in centrifuge testing are derived from dimensional analysis using linear dimension scale. Some of the scaling factors for basic quantities in centrifuge modeling are presented in Table 3-1 (Taylor 1995).

**Table 3-1: Some scaling factors for centrifuge modeling (Taylor, 1995)**

<b>Parameter</b>	<b>Scale Factor (Prototype : Model ) at Ng</b>
Length	1 : 1/N
Stress	1 : 1
Strain	1 : 1
Density	1 : 1
Unit Weight	1 : N
Force	1 : 1/N <sup>2</sup>
Time (dynamic)	1 : 1/N

### **3.1.2 C-CORE CENTRIFUGE FACILITY**

C-CORE in St. John's, Newfoundland has a world class Acutronic 680-2 geotechnical centrifuge, which has the radius of 5.5 m and can work up to 200g. This centrifuge has been also designed to incorporate a payload volume of 1.1 m × 1.4 m × 1.2 m. The C-CORE centrifuge has been used for modeling many geotechnical problems including pipe–soil interaction modeling (Paulin et al., 1998; Phillips et al., 2004a; PRCI 2009).

### 3.2 EXPERIMENTAL SETUP

The test setup developed by Daiyan (2013) and Daiyan et al. (2010), with minor modifications, is used in this study to conduct test on oblique pipe–soil interaction events. In the tests conducted by Daiyan (2013), a steel pipe of 41 mm outside diameter and 6.35 mm wall thickness was used. The thick-walled pipe, with a  $D/t$  of 6.5, could ensure a rigid pipe configuration; however its weight significantly influenced the force–displacement behavior and failure mechanisms. In the present study, a lighter pipe of 46 mm outer diameter and 3.9 mm wall thickness ( $D/t$  of 12) was used and centrifuge tests were conducted using the test setup developed by Daiyan (2013). This pipe configuration provided sufficient rigidity to investigate the load–displacement relationships. The geometric dimensions of the centrifuge strongbox and model pipe are summarized in Table 3-2.

**Table 3-2: Key parameters of pipe model**

Test configuration	Values
Centrifuge strong box	1180 mm × 940 mm × 400 mm
Model pipe outer diameter (D)	46 mm
Model pipe thickness (t)	3.90 mm
Model pipe length (L)	368 mm
Pipe springline burial depth to pipe diameter ratio (H/D)	2
Pipe cover depth (C)	69 mm
Pipe to diameter ratio (L/D)	8

The test setup, within the centrifuge strongbox, is shown in Figure 3-2 with some photographs in Figures 3-3 to 3-5. Various components of the centrifuge model are listed in Table 3-3. As shown in these figures, the model pipe (#1) is connected to the centrifuge actuator (#11), which is the prime mover to drag the pipe through the soil in a direction perpendicular to the support beams (Figure 3-2), by the stanchions (#4 & #5) and guiding plate (#9). The relative orientation of pipe movement (i.e., attack angle or oblique loading angle) through the soil can be adjusted using the guiding plate (#9) from purely axial ( $0^\circ$ ) to purely lateral bearing ( $90^\circ$ ). Two ball races (#7 & #8) were bolted to each end of the guiding plate (#9) to allow for vertical movement of the pipe (#1) and stanchions (#4 & #5). The stanchions (#4 & #5) were tied via a dogbone (#6) to provide additional support and stiffness for the loading system.

Two load cells (#2 & #3), connected at each end of the model pipe segment, measured the axial and lateral forces imposed on the pipe during the relative motion through the soil test bed. The load cell design is based on Stroud (1971) as shown in Figure 3-6. The load cell consists of 4 longitudinal webs and 2 horizontal webs. The longitudinal webs measure the axial load ( $N$ ) and the horizontal webs measure lateral load ( $S$ ). There is a cross sensitivity that exists between the axial and lateral strain gauges. The load cells are connected with ball bearing to the both ends of pipe through which loads are transmitted from the pipe to load cells as the ball bearings acts like a pinned (i.e., moment free) joint. The loads cells are recalibrated for this test series using a coupled calibration matrix, as described in Stroud (1971), and calibration results are presented in Appendix A.

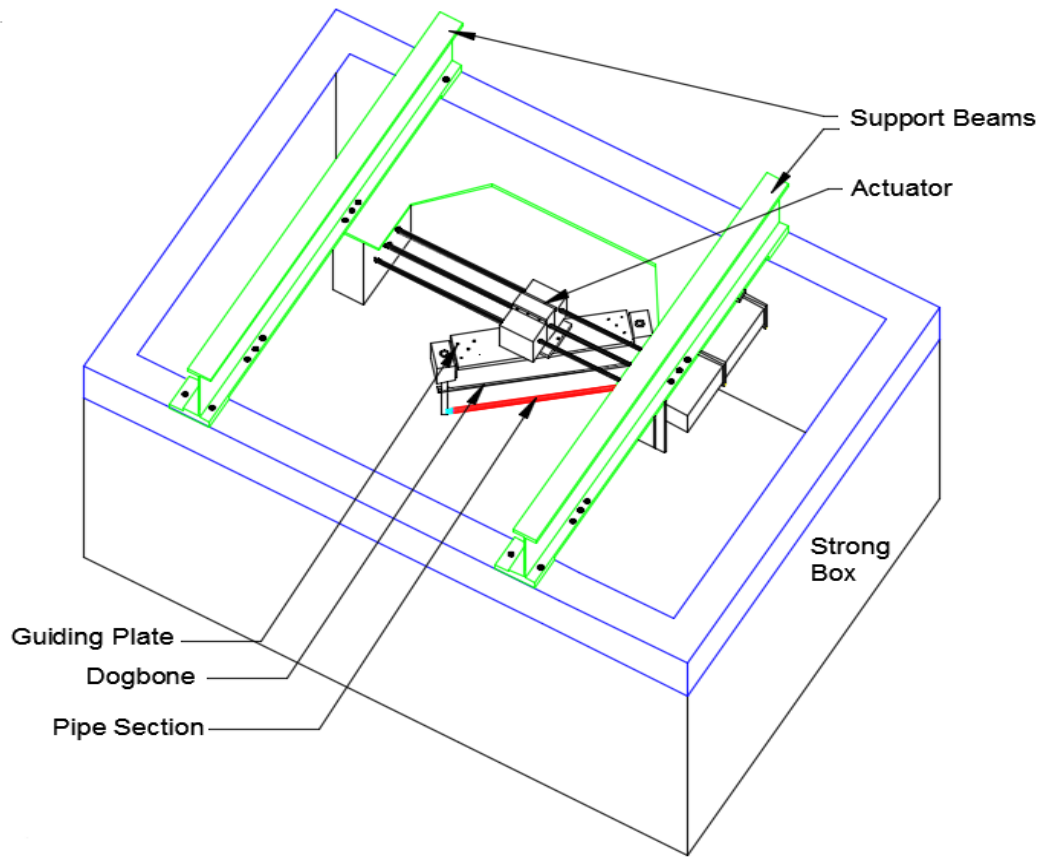


**Figure 3-2: Pipe setup in the strongbox for centrifuge tests**

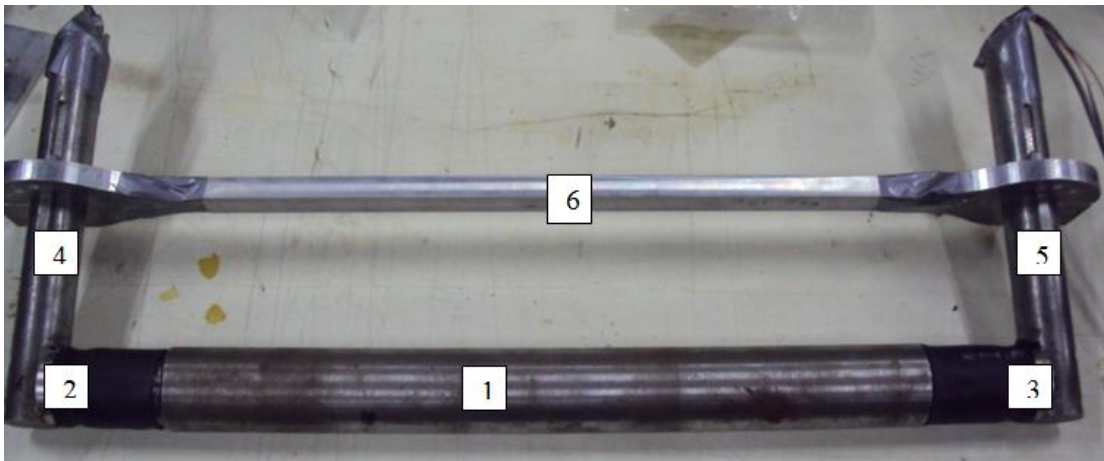


**Figure 3-3: Model pipe (#1) with load cell (#2, #3), stanchions (#4, #5) and dogbone (#6)**

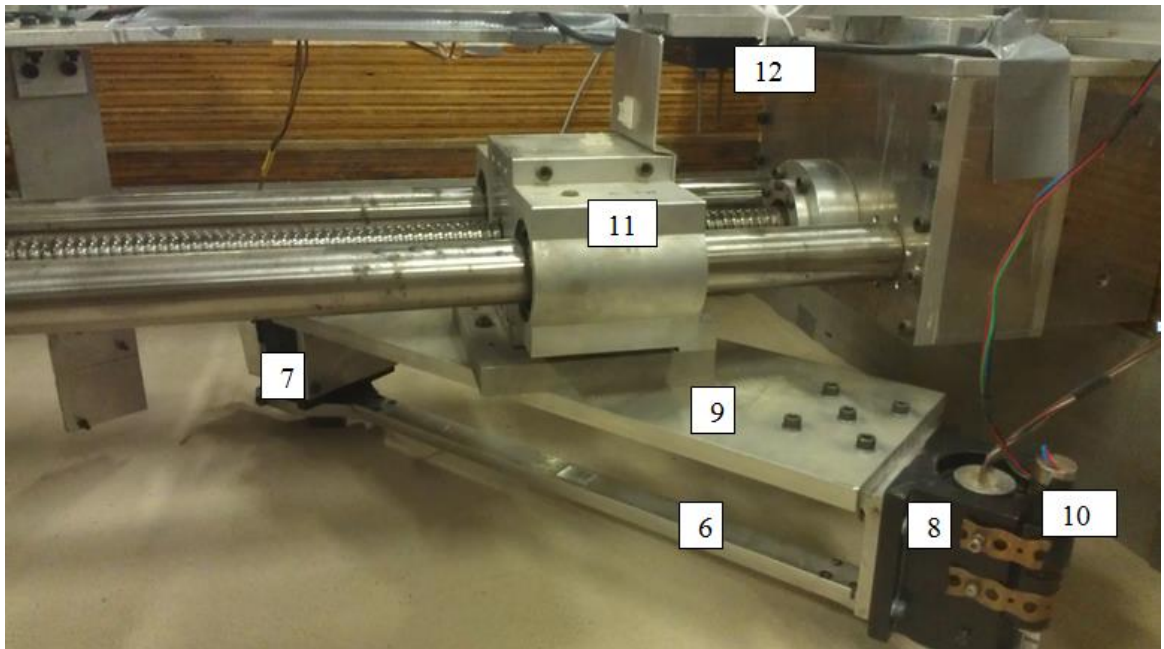


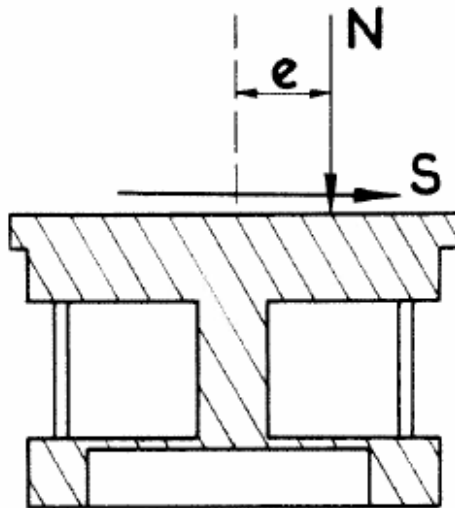
**Figure 3-4: Test setup for Test 3**



**Figure 3-5: Test setup for Test 5**

**Table 3-3: Main components in centrifuge model test**

No.	Description	No.	Description
1	Steel Model Pipe (46 mm Outer dia.)	8	Ball Race-2 (allow the vertical movement of stanchions)
2	Load Cell-1 (connected with the end of pipe through small bearing )	9	Guiding plate (connected with two ball races)
3	Load Cell-2 (connected with the end of pipe through small bearing )	10	LVDT-1 (to measure vertical displacement)
4	Stanchion-1 ( hold the load cell -1)	11	Motorized Carriage of the Actuator
5	Stanchion-2 ( hold the load cell -2)	12	Laser-1 (to measure horizontal displacement)
6	Dogbone ( cross beam to tie two stanchions together)	13	Laser-2 (to measure horizontal displacement)
7	Ball Race-1 (allow the vertical movement of stanchions)	14	LVDT-2 (to measure vertical displacement)

**Figure 3-6: Load cell configuration, after Stroud (1971).**

Horizontal displacement was measured using two laser sensors (#12 and #13 in Figures 3-5 and 3-6) located at the level of the actuator and the dogbone, which could be also used to measure any differential motion. Two LVDTs (Linear Variable Differential Transformer, #10 and #14), connected at the two ball races (#7 and #8), are used to measure the vertical movement.

### **3.3 TESTING PROGRAM**

A series of centrifuge tests were conducted, with dense and loose sand test beds, to investigate the coupling effects of oblique pipe–soil interaction in the axial-lateral (i.e., longitudinal-transverse horizontal) plane. As presented later in this thesis, the experimental data are compared with and verified by analytical solutions, physical modelling data and numerical simulations available in the public domain. All tests are conducted at a centrifuge acceleration of 13.25g and pipe displacement rate of 0.04 mm/s.

As shown in Table 3-4, a total of 10 centrifuge tests were conducted in this study. For brevity, test identifications (ID) number which refers to the density of sand test bed and oblique attack angle, is used in the following sections. For example, TD50 refers to the **Test on Dense sand condition for a 50° oblique attack angle.**

**Table 3-4: Test identification, load configuration and soil density**

Test No.	Test ID	Attack angle (degree)	Soil density (kg/m <sup>3</sup> )	Average soil density (kg/m <sup>3</sup> )
1	TD90	90 (pure lateral)	1571.8	1567
2	TD70	70	1575.6	
3	TD50	50	1570.6	
4	TD40	40	1562.8	
5	TD20	20	1543.9	
6	TD0	0 (pure axial)	1575.4	
7	TL90	90 (pure lateral)	1460.7	1467
8	TL70	70	1476.9	
9	TL40	40	1478.3	
10	TL0	0 (pure axial)	1453.8	

### 3.4 MATERIAL PROPERTIES

This section provides the information about the materials used in this testing program.

Geotechnical laboratory tests conducted for shear strength of the sand used for centrifuge tests are also described.

#### 3.4.1 MATERIALS USED IN PHYSICAL TESTING

In centrifuge modeling SCH 80s steel pipes were used. The test bed was prepared using silica sand. The particles size distribution curve of this sand shown in Figure 3-7 which shows that this is a poorly graded sand having  $D_{50} = 0.22$  mm and coefficient of uniformity  $C_u = 1.92$ .

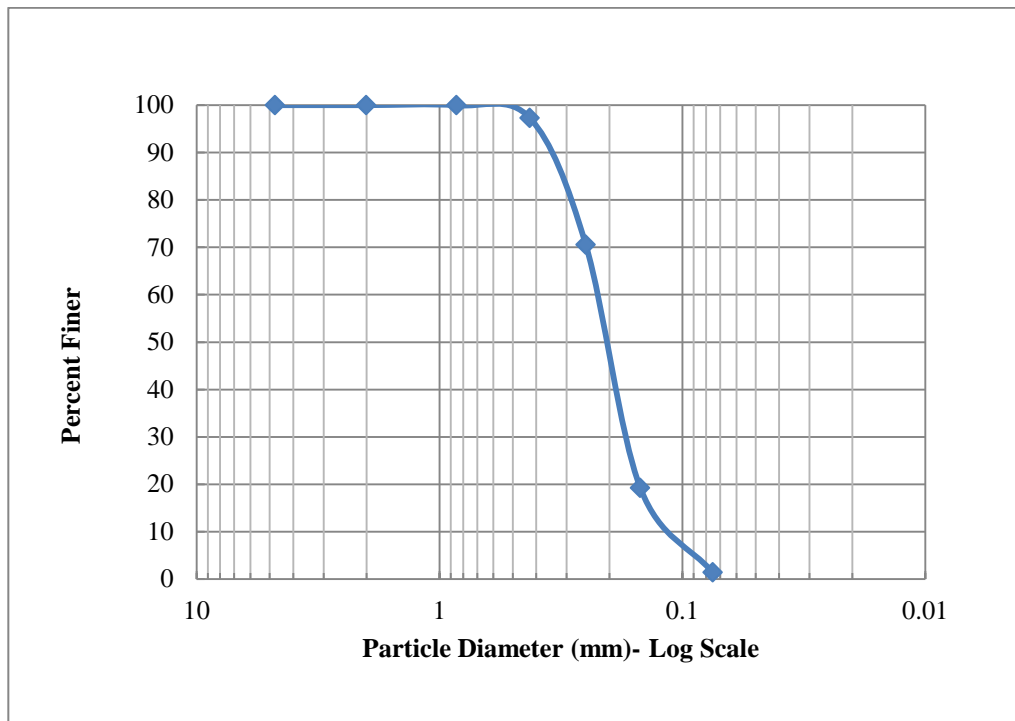


**Figure 3-7: Particle size distribution of silica sand used in experiments.**

### **3.4.2 LABORATORY TESTING FOR SHEAR STRENGTH OF SAND**

Direct shear tests were performed on this sand both at dense and loose states to get the shear strength parameters. Tests were conducted under normal stresses ranging from 8 kPa to 64 kPa, which are relatively lower than typical geotechnical engineering practice, because the stresses around the pipeline is low as compared to many geotechnical engineering problems such as foundations. All the tests were conducted using a recently acquired advanced direct shear test apparatus in the geotechnical laboratory at Memorial University of Newfoundland, which has fully automated load, displacement control and data acquisition system using a computer with high level of accuracy.

### 3.4.2.1 DIRECT SHEAR TEST ON DENSE SAND

In the direct shear tests, an average density of  $1577 \text{ kg/m}^3$  ( $D_r = 72.5\%$ ) was maintained which is comparable to the target density  $1567 \text{ kg/m}^3$  ( $D_r = 71.5\%$ ) in the centrifuge test program in dense sand. The measured shear stress at the peak and large strains (i.e., critical state) for different normal stresses are shown in Figure 3-8. For the normal stress ( $\sigma_n$ ) level greater than 32 kPa, the angle of internal friction at peak ( $\phi'_p$ ) and critical state ( $\phi'_c$ ) are  $41^\circ$  and  $32^\circ$ , respectively. However, at low normal stress levels (i.e.,  $\sigma_n = 8$  and 16 kPa) both  $\phi'_p$  and  $\phi'_c$  are higher than their values at high normal stresses. Drawing a line from the origin to the data points, it can be shown the  $\phi'_p$  and  $\phi'_c$  decreases with normal stress. The decrease in  $\phi'_p$  and  $\phi'_c$  with normal stress or confining pressure has been reported by a number of researchers (e.g., Bolton 1986; Lings and Dietz 2004), which has a significant effects on pipe–soil interaction modeling as shown in recent finite element modeling (Jung et al. 2013; Roy et al. 2015). Therefore, it is expected that the shear strength behavior obtained from the laboratory test will explain the pipe–soil interaction in centrifuge tests as presented in the following chapter. But for the normal stress from 8 kPa to 64 kPa, the average peak friction angle and average critical friction angle are  $47^\circ$  and  $40^\circ$ .

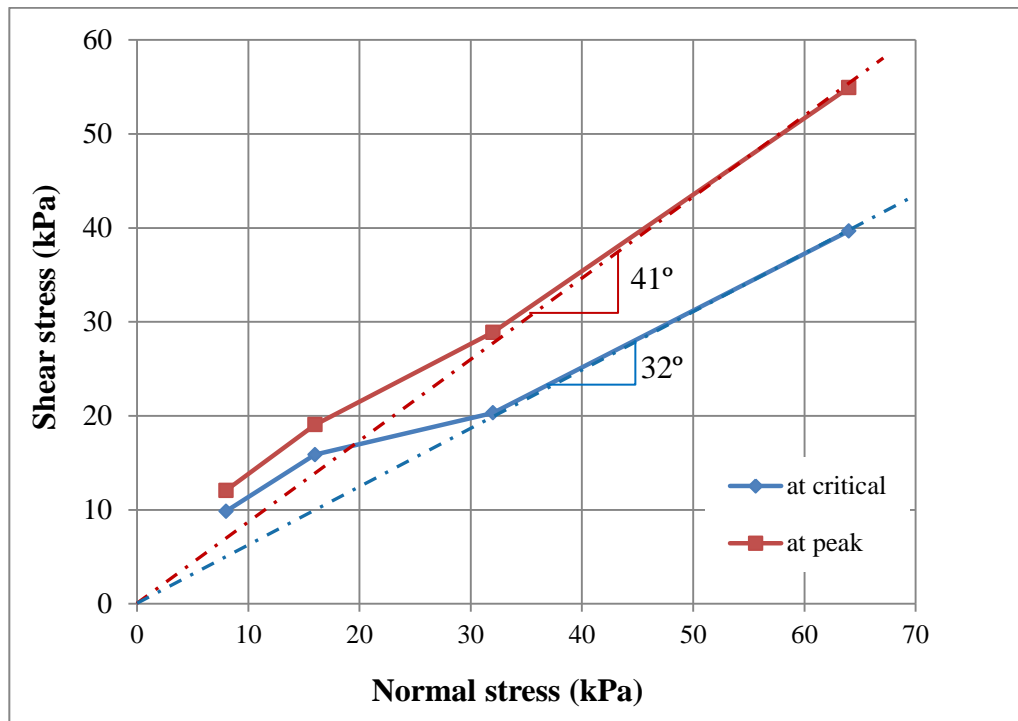


**Figure 3-8: Direct shear test results on dense sand (average density = 1577 kg/m<sup>3</sup>).**

### 3.4.2.2 DIRECT SHEAR TEST ON LOOSE SAND

Using the same direct shear apparatus, tests were conducted for loose sands of average density 1493 kg/m<sup>3</sup> ( $D_r = 33\%$ ) which is comparable to the target density of 1496 kg/m<sup>3</sup> ( $D_r = 34.5\%$ ) in the centrifuge test program for loose sand. Similar to dense sand in Figure 3-8,  $\sigma_n$  greater than 32 kPa,  $\phi'_p$  and  $\phi'_c$  are 36° and 32° respectively (Figure 3-9). Moreover,  $\phi'_p$  and  $\phi'_c$  decreases with normal stress; however, as expected, the decrease is less than in this case than dense sand in Figure 3-8. It is to be noted here that, as expected, in both dense and loose state  $\phi'_c = 32^\circ$ . But for the normal stress from 8 kPa to 64 kPa, the average peak friction angle and average critical friction angle are 40° and 36°.

In summary, the angle of internal friction is not a constant value, rather than it depends upon density, confining pressure/normal stress and strain level (e.g. critical state or the peak). These factors should be considered while interpreting physical modeling tests results and numerical modeling.

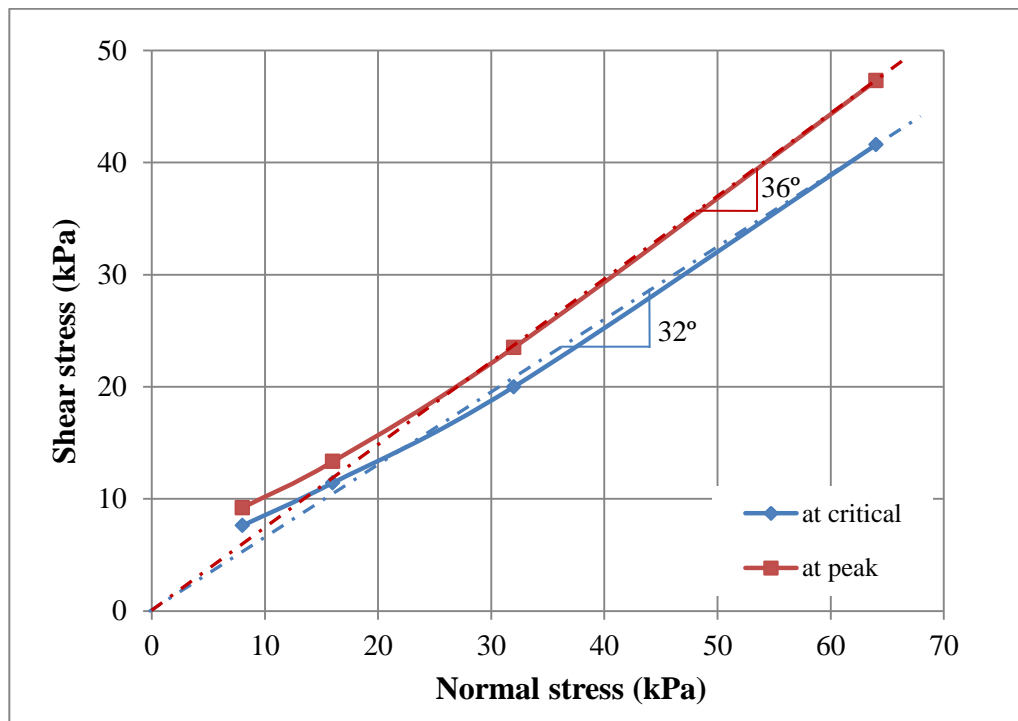


**Figure 3-9: Direct shear test results on loose sand (average density =  $1493 \text{ kg/m}^3$ ).**

### 3.5 TEST BED PREPATION FOR CENTRIFUGE MODELING

All the test beds were prepared by maintaining the same sand raining condition (i.e., height, aperture size and funnel moving speed). To achieve the required relative density,

several trials beds were prepared at different of raining heights. Plotting achieved density against drop height (Figure 3-10), the required drop height for targeted density is selected.

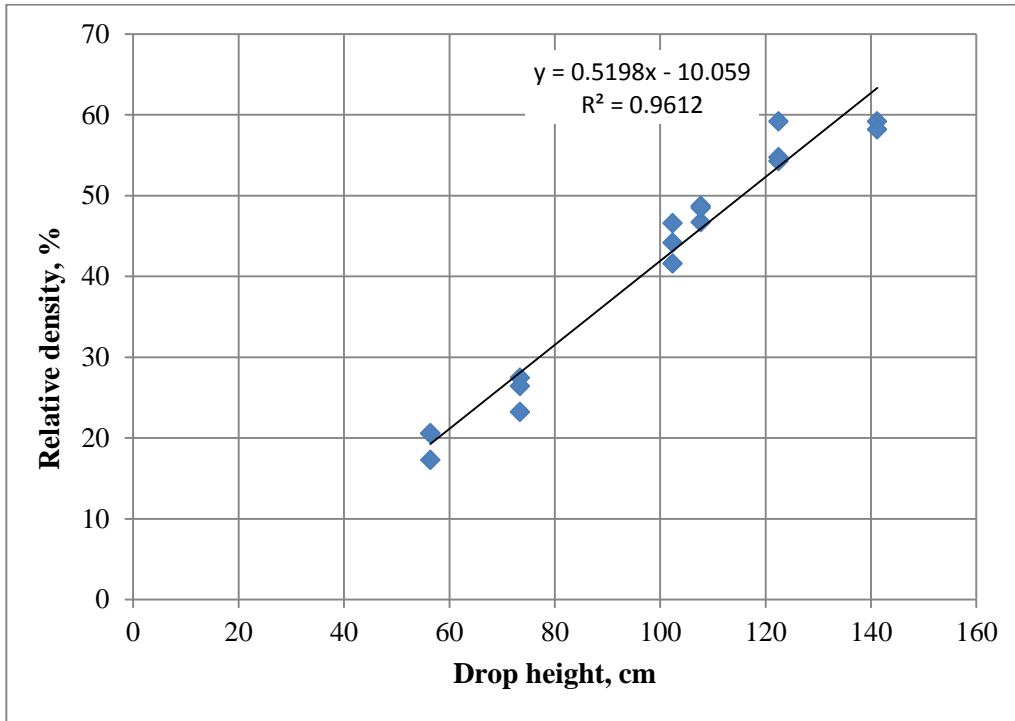


**Figure 3-10: Density trial test results for sand raining.**

## **4 AXIAL-LATERAL PIPE–SOIL INTERACTION IN DENSE SAND**

### **4.1 INTRODUCTION**

Centrifuge tests conducted in dense sand are presented in this chapter. As mentioned in Chapter 3, a total of 6 centrifuge tests were conducted in dense sand of an average density  $1567 \text{ kg/m}^3$  (Table 3-4) using a 46 mm diameter model pipe that represents the 609 mm diameter pipe in prototype scale at 13.25g. All tests were conducted at burial depth of 2D. Collected raw data was analyzed writing a MATLAB code. The synthesized data were further analyzed using MS Excel to examine force–displacement behavior, scale effects and coupling effects of displacements on failure envelope. In addition deformation pattern and failure mechanisms are examined based on a number of photos during and after tests. Only some of them are enclosed in this thesis because of space limitation. The results of the present study are also compared with previous analytical, numerical, experimental work as well as with the current design guidelines. Tests performed in loose sand are presented in Chapter 5.

### **4.2 TEST RESULTS, ANALYSIS AND DISCUSSION**

First of all the test results are plotted in form of load–displacement relationships. TD90 and TD0 were performed for purely lateral and purely axial condition whereas TD70, TD50, TD40 and TD20 were conducted at 4 different oblique angles of attack ( $70^\circ$ ,  $50^\circ$ ,  $40^\circ$  and  $20^\circ$ ). Two key parameters identified from the load–displacement curves are; (i)

peak load, and (ii) mobilized displacement to reach the peak load. To define the peak load, where a clear peak does not exist, there are several methods that have been proposed in the past. Pike et al. (2011) discussed the available methods to define the peak, which are summarized in Figure 4-1. The peak load using the Method (1) is defined as the load at point of intersection of the tangents to the curve at small and large displacements (Wantland et al.1982). Method (2) uses the load at which the load–displacement curve passes into steep straight tangent based on Trazaghi’s definition for local shear failure. The Method 3 simply uses the load at large displacement. Daiyan et al. (2009) also used these methods to define the peak loads. In this thesis, the Methods (1) and (2) are used to estimate the peak load and mobilization distance.

The test results for TD70, TD50, TD40 and TD20 are corrected according to Equation 4-1 to account the actuator compliance as described in Daiyan (2013). Daiyan (2013) conducted a series of in-air tests where a lateral load was applied at the middle of the pipe and displacements at carriage and top ball race level and rotation of the guiding plate were measured. He found that actuator compliance occurs because of rotation of the loading system including stanchions, ball races, guiding plate and carriage along a point at the center of carriage. To get the correct displacement at the pipe level, Daiyan (2013) established an equation based on the in-air test a result which is given below:

$$\text{Eq. 4-1} \quad d_{\text{pipe}} = d_{\text{actuator}} - 1.5(d_{\text{actuator}} - d_{\text{dogbone}})$$

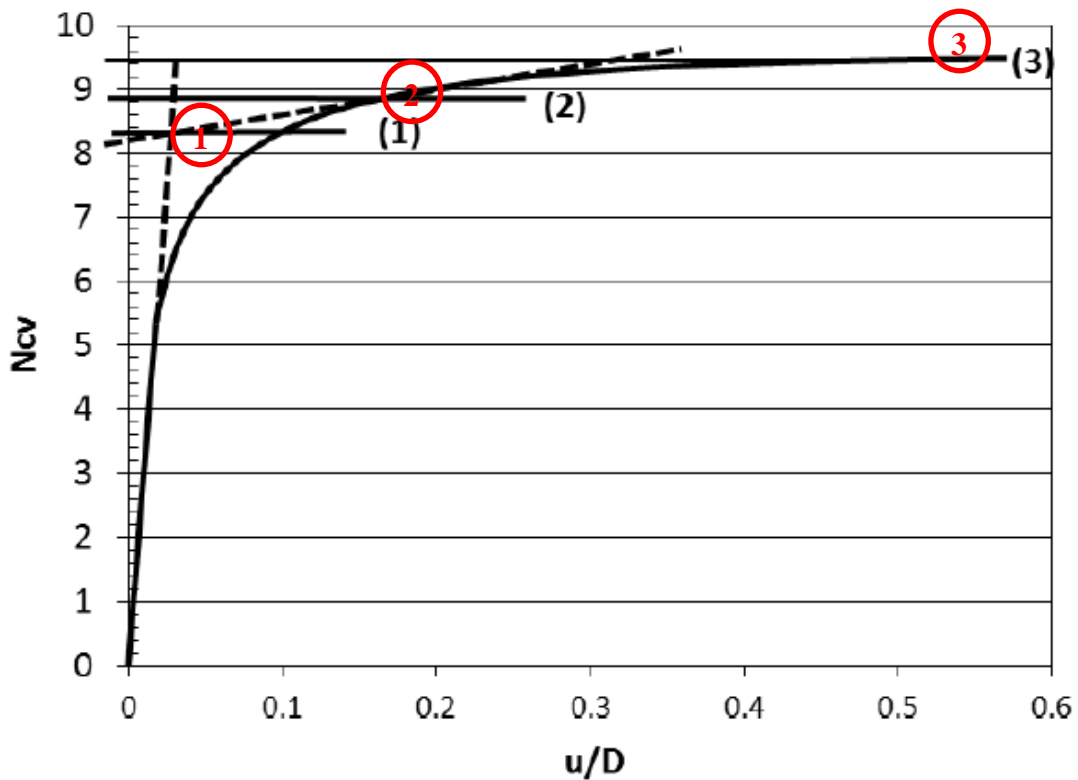


**Figure 4-1: Schematic illustration of how the peak force was defined to define ultimate load (after Pike et al., 2011).**

#### 4.2.1 PURE AXIAL TEST

The result of the purely axial test (TDO) is presented in Figure 4-2 in actual force ( $T_u$ ) and Figure 4-3 in normalized form. The normalized force ( $N_t$ ) in the vertical axis of Figure 4-3 represents  $T_u/\gamma D H L$  where  $\gamma$  is the dry unit weight of soil,  $H$  is the burial depth to pipe springline,  $L$  is the length of the pipe section and  $D$  is diameter (Equation 2-3) which presents in the vertical axis; and the normalized axial displacement ( $u/D$ ) is defined by the mobilized soil displacement divided by the pipe diameter which presents in horizontal axis. Maximum normalized axial force ( $N_t$ ) and normalized yield displacement ( $Y$ ) are

selected at the peak normalized force of the normalized force–displacement curve. Figure 4-3 shows that, in test TD0,  $N_t$  increases to a peak value of 2.6 at a normalized yield displacement of 0.5 (23 mm at model scale, see Figure 4-2) and then decrease with further displacement. The peak force is considered as “yield force” and the displacement required to mobilize it is denoted as “yield displacement”. As shown in Figure 4-4, the peak value of  $N_t$  obtained from this test is comparable with other studies (e.g. Schaminee et al. 1990) and current guidelines (ALA, 2005).

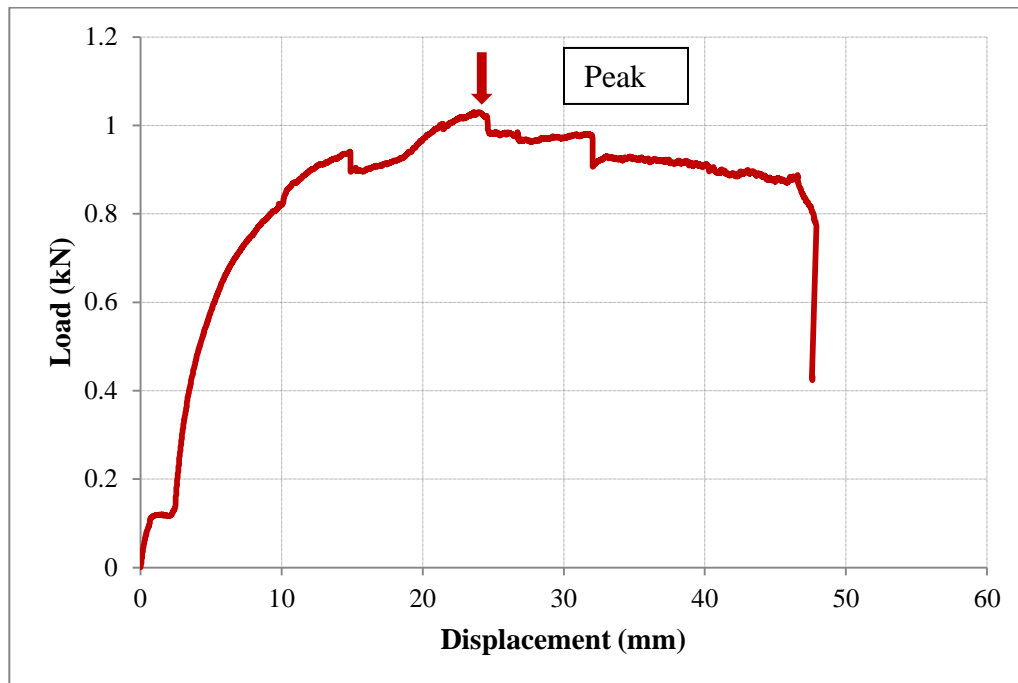


**Figure 4-2: Load–displacement relationship for test TD0**

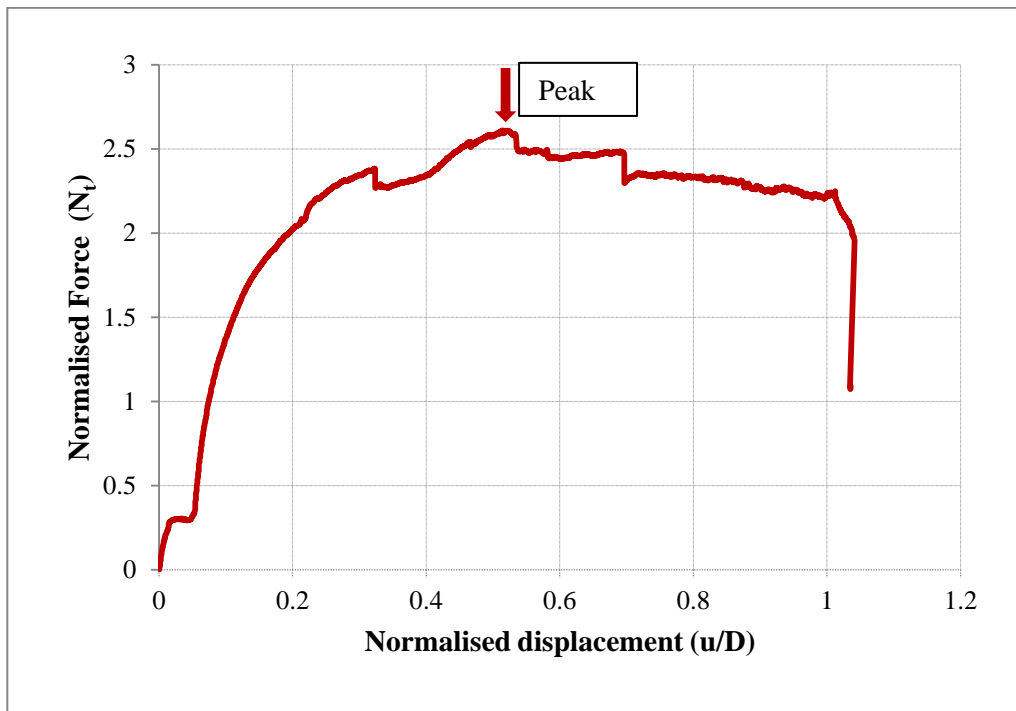


**Figure 4-3: Normalized load–displacement relationship for test TD0.**

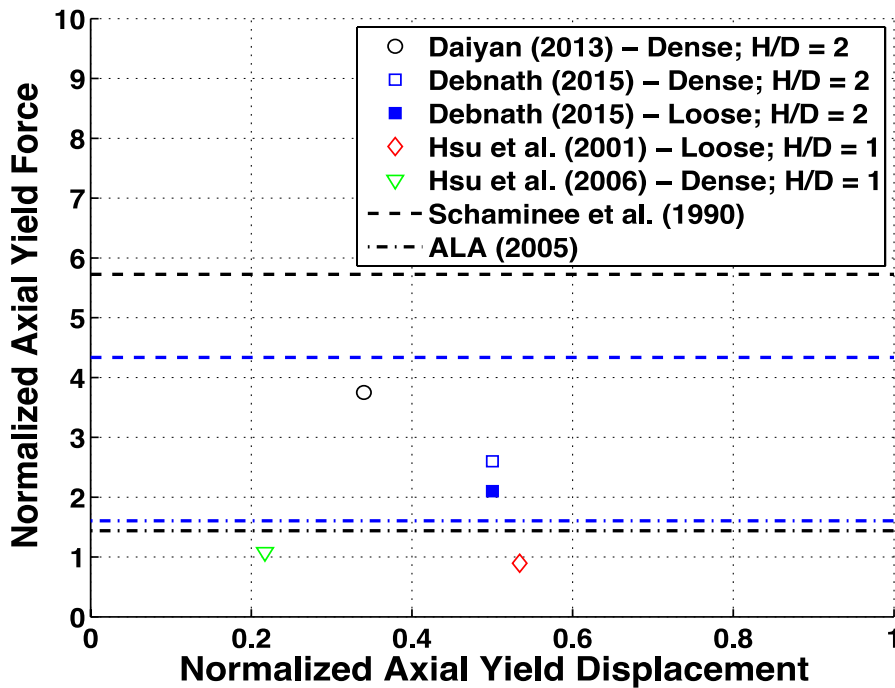


**Figure 4-4: Comparing the normalized axial force for axial pipe–soil interaction with some other test results**

Figure 4-4 shows that the measured yield force of this test and Daiyan (2013) is greater than ALA (2005) guidelines by a factor of 1.6 and 2.6, respectively, for this test as  $H/D = 2$ . In this calculation using ALA (2005), Equation 2-2 is used for the maximum axial force where  $K_0$  for dense sand is estimated using Equation 2-5 (Sherif et al. 1984) and a friction factor of 0.7 is used for smooth steel pipe (Table 2-1). Hsu et al. (2006) reported the normalized axial yield force less than 1.0 for dense sand (peak friction angle of  $42^\circ$ ) across a range of  $H/D = 1, 2, 3$  from a series of full-scale tests, in other word, the yield force of Hsu et al. (2006) is lower than the ALA (2005) guidelines and centrifuge tests. The experimental setup, instrumentation and test procedure in these centrifuge test programs and full-scale tests (Hsu et al. 2006) are similar. Hsu et al. (2001 & 2006) used

a rigid blanking plate on the end pipe segment where in these centrifuge tests, compliant foam blocks are used on the leading face of the stanchions which reduces end-bearing loads effects and thereby mitigate soil deformations and failure processes on the leading face. Differences in test results may be attributed to boundary conditions, pipe self-weight and local failure mechanisms.

Karimian (2006) conducted full-scale axial pull-out test in loose sand and showed that the axial yield resistance obtained from physical modeling is consistent with the ALA (2005). However, for the dense sand condition, the measured axial yield force is 2 to 3 times greater than the ALA (2005) guidelines. The author argued that the difference might be attributed to the increased normal stress with loading that significantly influences the localized shear failure of soil around the pipeline under some *constrained dilation* (see Figure 2-3). It has also been suggested that the conventional earth pressure co-efficient “at rest” ( $K_0$ ), as defined in Equation 2-2, may not adequately represent the stress condition and failure mechanisms for dense sand conditions. Therefore, instead of  $K_0$  an equivalent lateral earth pressure co-efficient ( $K > K_0$ ) in the range of 1.0 to 2.25 has been recommended for the shear zone of about 1.0 mm thickness around the circumference of the pipeline to calculate axial resistance (Wijewickreme et al. 2009). They also showed good agreement between measured axial resistance and calculated values with this equivalent earth pressure coefficient. Following Wijewickreme et al. (2009), if  $K=1.6$  is used, instead of  $K_0$ , the peak axial resistance can be obtained using Equation 2-2 (Figure 4-5). Similarly,  $K=2.6$  gives comparable peak value of Daiyan (2013). In summary, centrifuge test results are consistent with full-scale test results—both gave higher axial

resistance as compared to ALA guidelines—which could be estimated using an equivalent earth pressure coefficient.

It is also noted here that a slight change in direction from axial direction could increase the axial resistance as discussed in the following sections. Moreover, higher values obtained by Daiyan (2013) might be due to heavy weight of the pipe as compared to present study.

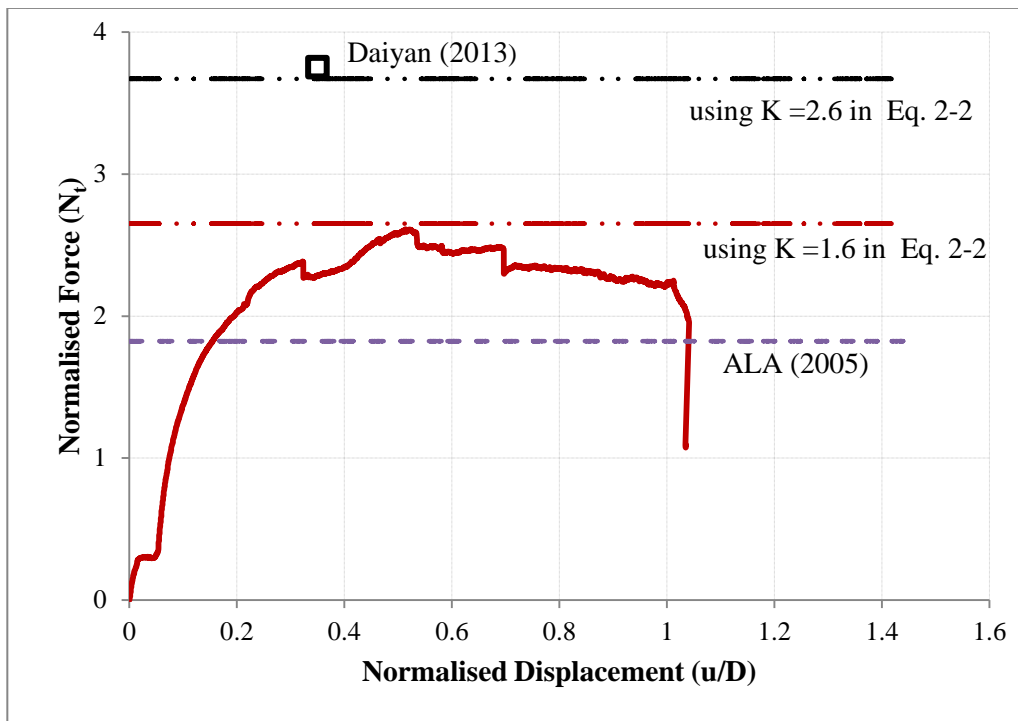


**Figure 4-5: Comparison of the axial test results (TD0) with ALA (2005) and Karimian (2006)**

The yield displacement ( $0.5D$ ) of this centrifuge test (Figure 4-3) and for Daiyan's (2013) physical test result are much greater than ALA (2005) and the results of Karimian (2006) full-scale tests, which are on the order of millimeters (i.e.,  $0.005D$  to  $0.01D$ ). This may

due to the test set up, end bearing effects and boundary conditions in the centrifuge test. Daiyan et al. (2011) demonstrated the axial load–displacement response becomes moderated at low oblique attack angles through numerical simulation, which can be associated with misalignment of the test frame, where the peak load occurs at greater mobilization distance. It is also noted here that Palmer et al. (2003) recognized that the centrifuge model could simulate the peak uplift resistance; however, the centrifuge gives higher mobilization distance as compared to full-scale test. As the test setup and loading condition in centrifuge and full-scale tests (Karimian 2006) are different, it is difficult to conclude whether the higher mobilization distance in the present centrifuge modeling is due to the limitation of centrifuge modeling as Palmer et al. (2003) suggested in uplift tests or it resulted from test setup. Further studies are required to address this issue.

#### **4.2.2 PURE LATERAL TEST**

The result of the pure lateral test (TD90) is presented in Figures 4-6 and 4-7. Figure 4-7 shows the measured normalized values where the normalized lateral force in the vertical axis is defined as the lateral force per unit length divided by the dry soil unit weight ( $\gamma$ ), the burial depth to pipe spingline ( $H_s$ ) and pipe diameter ( $D$ ) (Equation 2-13). The horizontal axis shows the normalized lateral displacement ( $u/D$ ). The maximum normalized lateral force ( $N_h$ ) and normalized yield displacement ( $Y$ ) represent the values at the peak normalized force of the force–displacement curve. The force–displacement curve for the test TD90 (Figure 4-6) shows an increase in force with displacement. After

50mm displacement, the gradient of the curve decreases. Figure 4-7 shows no clear peak and therefore the Method (1) and Method (2) as discussed Figure 4-1 are used to determine the peak load. In Method (1), the tangent at the steepest segment is drawn neglecting the initial flat segment of the force–displacement curve as shown in Figure 4-7. The Method (3) in Figure 4-1 is not applicable here because the force–displacement curve does not become horizontal. The vertical arrows in Figure 4-7 show the estimated normalized peak loads.

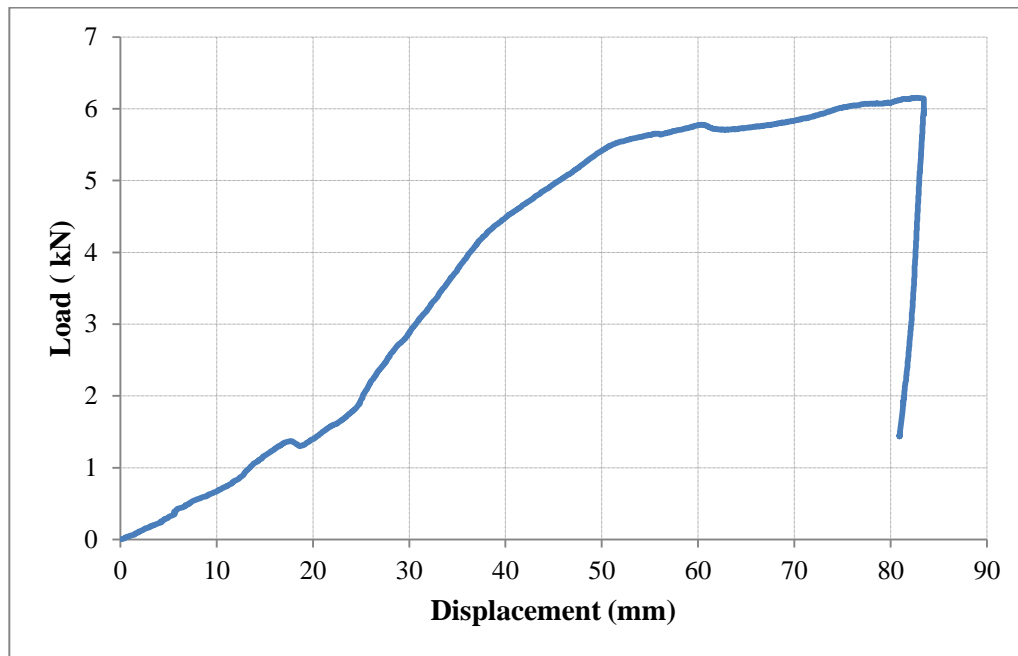


**Figure 4-6: Load–displacement relationship for pure lateral test (TD90).**

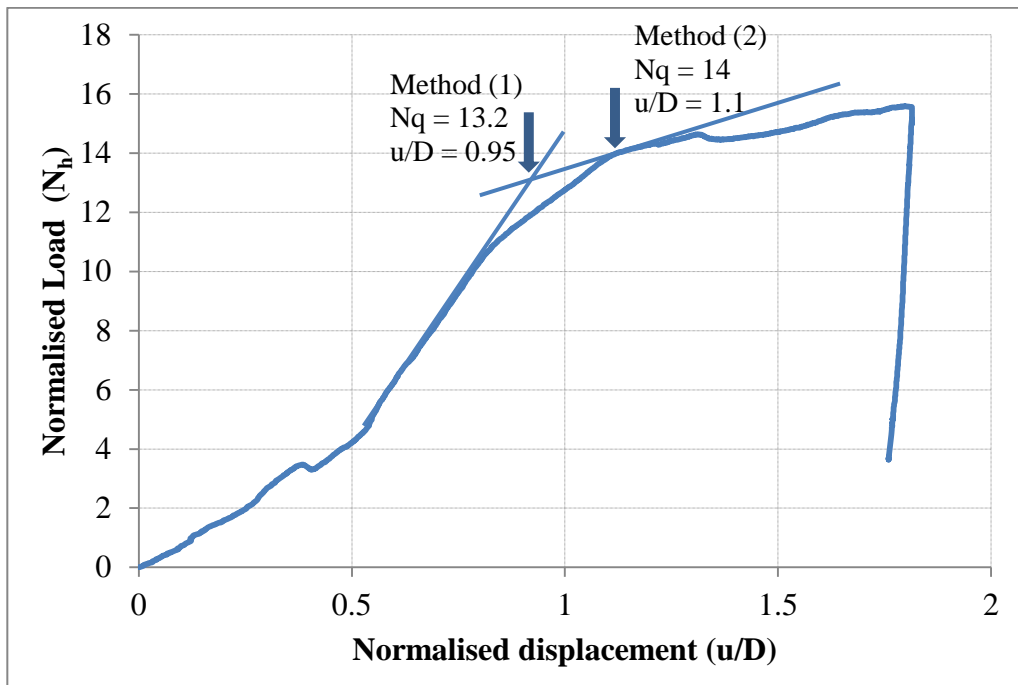


**Figure 4-7: Normalized load–displacement relationship for pure lateral test (TD90).**

The measured normalized lateral force of this test is 13.2 and 14.0 for Method (1) and Method (2), respectively which are lower than PRCI (2004) and ALA (2005) guidelines by a factor of 0.61 and 0.65 respectively as shown in Figure 4-8. ALA (2005) guideline defines the maximum lateral force by Equation 2-13 as discussed in Chapter 2. Guo and Stoll (2005) conducted a numerical study to assess the effects of burial depth, overburden ratio, soil dilatancy, strain hardening and scale effect (ratio between pipe diameters with respect to reference pipe diameter) on the peak load and ultimate displacement. Accounting these scale and burial effects, Guo and Stoll (2005) proposed the following empirical equation.

$$\text{Eq. 4-2} \quad N_h = k \left(\frac{H}{D}\right)^m \left(\frac{D_{ref}}{D}\right)^n$$

where  $D_{ref}=1$  m,  $k=6$ ,  $m=0.35$  and  $n=0.2-0.25$ .

The estimated normalized lateral forces, using Equation 4-2, are much lower than the ALA (2005) guidelines by factor of 0.4, which are also less than the observed test result. Also the measured normalized lateral force is very close to the Audibert and Nyman (1977) test result for the friction angle of  $40^\circ$  (see Figure 4-8).

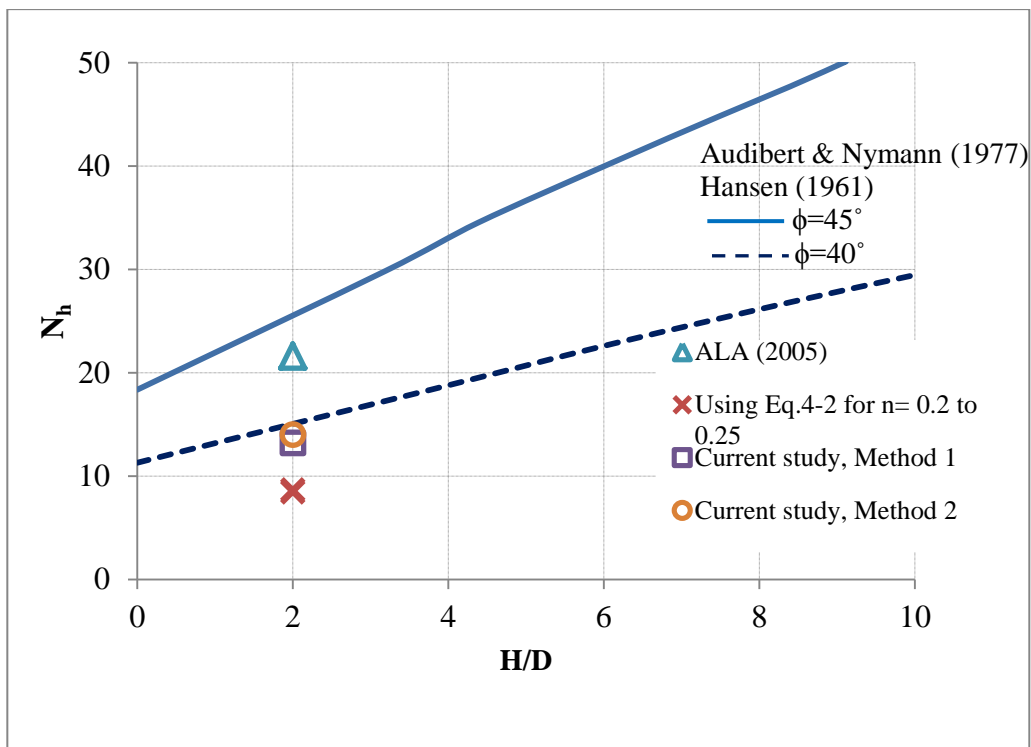


**Figure 4-8: Comparison of the test results with Audibert and Nyman (1977) and Guo and Stoll (2005).**

The normalized lateral force versus H/D ratio is presented in Figure 4-9. For comparison, physical model test results available in the literature are also plotted in this figure (e.g., Audibert and Nyman, 1977; Trautmann and O'Rourke, 1983; Turner, 2004; Karimian,

2005; Calvetti, 2004 and Daiyan, 2013). The discrepancy between the results might be the result of soil strength parameters, pipe diameter and H/D ratio as shown in the legend of Figure 4-9. The normalized lateral resistance increases with increasing soil strength (e.g., friction angle) and H/D. For the dense sand conditions presented in Figure 4-9, the normalized lateral load decreases with increasing diameter. This was attributed to scale effects for small diameter pipe at shallow burial depth (i.e., Guo and Stolle, 2005) and discussed in the conference paper (Kenny et al., 2015) presented in Appendix C.

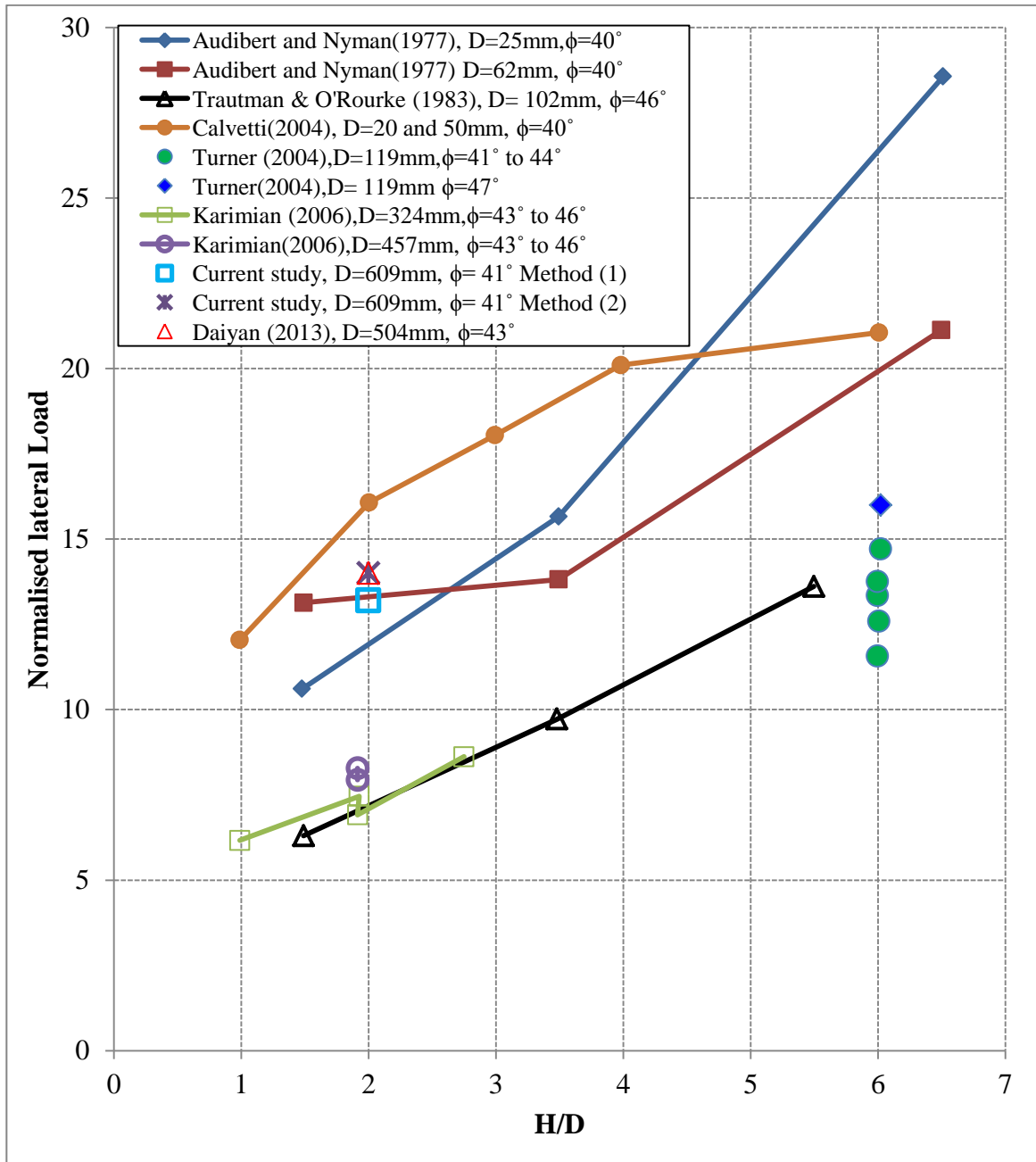


**Figure 4-9: Comparison of the normalized peak loads with several published test results.**

A wide variation is observed in  $N_h$  depending on soil properties (i.e., soil density, friction angle) and H/D ratios (Figure 4-9). Although there are many factors, for the same peak friction angle,  $N_h$  tends to increase with the decrease of pipe diameter and H/D ratio. On the other hand, for the same pipe diameter,  $N_h$  increases with the soil friction angle along the same H/D ratio. However, it is not clear how  $N_h$  changes due to combined effects of soil friction angle, pipe diameter and H/D ratios.

It is recognized that the normalized load increased with the soil friction angle and burial depth ratio (e.g., Trautmann and O'Rourke, 1985). The pipe is buried at shallow depth and therefore the behavior of the soil at low stress levels needs to be considered. Roy et al. (2014, 2015) demonstrated the behavior of dense sand by investigating the failure mechanisms considering the stress-strain behavior of soil at low stresses using Abaqus/Explicit FE software. They successfully simulated the triaxial test results under low confining pressure and also the strain localization/shear bands during lateral movement of the pipe. With displacement of the pipe, plastic shear strain mainly accumulates in the shear band resulting in decrease of mobilized shear resistance (friction and dilation angle). They also showed that the mobilization of friction and dilation angle significantly influence the lateral resistance. It has been also recognized that both friction and dilation angles increases with decrease in confining pressure (Bolton 1986), which might be also cause of higher  $N_h$  at shallow burial depth. However, the measured  $N_h$  of this test is consistent with Daiyan (2013), Audibert and Nyman (1977) for H/D ratio of 2, which provides further confidence in the centrifuge test results.

The displacement at the peak lateral force of this centrifuge test is about  $0.95D$  and  $1.1D$  for Method (1) and Method (2) respectively, which is higher than ALA (2005) and PRCI (2004) guidelines. Trautmann (1983) reported this displacement within  $0.05D$  to  $0.075D$  from his large-scale test. Hsu et al. (2006) also shows this displacement is about  $0.25D$ . There are several causes that may result in this higher displacement including variation in test bed preparation and soil density around the pipe during pluviation. Also, Palmer et al. (2003) reported that there is a discrepancy between the full-scale test and centrifuge test for mobilized displacement, as discussed before for axial loading. They observed the mobilization distance does not scale properly, between reduced scale centrifuge and full-scale physical modelling tests, in their uplift modeling. Although it is difficult to conclude from one test, it could be also a potential cause of discrepancy of mobilization distance in centrifuge and full-scale tests for lateral loading.

The potential scale effects on the yield load and displacement to yield load for the lateral pipe–soil interaction is shown in Figure 4-10. The centrifuge test results reveals higher mobilization distance to peak load which may be related to the kinematics of soil failure mechanisms and formation of shear zones. Other factors that may influence this response include the soil particle shape, gradation and relative density.

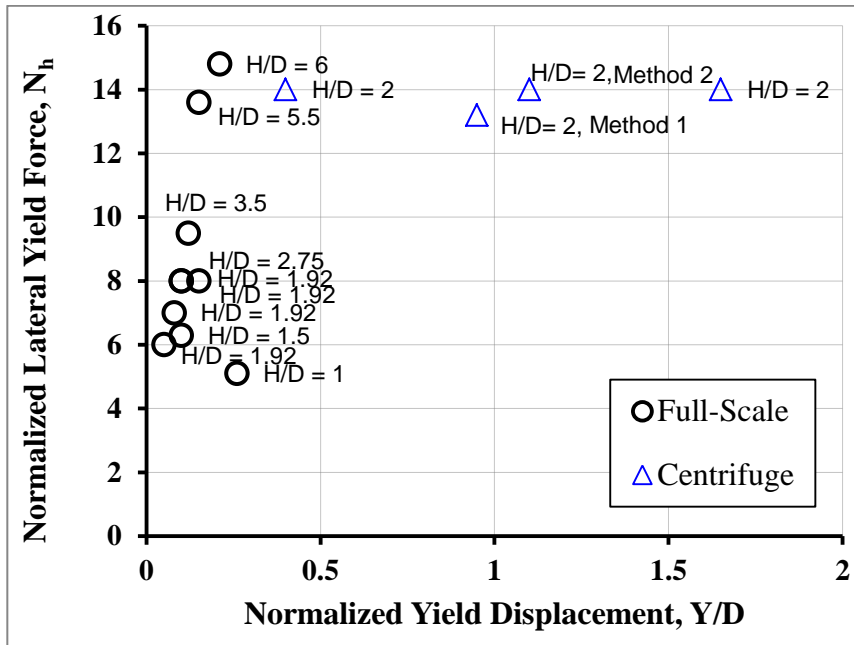


**Figure 4-10: Effects on normalized yield load and displacement for lateral pipe–soil interaction**

### 4.2.3 OBLIQUE ANGLE TESTS

The test results for oblique loading events TD70, TD50, TD40, and TD20 are shown in Figure 4-11 to 4-14 in terms of normalized force–displacement curves for the attack angles of 70°, 50°, 40° and 20°, respectively. For tests TD70 and TD20, the force–displacement curve (Figure 4-11 and 4-14) does not exhibit any local maximum where Method (1) and Method (2), as shown in Figure 4-1, are used to determine the peak load. The vertical arrows identify the peak load estimate, based on the method used, for each normalized force–displacement curve.

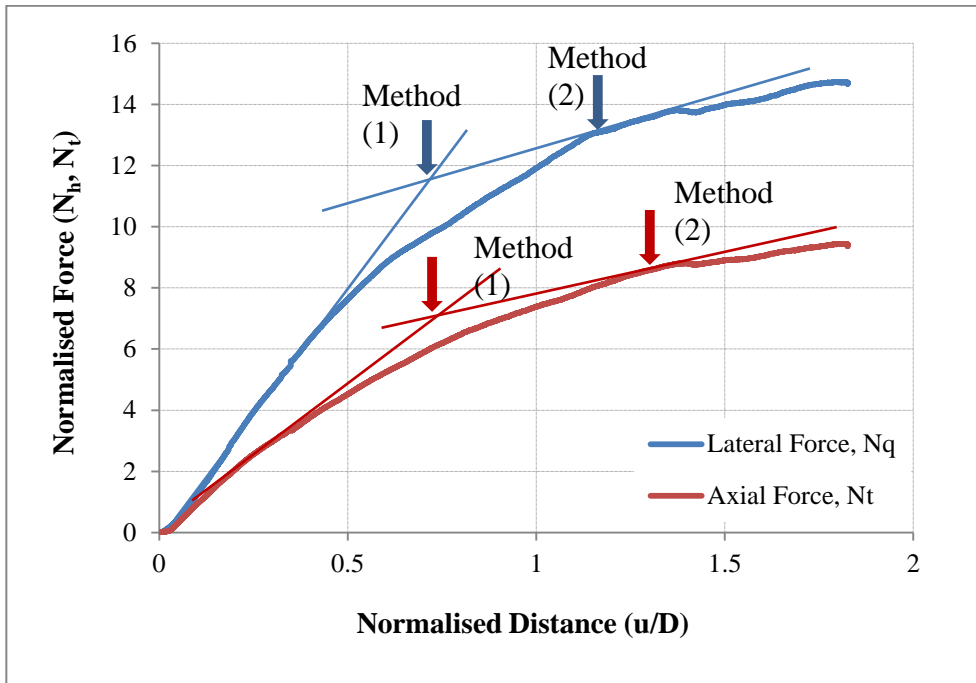


Figure 4-11: Normalized load–displacement relationship for oblique angle test (TD70).

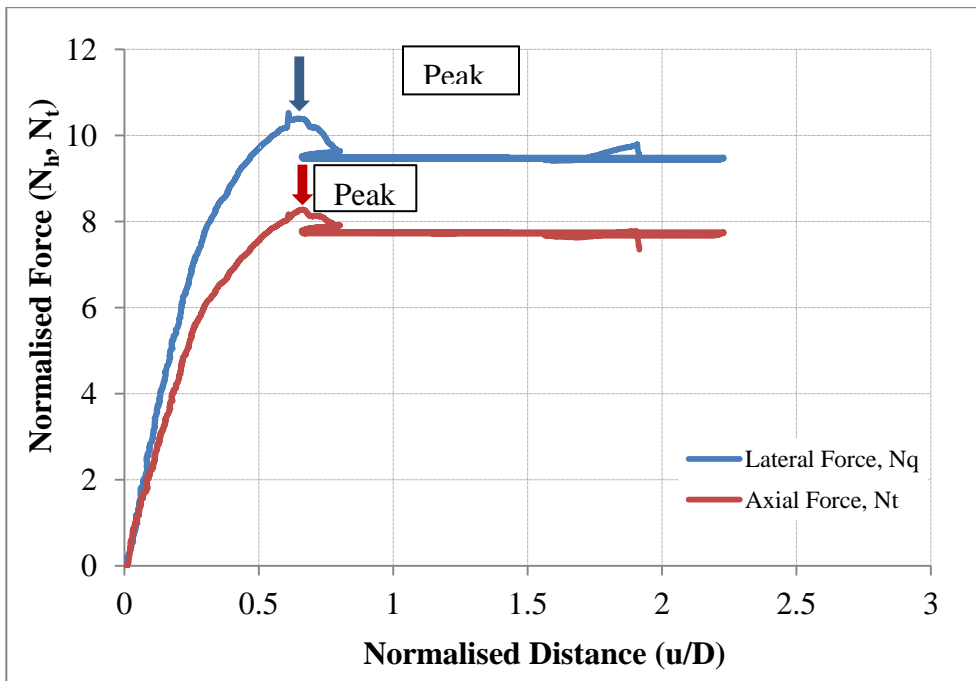


Figure 4-12: Normalized load–displacement relationship for oblique angle test (TD50).

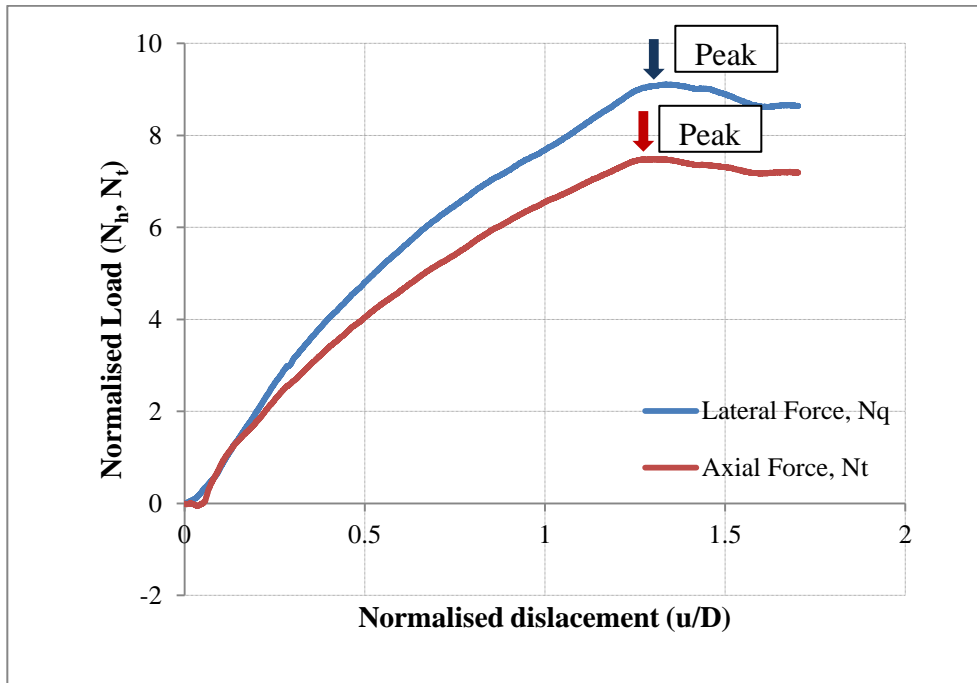


Figure 4-13: Normalized load–displacement relationship for oblique angle test (TD40).

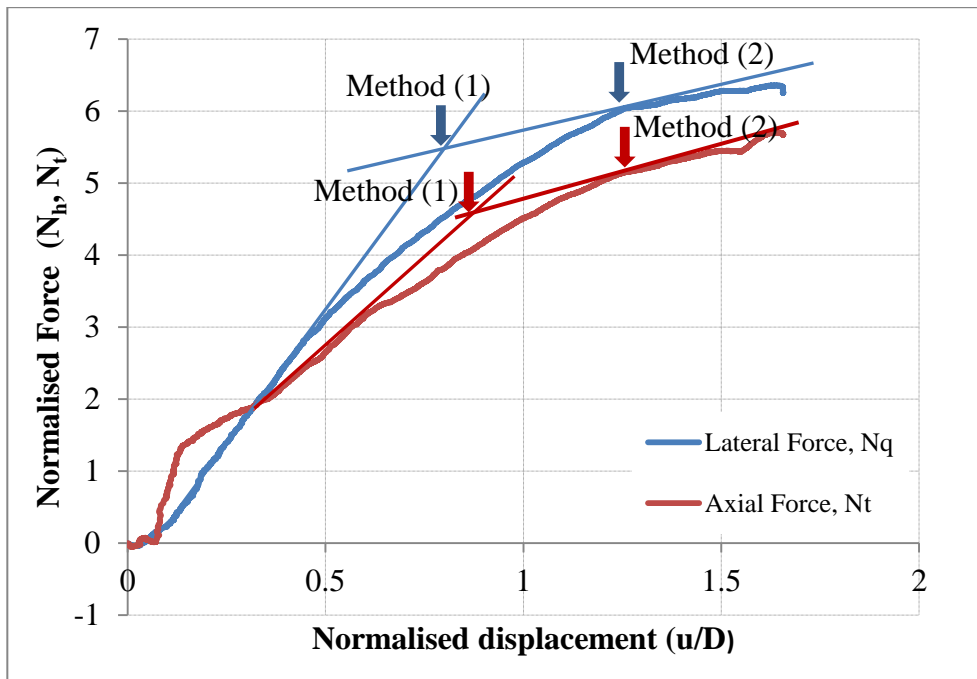
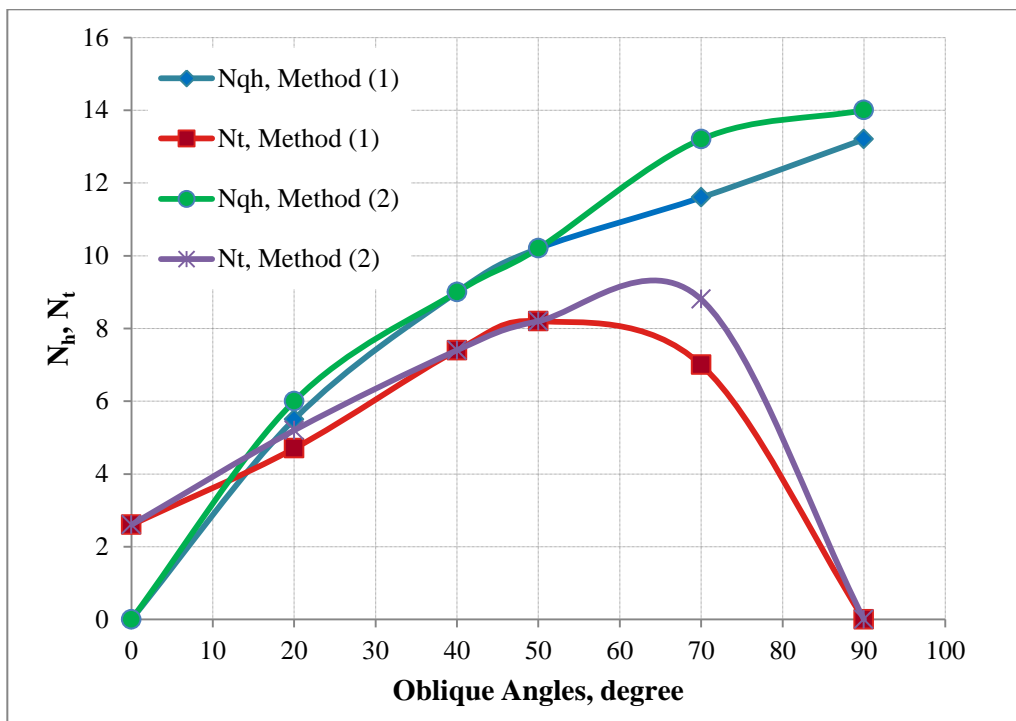


Figure 4-14: Normalized load–displacement relationship for oblique angle test (TD20).

Though synthesis of the oblique angle test results, it is observed the axial and lateral interaction factors vary with the oblique attack angles as shown in Figure 4-15. The normalized lateral load ( $N_h$ ) increases from zero load condition associated with pure axial motion with increasing attack angles whereas the normalized axial load ( $N_t$ ) has an initial offset due to axial restraint that increases with the attack angles until a peak load is reached and then reduces. The angle of attack associated with a change in the failure mechanism is influenced by the method used to estimate the peak load, which is also related to soil deformation, kinematics and failure mechanisms. This is illustrated in Figure 4-15, where the transition from axial to lateral bearing failure mechanisms, associated with decreasing axial forces, may occur between  $50^\circ$  and  $70^\circ$  depending on which method is used to estimate the normalized axial force for the oblique load test.



**Figure 4-15: Variation of axial and lateral interaction factor using Method (1) and Method (2).**

Here, it is also noted that the normalized force–displacement curves of test TD20 and TD70 doesn't have the discrete peaks as the oblique angle of attack for  $20^\circ$  and  $70^\circ$  tends to pure axial and pure lateral respectively. For the  $20^\circ$  oblique angle test, initially it acts like an axially loaded pile as the axial load rapidly increases within a very small displacement is which shown in Figure 4-14. Considering the load ratio (axial/lateral) aspects, the  $20^\circ$  oblique angle test has the higher load ratio (axial/lateral) within the first 10 mm pipe displacement which supports this rapidly increased axial load behavior whereas the  $70^\circ$  oblique angle test has lower the load ratio for large pipe displacement. It is also evident from figures 4-11 to 4-14 that the ratio of axial to lateral normalized force tends to a constant ratio for large pipe displacement.

In this study, the failure surface in front of the pipe was also examined during the oblique angle test (TD50) using very thin layers, approximately 2 mm thickness of colored sand. As shown in Figure 4-16, a passive wedge, formed in front of the pipe, and heave surface parallel to the pipe movement can be identified, which are observations consistent with those presented by Daiyan (2013).

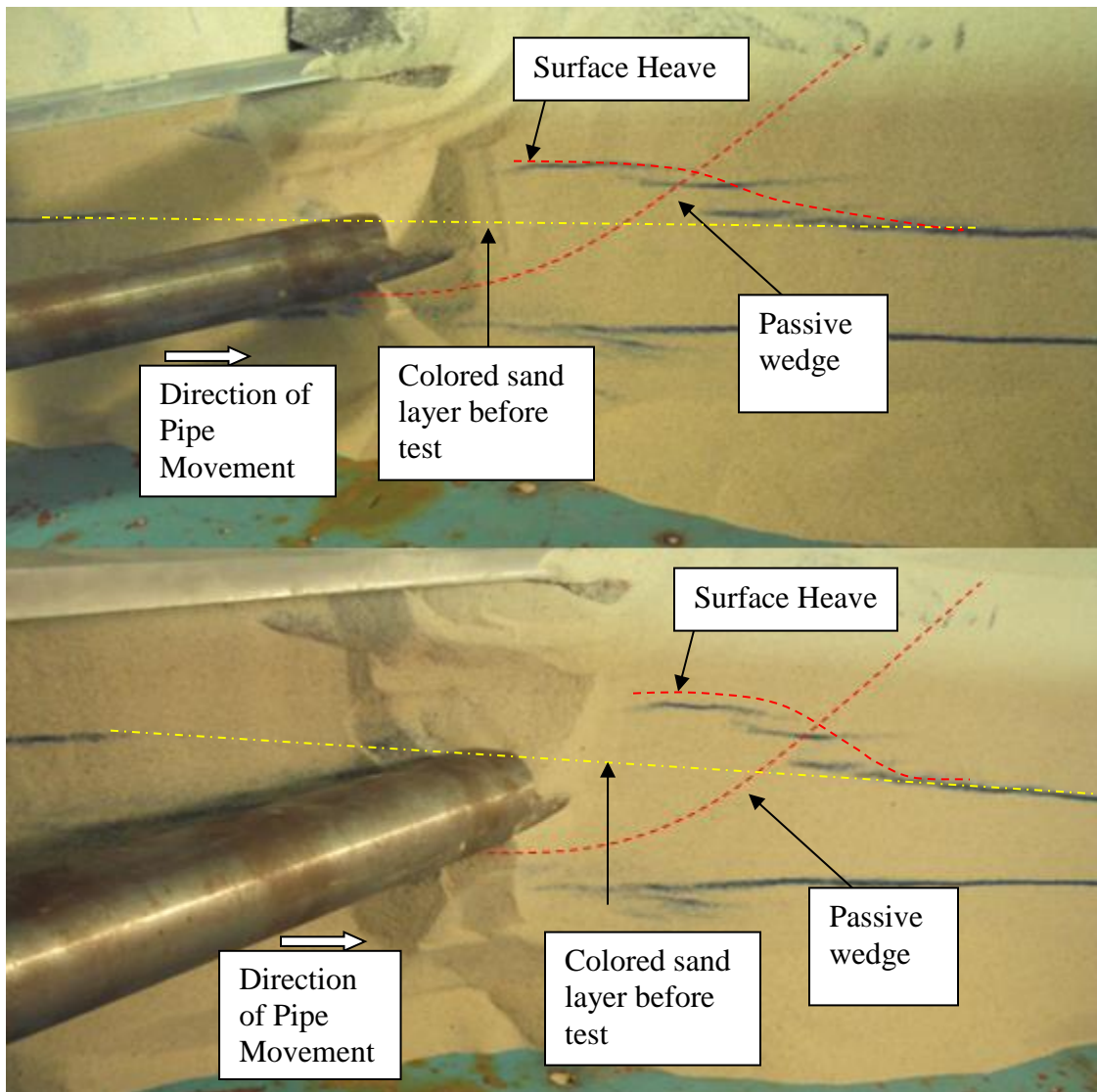


**Figure 4-16: Deformed colored soil layers for the oblique loading test (TD50) after centrifuge test.**

Using the data presented in Figure 4-15, a failure or yield load envelop can be constructed (Figure 4-17) and compared with the test results from other recent centrifuge (Daiyan 2013) and full-scale (Hsu et al., 2006) oblique pipe–soil interaction events. The failure envelope illustrates the coupling between the normalized axial and lateral interaction

forces that are dependent on the relative oblique attack angle. This is supported by the data presented in Figure 4-15 where the normalized lateral load ( $N_h$ ) increases from zero load condition, associated with pure axial motion (i.e.,  $0^\circ$ ), with increasing attack angle, whereas the corresponding normalized axial load ( $N_t$ ) has an initial offset, due to pure axial motion, that increases with the attack angle and subsequently reduces when the interaction event is dominated by lateral motion (i.e.,  $90^\circ$ ).

The coupled load interaction, as illustrated by the yield envelope, is associated with two failure mechanisms. At low oblique angles, the soil failure is controlled by shear strength and friction along the pipe–soil interface. This failure mechanism is associated with the increased effective axial force with increasing oblique angle, which has also been observed in numerical modeling studies for cohesive (Phillips et al., 2004a; Pike and Kenny, 2012a, b) and non-cohesive soil (Daiyan, 2013; Daiyan et al., 2011, 2010). As the attack angle increases, the axial-lateral interaction coupling effects are moderated where the failure mechanism is governed by the shear failure through the soil mass associated with lateral bearing action. Through a numerical modeling parameter study, Daiyan (2013) developed a family of yield envelopes dependent on soil peak friction angle, pipe–soil interface friction angle and pipe springline burial depth to diameter ratio ( $H/D$ ). There was agreement between the numerical simulations and centrifuge data with respect to yield load estimates, envelop characteristics and failure mechanisms. The load coupling is also supported by results from other numerical modeling (e.g., C-Core 2008; Phillips et al., 2004a; Pike and Kenny, 2012a, b). Differences in the normalized loads and failure envelopes between the centrifuge test results by Daiyan (2013) and this study, may in

part, be attributed to the heavier pipe used in the previous modeling studies by Daiyan (2013).

Depending on the method used to estimate the peak load, as described in Figure 4-1, the transition point between linear and non-linear portion of the failure surface changes. Using Method (1), the transition of the failure surface occurred at an oblique angle of about  $50^\circ$ , whereas using Method (2) the transition occurred in between  $60^\circ$  to  $70^\circ$ . The ordinate (i.e., pure bearing) and abscissa (i.e., pure axial) intercepts were not sensitive to the method selected. The influence of the methodology to determine the peak load and mobilization distance to peak load was not addressed in the previous study by Daiyan (2013).

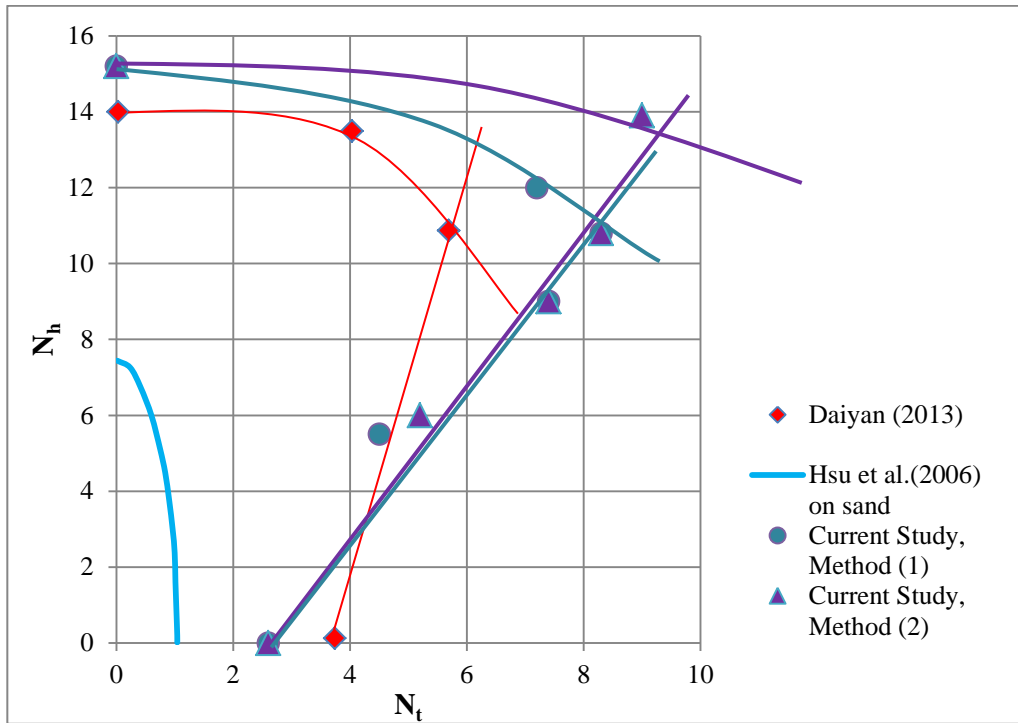


**Figure 4-17: Axial-lateral interaction curve for dense sand.**

### 4.3 SUMMARY OF THE CHAPTER

A series of centrifuge tests were conducted in dense sand, which includes axial, lateral and oblique angle tests for 20°, 40°, 50° and 70°, mostly examining peak load, yield displacement at peak load and scale effect on displacement, the failure envelop characterizing the load coupling, failure mechanisms and compared the test results with available experimental data and analytical expressions. Some of the key findings are summarized below:

- 1) The measured normalized axial force of this test is greater than ALA (2005) guidelines by a factor of 1.6. Karimian (2006) recommended the equivalent lateral earth pressure co-efficient would be in the range of 1.0 to 2.25 for the centrifuge test parameters to estimate the axial resistances in Equation 2-2 instead of using  $K_o$ . Using Equation 2-2 with the equivalent lateral earth pressure co-efficient of 1.6, the estimated value matches with the peak axial yield force of this centrifuge test. So it is very important to use proper lateral stress coefficient to get axial load which should be considered to improve design guidelines of pipe–soil interaction problems.
  
- 2) The measured normalized lateral force is lower than PRCI (2004) and ALA (2005) guidelines, but higher than other studies. The soil constitutive behavior was investigated at low confining stress of a buried a pipe subjected to lateral movement by Roy et al. (2014, 2015) which support the centrifuge test results of this study. Also the measured result of this test is consistent with Daiyan (2013) and Audibert and Nyman (1977) test results for H/D ratio of 2 which exits enough confidence in this centrifuge tests.
  
- 3) There is a potential scale effect observed in centrifuge test results with respect to mobilization distance to yield as observed by Palmer et al. (2003) for the vertical mobilization distance. The centrifuge test results exhibits higher mobilization distance to peak load that may be related to kinematics, soil failure mechanisms and formation of shear zones.

- 4) The interaction factor changes with the oblique attack angles (Figure 4-15) where the normalized lateral load ( $N_h$ ) increases from zero load condition and the normalized axial load ( $N_l$ ) has an initial offset due to axial restraint that increases with the attack angles until a peak load is reached and then reduces.
- 5) During failure, there is a passive wedge formed in front of the pipe where a surface heave is identified parallel to the pipe movement according to the layered colored sand, which is consistent with Daiyan (2013).
- 6) The normalized axial and lateral interaction forces are coupled and dependent on the pipe–soil oblique attack angle (Figure 4-17). The coupled interaction is associated with two mechanisms characterized by the bounding surfaces of two yield envelope. At low oblique angles, the soil failure is controlled by shear strength and friction along the pipe–soil interface which represents the linear portion of the envelope and as the attack angle increases, the axial-lateral interaction coupling effects are moderated where the failure mechanism is governed by the shear failure through the soil mass which represents the non-linear portion of the envelope. This degree of coupling is supported by results from continuum finite element simulations (e.g., Daiyan, 2013; Daiyan et al., 2011; Phillips et al., 2004a; Pike and Kenny, 2012a, b; C-Core, 2008). Depending upon the method to estimate the peak load, the transition of failure surface changes from 50° oblique angle (using Method (1)) to in-between 60° and 70° oblique angle (using Method (2)).

## **5 AXIAL-LATERAL PIPE–SOIL INTERACTION IN LOOSE SAND**

### **5.1 INTRODUCTION**

This chapter describes the test results for pure axial, pure lateral and axial-lateral oblique angle loading of a buried pipe in loose sand test bed condition. There were 4 centrifuge tests conducted in loose sand with an average density of  $1467 \text{ kg/m}^3$  (see Table 3-4 for the test specific soil density), using a 46mm diameter model pipe (609 mm diameter prototype) with H/D of 2. The experimental test results in loose sand conditions are presented and discussed based on force–displacement behavior, failure envelope characterizing the coupled load effects, deformation pattern and failure mechanisms. The results are finally compared with previous analytical, numerical and experimental work as well as with the current recommended design guidelines to verify the test results and summarize the findings.

### **5.2 TEST RESULTS, ANALYSIS AND DISCUSSION**

All the test results are presented in terms of load–displacement relationships. Test TL90 and TL0 were performed for pure lateral and pure axial conditions whereas TL70 and TL40 were conducted for oblique angles of attack ( $70^\circ$  and  $40^\circ$ ) condition. The load–displacement curves are characterizes based on peak load and mobilization distance to peak load. All the tests were performed using the test setup as described for dense sand (Section 4.2) except test bed condition (i.e., soil density). The test results for TL70 and

TL40 are corrected for the displacement correction at the pipe level, as for the dense sand, according to Equation 4-1 as given in Chapter 4.

### **5.2.1 PURE AXIAL TEST**

The measured force–displacement relationship for the pure axial test (TL0) in the horizontal plane is presented in Figure 5-1. The normalized force–displacement response is shown in Figure 5-2, where the normalized axial displacement ( $u/D$ ) is the mobilized soil displacement divided by the pipe diameter and the normalized axial load is expressed in Equation 2-3. Using the methods described in Chapter 4, the maximum normalized axial force ( $N_t$ ) and normalized yield displacement ( $Y$ ) was established. For the axial load event (Test TL0), the peak normalized force was 2.1 with a normalized yield displacement of 0.48D (22 mm at model scale).

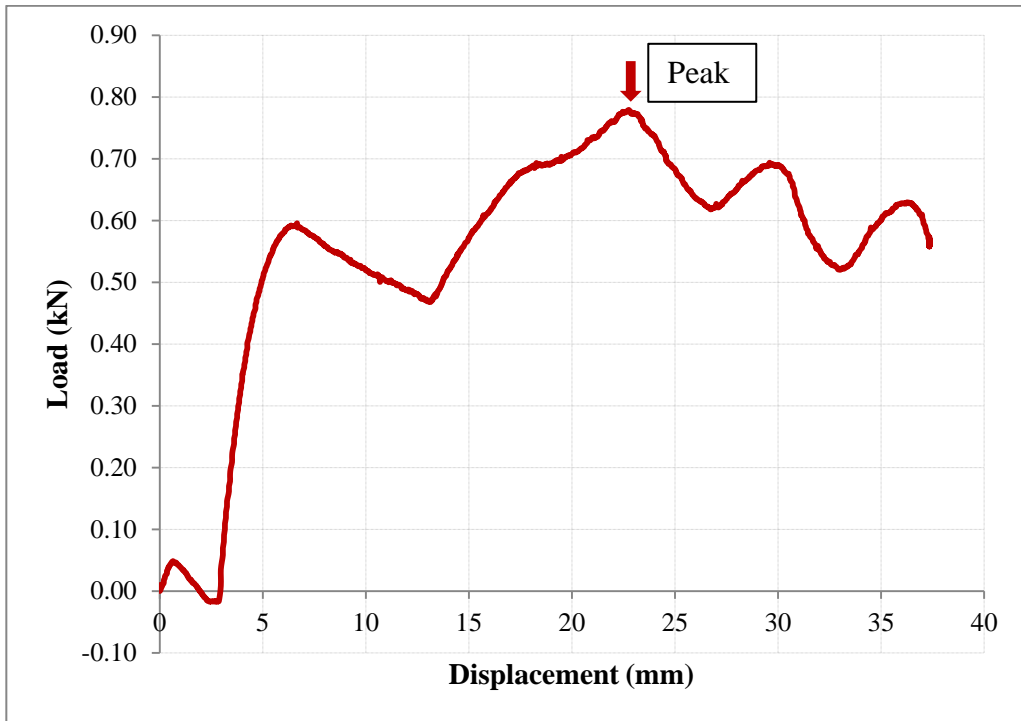


Figure 5-1: Load–displacement relationship for test TL0.

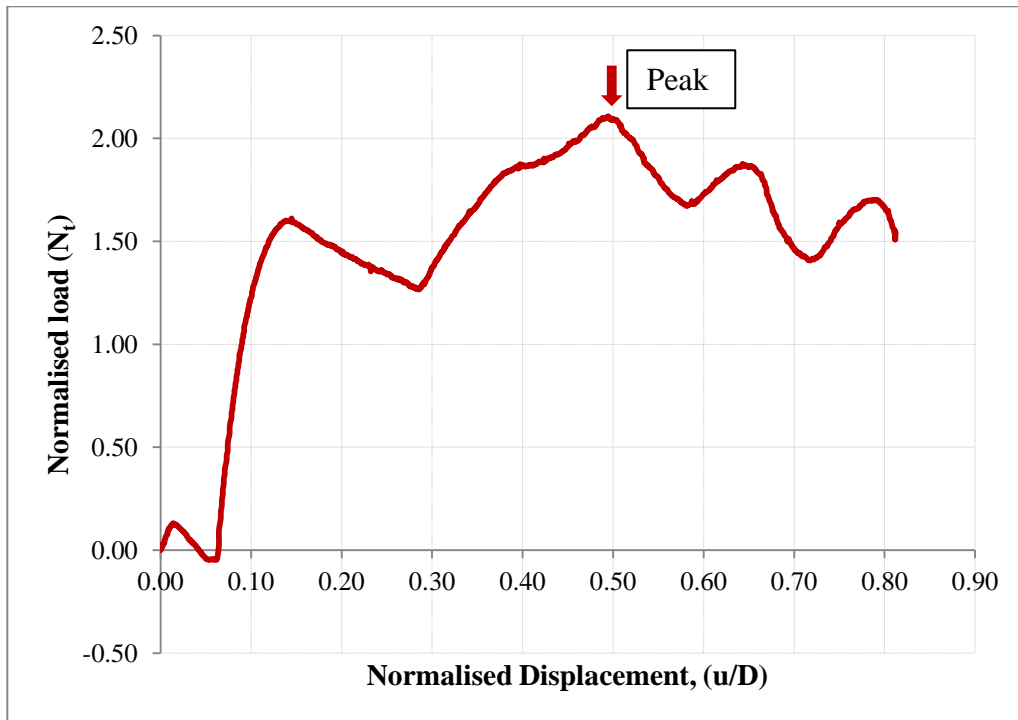


Figure 5-2: Normalized load–displacement relationship for test TL0.

From the load–displacement relationship, it was observed that, the axial load increased and then suddenly decreased within the small displacement and this pattern happened repeatedly with the displacement. As the pipe was in loose test bed conditions, and moved in the axial direction on the horizontal plane, the soil was getting compressed by the pipe which caused the increasing load. This compression occurs within a small region of the soil and when the pipe moves further that leads to the shear failure of soil and decreasing load with displacement. There might have been some variation in the test bed around the pipe as it is very difficult to maintain the same density all over the soil field especially near the pipe for loose conditions due to interaction effects between the soil particles and pipe during the free fall pluviation process. Also Wang et al. (2010) reported that a multiple shear surface is formed in front of the pipe (based on total shear strain evolution) within the very small displacement which propagates through the backfill soil medium during the pipe uplift movement in loose sand at H/D ratio of 2. Although, it is very difficult to conclude from this test, it could be also a potential cause for this pattern in the loose sand condition for axial loading. This behavior was also observed in pure axial test ( $0^\circ$ ) for dense condition (Figure 4-3) before the axial load reached to peak which was not as significant as in loose condition.

The measured normalized axial force exceeds the axial force estimate, as proposed by the ALA (2005) guidelines, by a factor of 1.6 for H/D of 2 as shown in Figure 5-3, which is similar to the observations in the dense sand tests (Section 4.2.1, Figure 4-4). For cohesionless, soil ALA (2005) guidelines defines the maximum axial force by Equation 2-2 as discussed in Chapter 2 where  $K_o$  is estimated for the loose sand test bed condition

using the expression presented by Jacky (1944), using Equation 2-4. A friction factor of 0.7 is used to represent the smooth steel surface of the model pipe. The importance of selecting the appropriate  $K_0$  value has been discussed in Chapter 2 and Chapter 4. Karimian (2006) defined an equivalent lateral earth pressure co-efficient used to estimate the axial resistance as defined by Equation 2-2 rather than using  $K_0$ . For the test parameters in this study, the equivalent lateral earth pressure coefficient would be in the range of 1.0 to 2.25. Using Equation 2-2 with an equivalent lateral earth pressure coefficient of 1.5, the estimated normalized axial load is in agreement with the measured peak axial yield force for the centrifuge test in loose sand.

For this testing program, the peak axial force for dense sand was 1.2 times greater than the loose sand test bed condition. In large scale axial pipe–soil interaction tests, Paulin et al. (1998) found that post-peak axial loads in dense sand were on average approximately 1.6 times greater than tests on loose sand.

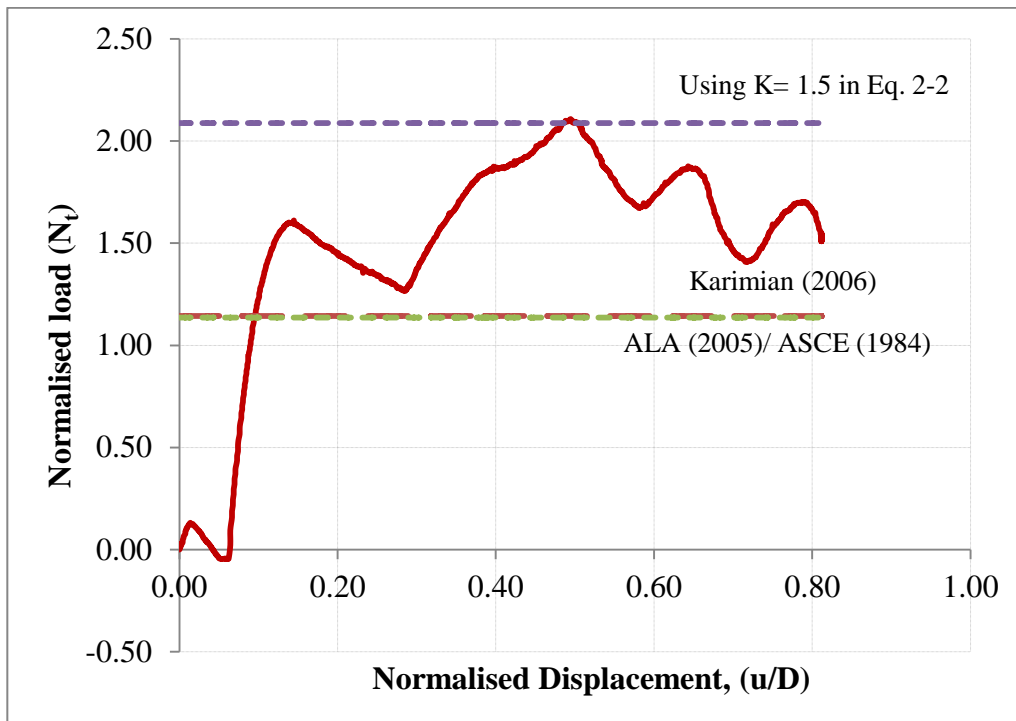


**Figure 5-3: Comparison of the axial test results (TL0) with ASCE (1984) and Karimian (2006).**

The normalized yield displacement ( $0.48D$ ) (22 mm at model scale) of this centrifuge test (see Figure 5-2) is greater than that estimates using ALA (2005), which is in the range from  $0.005D$  to  $0.01D$ . This may be due to end bearing effects as the pipe moves through the soil, and test preparation procedures where the soil density adjacent to the pipe may not be the same as the far field soil density due to interaction effects between the soil particles and pipe during the free fall pluviation process.

### 5.2.2 PURE LATERAL TEST

The force–displacement relationship for pure lateral test (TL90) in the horizontal plane is presented in Figure 5-4. In Figure 5-5 the corresponding normalized force–displacement relationship is illustrated where the normalized lateral displacement ( $u/D$ ) is defined by the mobilized soil displacement divided by the pipe diameter and the normalized lateral force is defined in Equation 2-13. The peak normalized force was 10.8 with a normalized yield displacement of 1D.

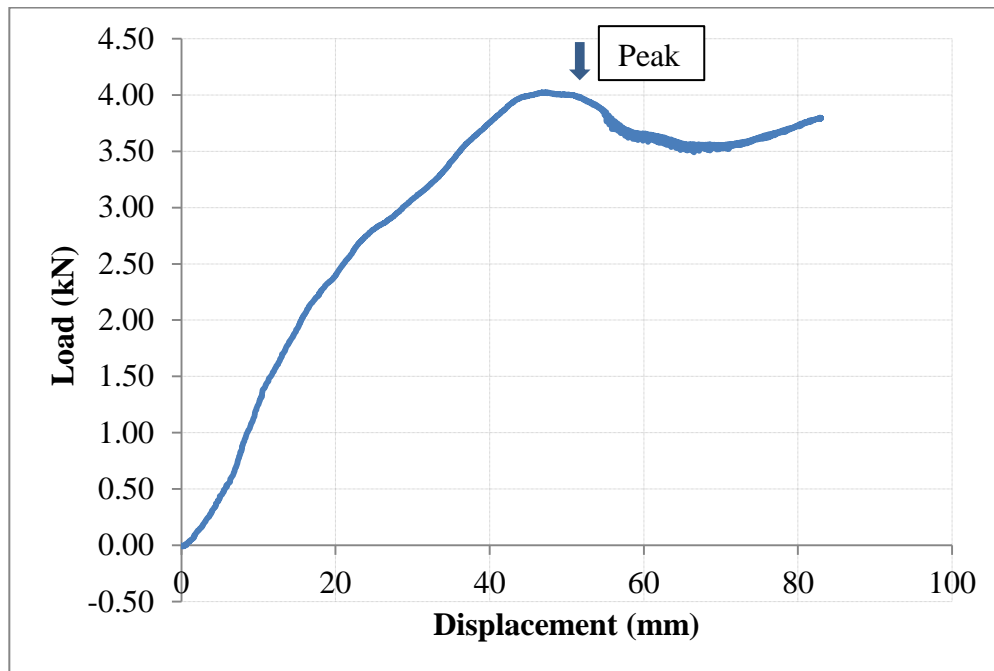


**Figure 5-4: Load–displacement relationship for pure lateral test (TL90).**

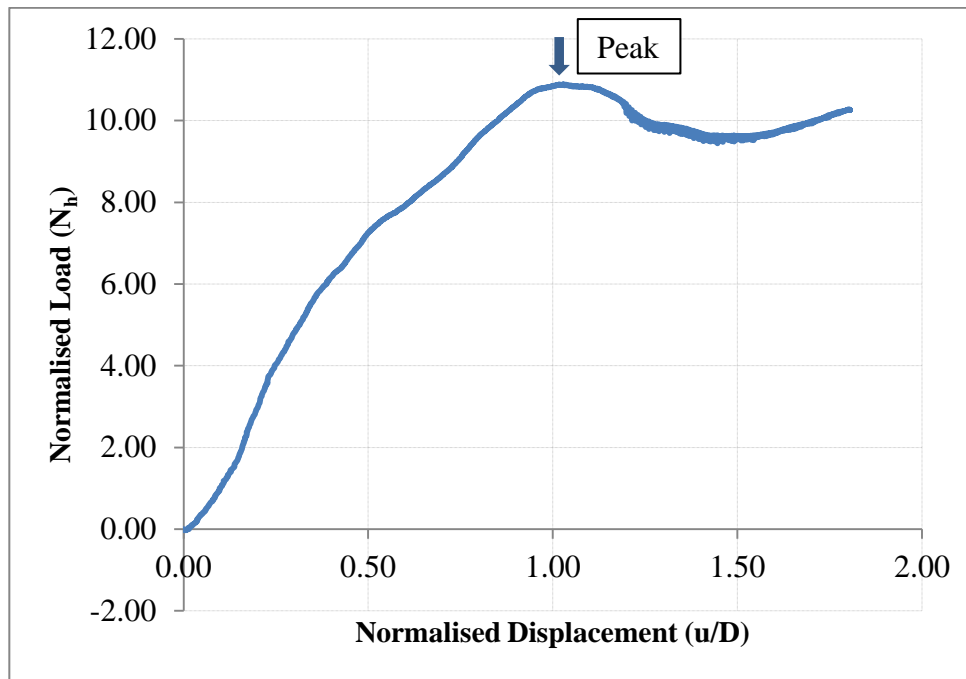


**Figure 5-5: Normalized load–displacement relationship for pure lateral test (TL90).**

ALA (2005) and PRCI (2004) guideline define the maximum lateral force based on an analytical model (Hansen, 1961) which is in agreement with the experimental study by Audibert and Nyman (1977) (Figure 2-6). As shown in Figure 5-6, the measured normalized lateral force, for  $H/D = 2$  and  $\phi = 35^\circ$ , is in agreement with Audibert & Nyman (1977) and Hansen (1961). Based on a numerical study, Guo and Stoll (2005) expressed an empirical relation (Equation 4-2) to assess the effects of burial depth, overburden ratio, soil dilatancy, strain hardening and scale effect (ratio between pipe diameters with respect to reference pipe diameter) on the peak load and ultimate displacement. Using Equation 4-2, the estimated normalized lateral forces are lower than the Audibert and Nyman (1977) results by factors over the range of 0.35 to 0.6, (see Figure 5-6).

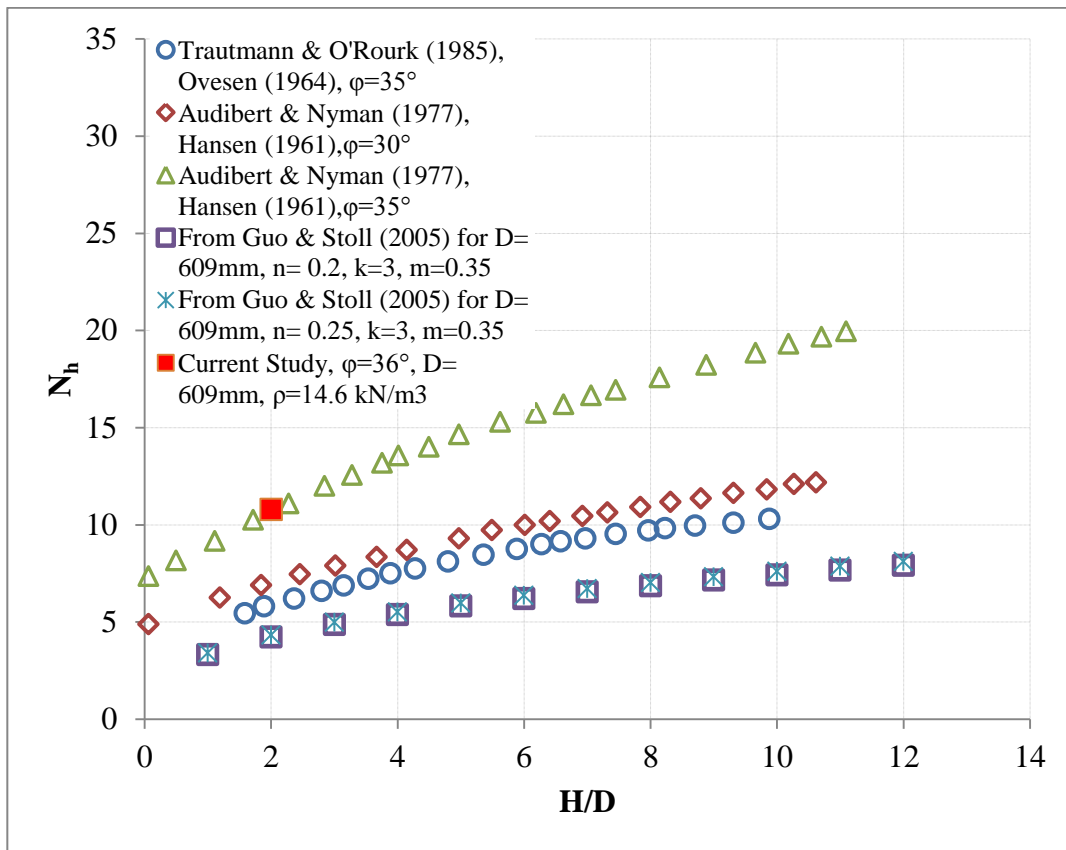


**Figure 5-6: Comparison of the test results for loose sand with Audibert and Nyman (1977) and Guo and Stoll (2005).**

The normalized lateral force as a function of H/D determined in this study is compared with other literature (e.g., Audibert & Nyman, 1977; Trautmann & O'Rourke, 1985; Smith, 1962 and Hsu et al., 2001) in Figure 5-7, which incorporates different soil properties (e.g., soil density, soil friction angle). The pipe diameter and peak soil friction angle, for each study, are summarized in the legend.

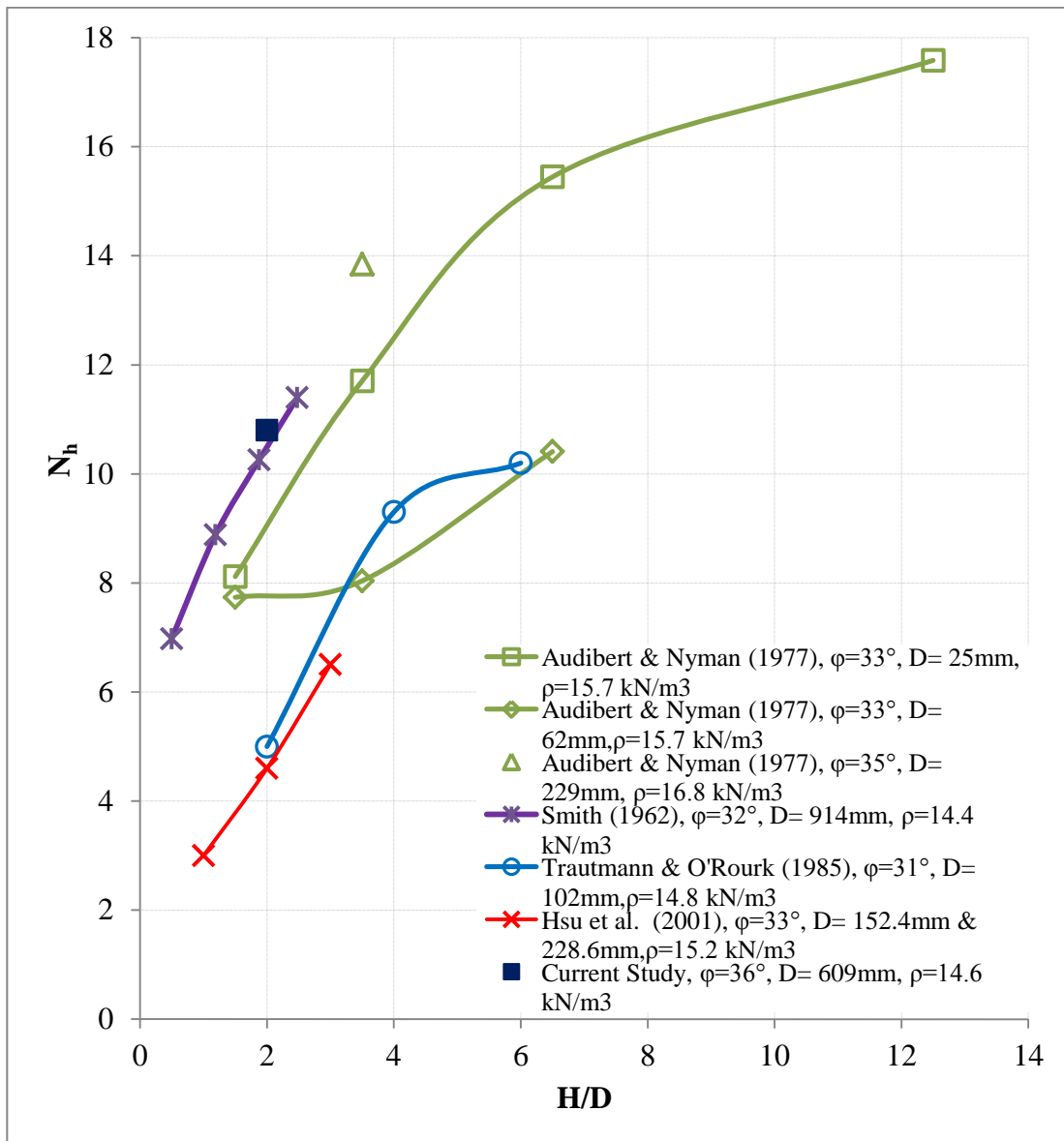


**Figure 5-7: Comparison of the normalized peak loads with several published test results for loose sand.**

The current study in loose sand is consistent with the normalized lateral force estimates presented by Audibert and Nyman (1977) and Smith (1962). For this study, the soil friction angle was measured through a direct shear test at low stress level (i.e., normal

stress 8 kPa to 64 kPa), which is consistent with the test conditions for a pipe buried at shallow depth. As discussed in Chapter 4, Roy et al. (2014, 2015) have investigated the mechanical response of a buried pipe subject to lateral movement at low stress using Abaqus/Explicit FE modeling procedures. The soil constitutive relationships were established through simulation of triaxial test results at low confining pressure. The numerical modeling procedures were able to capture strain localization and shear bands during lateral movement of the buried pipe. Based on examination of the failure mechanisms, the numerical simulations indicated an increase the dilation angle that in turn resulted in higher lateral forces (Roy et al. 2015). Guo and Stoll (2005) also observed higher normalized loads for shallow burial depth ratio when the effects of pressure dependency were considered for soil with higher friction angles. These observations support the centrifuge test results from this study.

The ultimate displacement at peak lateral force of this centrifuge test is about 1D, which much higher than that estimated by ALA (2005) and PRCI (2004) guidelines. Trautmann (1983) reported this displacement to peak load within 0.4D to 0.5D in his large scale tests. There are several reasons that may cause this higher displacement including variation in test bed preparation and soil density around the pipe during pluviation. Also Palmer et al. (2003) reported that there is a discrepancy between the full-scale test and centrifuge tests for the mobilization displacement for the uplift resistance of buried pipeline. But he explained this discrepancy as an effect of localized shear zone across which the shear stress is a function of the relative displacement, which is also similar to the lateral pipe movement.

### 5.2.3 OBLIQUE ANGLE TESTS

The test results for oblique loading events TL40 and TL70 are shown in Figure 5-8 and 5-9 in terms of normalized force–displacement curves for the oblique attack angles of  $40^\circ$  and  $70^\circ$ . Both the axial and lateral normalized load increases with the displacement until peak load is reached and then decreases. The vertical arrows identify the peak load estimate for each normalized force–displacement curve.

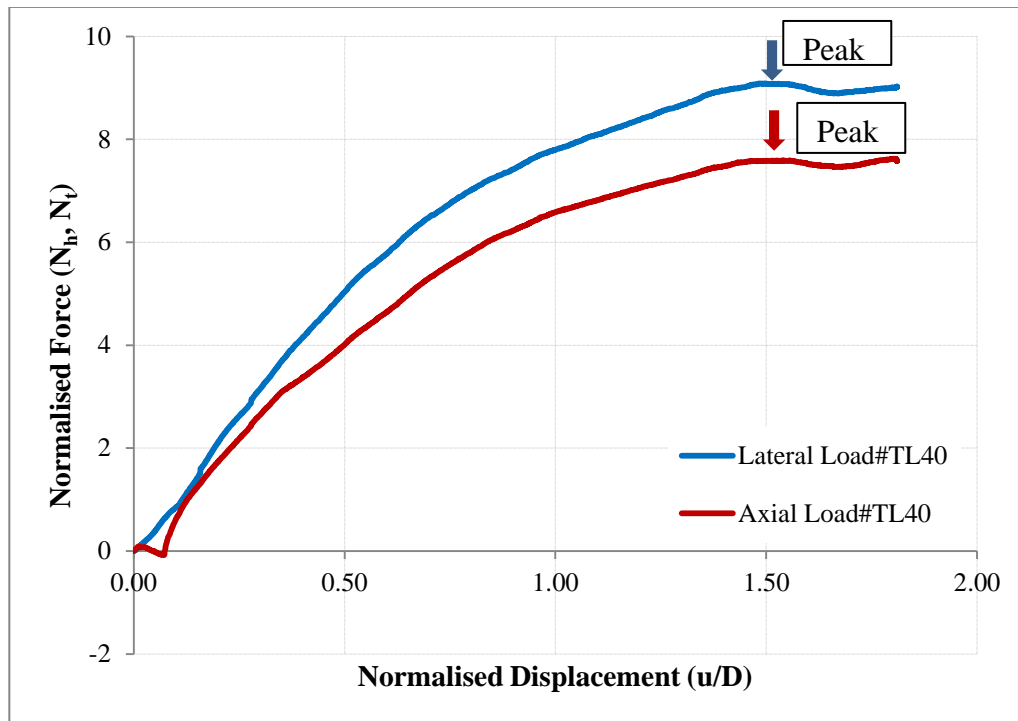


**Figure 5-8: Normalized load–displacement relationship for oblique angle test in loose sand (TL40).**

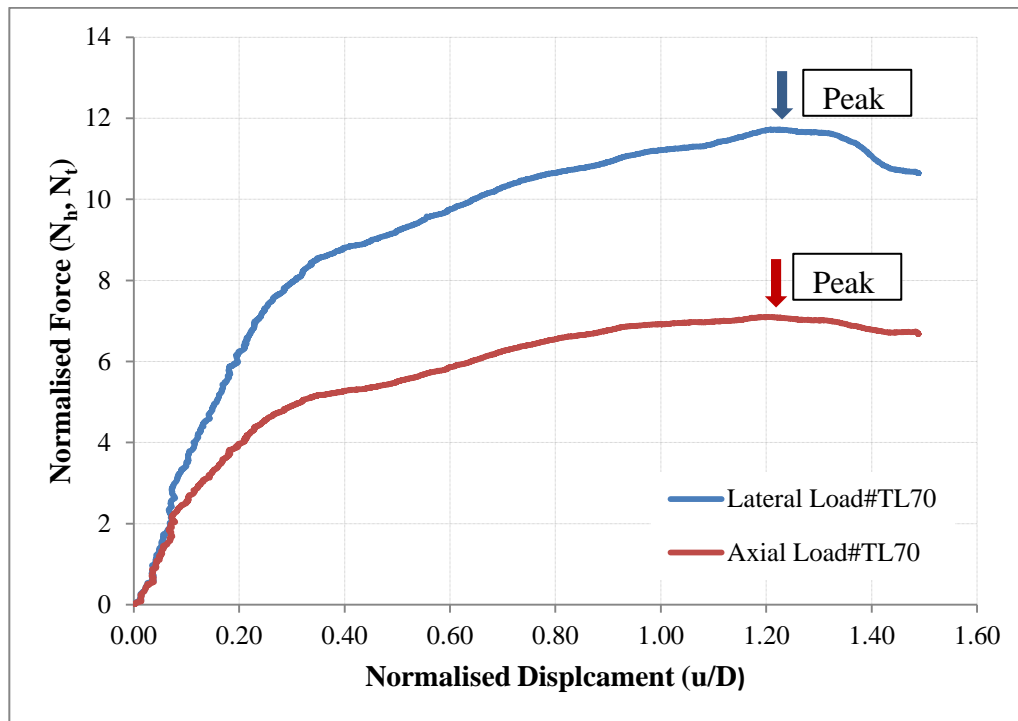


**Figure 5-9: Normalized load–displacement relationship for oblique angle test in loose sand (TL70).**

As shown in Figure 5-10 where the oblique angle test results (Figures 5-2, 5-5, 5-8 & 5-9) are summarized, it is observed the axial and lateral interaction factors vary with the oblique attack angles. The normalized axial load ( $N_t$ ) has an initial offset due to axial restraint that increases with attack angle until a peak load is reached and then reduces as the pipe–soil interaction event becomes dominated by lateral bearing failure mechanism. The normalized lateral load ( $N_h$ ) increases from zero load condition associated with pure axial motion with increasing attack angles. Here it is noted that that for the 70° oblique angle test, the lateral interaction factor is little bit higher than the pure lateral test (TL90) which is due to higher soil density (Table 3-4) as it is very difficult to maintain the same

density for loose condition and at the same time change the soil friction angle. The normalized load for lateral test ( $90^\circ$ ) was lower than the lateral load at an attack angle of  $70^\circ$  by a factor of 0.93. Possible explanations for this discrepancy include natural variation between tests, methods used to establish the peak load, greater mobilization distance for the oblique load event (Figure 5-9 in comparison with Figure 5-5), and possible scale effects (Section 4.2.2) and influences of failure mechanisms. This is illustrated in Figure 5-10 where the transition from axial to lateral bearing failure mechanisms, associated with decreasing axial forces, may occur in between  $50^\circ$  and  $60^\circ$ . This behavior is consistent with the test results for dense sand of this study which is already discussed in Chapter 4. Also, some other centrifuge test results such as Daiyan (2013) for dense sand and Phillips et.al (2004) for clay showed similar soil behavior where the lateral interaction factor also increases with the increase of oblique angles from  $0^\circ$  (pure axial condition) to  $90^\circ$  (pure lateral condition).

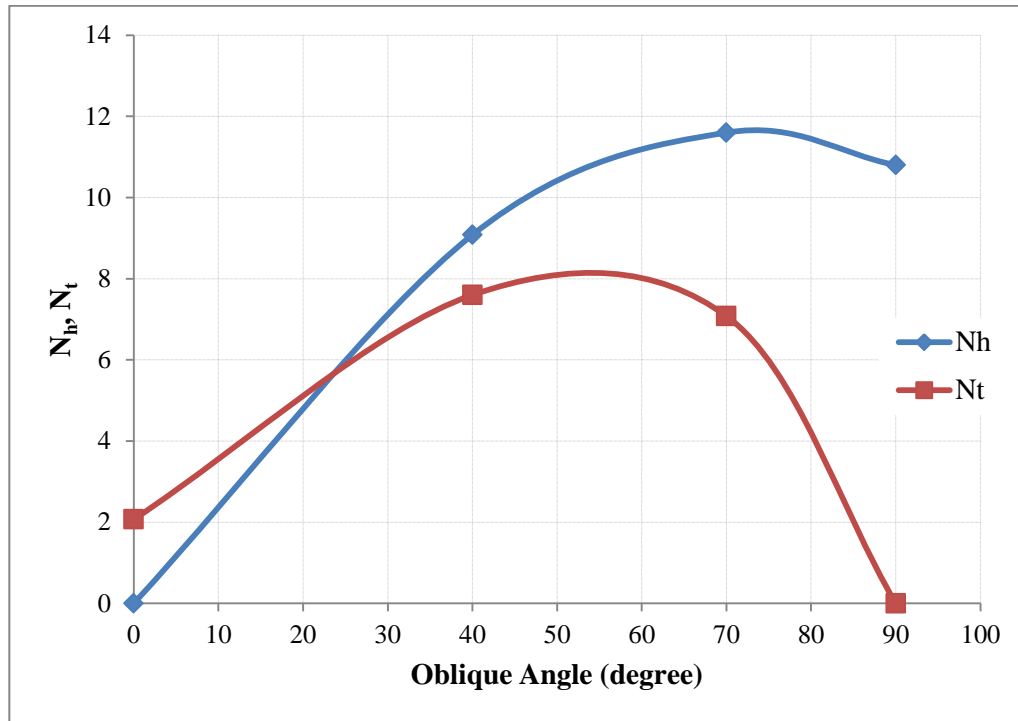


**Figure 5-10: Variation of axial and lateral interaction factor for loose sand**

In this study, the failure surface in front of the pipe was examined during the oblique angle test (TL40) using very thin layers approximately 2 mm thickness of colored sand. As shown in Figure 5-11, a passive wedge formed in front of the pipe (which was not as significant as for dense sand) and a caving wedge were identified in back of the pipe which was consistent with Audibert & Nyman (1977) for intermediate burial depth.

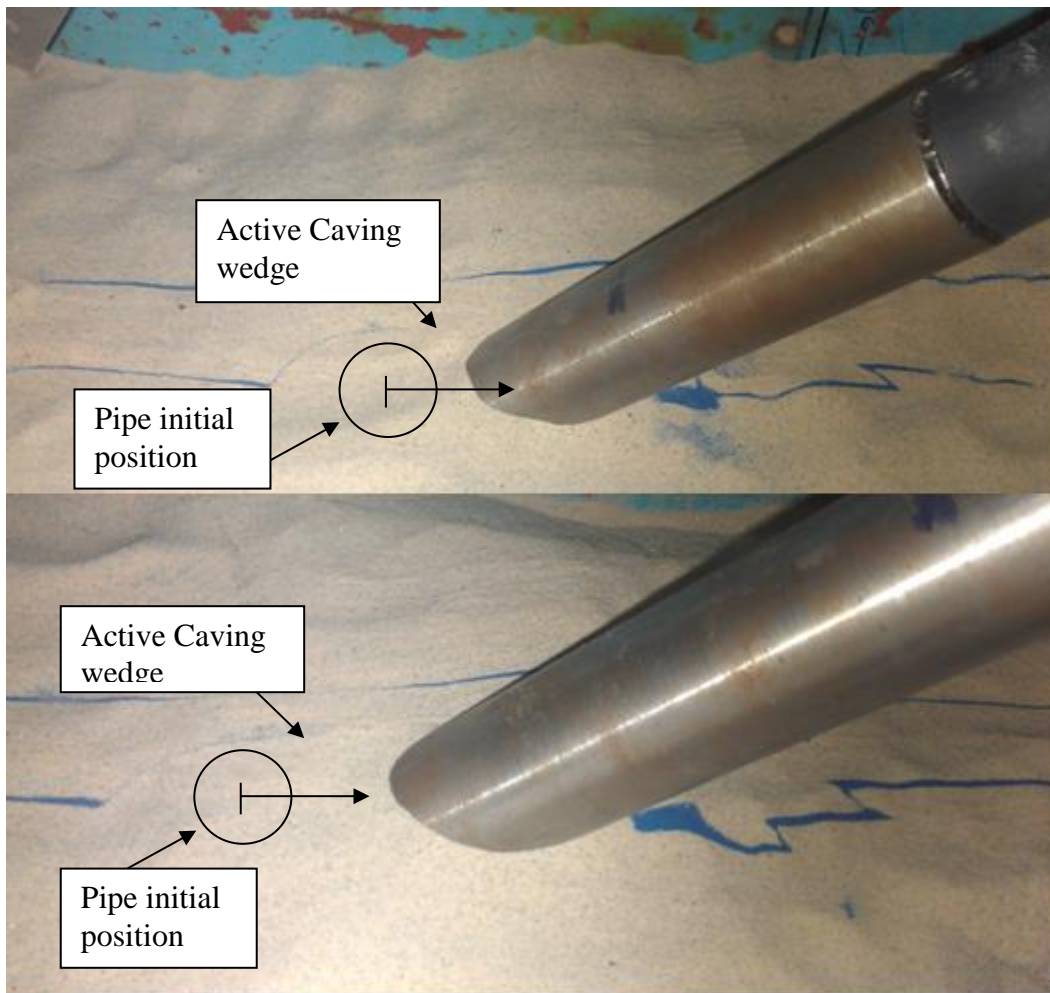


**Figure 5-11: Deformed colored soil layers for the oblique loading test (TL40) after centrifuge test.**

Using the data presented in Figure 5-10, a failure or yield load envelop can be constructed (Figure 5-12) and compared to test results for dense sand of this study. The failure envelope illustrates the coupling between the normalized axial and lateral interaction forces that are dependent on the relative oblique attack angle where the axial normalized force increases with the oblique attack angles from the pure axial condition, which has an initial offset, until a peak load is reached then decrease while the normalized lateral load

( $N_h$ ) increases from zero load with increasing oblique attack angle. This is also supported by the data presented in Figure 5-10. The coupled load interaction, as illustrated by the yield envelope, is associated with two failure mechanisms. At low oblique angles, the soil failure is controlled by shear strength and friction along the pipe–soil interface which is associated with increased effective axial force with increasing oblique angle. This curve is consistent with the curve of the dense sand as discussed in Chapter 4 (Section 4.2.3) which was supported by numerical studies on oblique pipe–soil interaction in cohesive (Phillips et al., 2004a; Pike and Kenny, 2012a, b) and non-cohesive soil conditions (Daiyan, 2013; Daiyan et al., 2011, 2010). As the attack angle increases, the axial-lateral interaction coupling effects are moderated where the failure mechanism is governed by the shear failure through the soil mass. Figure 5-12 shows the similar failure envelope as for dense sand consisting of the linear portion of the curve associated with the soil failure on the pipe surface and the non-linear portion associated with the shear failure in the soil mass. For this study in loose sand, the transition between linear and nonlinear components of the failure surface occurred at an oblique angle of approximately  $50^\circ$ . In Figure 5-12, Method (1) and Method (2) indicates the method of selecting peak load for the dense sand which is already presented in Chapter 4 (Figure 4-18).

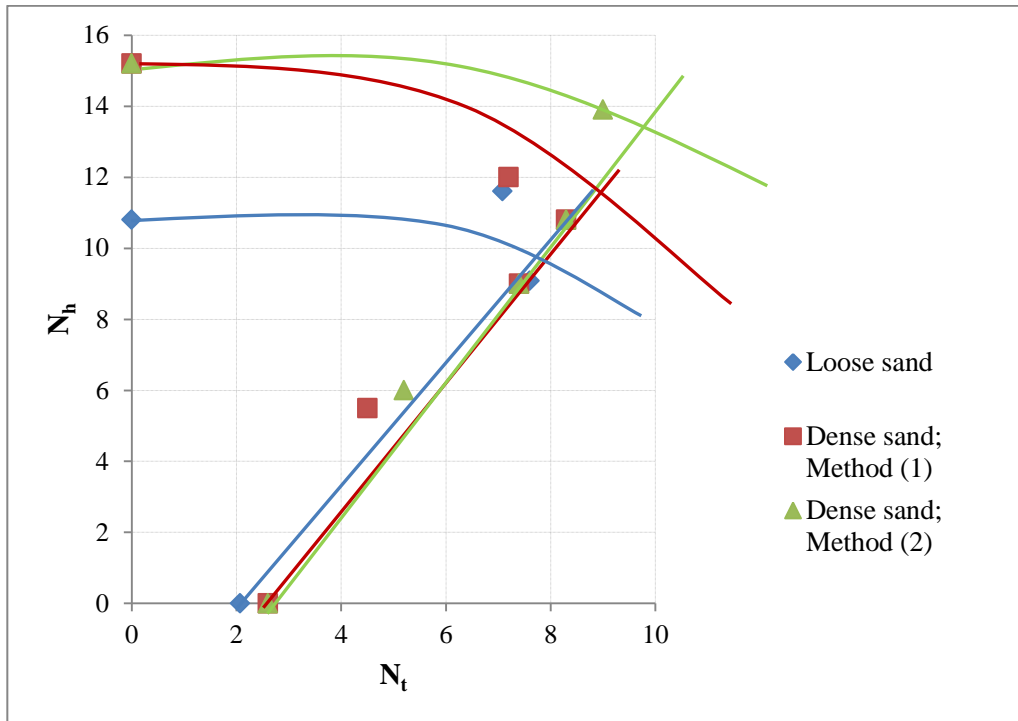


**Figure 5-12: Axial-lateral interaction curve for loose sand.**

### 5.3 SUMMARY OF THE CHAPTER

Similar to the dense sand test bed condition, a series of centrifuge tests were also conducted in loose sand condition which includes axial, lateral and some oblique angle tests. These tests mostly examine peak load, yield displacement at peak load and failure mechanisms. The axial and lateral test results were compared with other available results which gives confidence in the results of this study. Some of the key findings are summarized below:

- 1) The measured normalized axial force of this test is greater than ALA (2005) guidelines by a factor of 1.6 for H/D of 2. Using the equivalent lateral earth pressure co-efficient of 1.5 in Equation 2-2, which was recommended by Karimian (2006) in the range of 1.0 to 2.25, the estimated normalized axial force exactly matched with the measured test result as like for dense sand condition.
- 2) The measured normalized lateral force of this test is in good agreement with the Audibert & Nyman (1977) and Hansen (1961) results for H/D= 2,  $\phi= 35^\circ$  (Figure 5-6). Also the soil constitutive behavior was investigated at low confining stress of a buried pipe subjected to lateral movement by Roy et al. (2014, 2015) which support the centrifuge test results of this study. However, the measured normalized lateral force of this test is also consistent with Smith (1962) (Figure 5-7).
- 3) The interaction factor also changes with the oblique attack angles (Figure 5-10) where the normalized lateral load ( $N_h$ ) increases from zero load condition and the normalized axial load ( $N_t$ ) has an initial offset due to axial restraint that increases with the attack angles until a peak load is reached and then decreases which is consistent with dense sand test results.
- 4) During the failure, there is an active caving wedge formed in back of the pipe due to pipe movement where the passive wedge in the front of the pipe is not as significant.

- 5) The normalized axial and lateral interaction forces are coupled where, at low oblique angles, the soil failure is controlled by shear strength and friction along the pipe–soil interface which represents the linear portion of the envelop, and as the attack angle increases, the axial-lateral interaction coupling effects are moderated where the failure mechanisms is governed by the shear failure through the soil mass which represents the non-linear portion of the envelop. This degree of coupling is consistent with the dense sand test results which was supported by results from continuum finite element simulations (e.g., Daiyan, 2013; Daiyan et al., 2011; Phillips et al., 2004a; Pike and Kenny, 2012a, b; C-Core, 2008). The transition of failure surfaces occurred at an oblique angle of about  $50^\circ$ .

## 6 SUMMARY, CONCLUSIONS AND RECOMMENDATIONS

### 6.1 SUMMARY

Current engineering practice for modelling pipe–soil interaction events uses idealized structural beam/spring models to simulate the continuum response. The soil forces are idealized by discrete forces acting on the pipe section in three mutually orthogonal directions (i.e., longitudinal, transverse horizontal and transverse vertical) to the pipe cross section. The soil springs are independent and do not account for shear load transfer and coupling between adjacent soil spring elements.

The main objective of this study was to examine the effects of load coupling during axial-lateral pipe–soil interaction events through physical modelling using the geotechnical centrifuge. A model pipe with 46 mm outside diameter and 3.9 mm wall thickness ( $D/t$  of 12) was used to simulate prototype pipe diameter of 609 mm. Laboratory tests were conducted to obtain physical and mechanical strength properties of the soil. The soil test bed examined loose sand, with an average density of  $1467 \text{ kg/m}^3$ , peak friction angle of  $36^\circ$  and constant volume friction angle of  $32^\circ$ , and dense sand conditions, with an average density of  $1567 \text{ kg/m}^3$ , peak friction angle of  $41^\circ$  and constant volume friction angle of  $32^\circ$ .

Through examination of the soil force–displacement response, yield load envelopes were developed with respect to pure axial, lateral bearing and oblique axial-lateral interaction events. Methodologies used to establish the yield envelope, mobilization distance to yield and soil failure mechanisms were also evaluated.

The experimental results and analysis were also used to assess the significance of ignoring load coupling effects in current engineering practice for defining the load-displacement response used in engineering models predicting the pipe mechanical response.

## **6.2 FINDINGS FROM THE RESEARCH**

Based on the physical model tests on buried pipe in both dense and loose sand test bed conditions the key findings from this work is summarized as follows:

- 1) The measured normalized axial force was in agreement with theoretical considerations (Equation 2-2) when the equivalent lateral stress coefficient was 1.6 for dense and 1.5 for loose sand conditions. This is consistent with the recommendations by Karimian (2006) where the equivalent lateral stress coefficient ranges from 1.0 to 2.25 for the centrifuge test parameters examined in this study.

- 2) The peak axial force for dense sand is 1.2 times greater than the loose sand test bed condition. In large scale axial pipe–soil interaction tests, Paulin et al. (1998) found that post-peak axial loads in dense sand were on average approximately 1.6 times greater than corresponding tests conducted in loose sand condition.
- 3) The normalized lateral bearing load for both the dense (Figure 4-8 & Figure 4-9) and loose sand (Figure 5-6 & Figure 5-7) conditions were consistent with some data records in the public domain reported for full-scale and reduced scale physical models. Other public domain data sets suggest lower normalized lateral bearing loads. The discrepancy may be related to the effects of low stress level associated with shallow burial depth on soil strength parameters (e.g., Pike et al., 2013, Roy et al., 2014), scale effects due to pipe diameter (Guo and Stolle, 2005), and scale effects on higher mobilization distances to yield load associated with soil kinematics and failure mechanisms (e.g., Palmer et al., 2003).
- 4) The failure envelope for oblique pipe–soil interaction events exhibits a linear and non-linear failure surface, which was observed for both the dense (Figure 4-15 & Figure 4-17) and loose (Figure 5-10 & Figure 5-12) sand test beds. The linear surface is mobilized at low, oblique attack angles and is associated with soil failure within a zone circumscribing the pipe circumference that is controlled by soil shear strength and friction along the pipe–soil interface. The nonlinear failure surface is associated with bearing failure through the soil mass at higher angles. The failure mechanism transition for dense sand occurred at oblique angles

between  $60^\circ$  and  $65^\circ$  (Figure 4-15 and Figure 4-17) and  $50^\circ$  and  $55^\circ$  for loose sand (Figure 5-10 and Figure 5-12). These results are consistent with other physical modelling (Daiyan, 2013) numerical simulations (e.g., Daiyan, 2013; Daiyan et al., 2011; Phillips et al., 2004a; Pike and Kenny, 2012a, b; C-CORE, 2008) for pipe–soil interaction events. As shown in Figure 4-15 and Figure 5-10, for small oblique angles, the axial force increases with increasing attack angle until the soil failure mechanism is dominated by lateral bearing, where the axial force decreased to zero with increasing attack angle to pure lateral bearing ( $90^\circ$ ). The discrepancy between the current results and observations (Hsu et al., 2001, 2006) may be due to a number of factors including scale effects associated with the small pipe diameter and shallow burial depth at full-scale, scale effects in the centrifuge model with respect to soil kinematics and failure mechanisms, and differences in the pipe end bearing conditions and stiffness of the pipe and test frame.

- 5) As shown in Figure 4-17 and Figure 5-12, for both the dense and loose sand test beds, the method used to determine the yield load only influenced the transition point (i.e., hinge point) of the failure surface from the axial to lateral bearing failure modes.
- 6) For dense sand, a passive wedge was formed during the pipe horizontal movement in oblique directions in front of the pipe (Figure 4-16), which is similar to the results from Daiyan (2013). Whereas for the loose sand condition, an active

caving wedge formed at the back of the pipe (Figure 5-11) due to pipe movement and where the passive wedge in the front of the pipe was not so significant.

### **6.3 FUTURE RESEARCH RECOMMENDATIONS**

Based on the research findings established in this study, it is recommended the following investigations can be undertaken to reduce uncertainty, improve knowledge and advance current practice. There is observed agreement between reduced scale-centrifuge test results and continuum finite element simulations on the load coupling effects for axial-lateral pipe–soil interaction. There are some uncertainty exists on the characteristics of the yield envelop for oblique axial-lateral interaction events when this reduced scale-centrifuge test results are compared with full scale test data which may be related to differences in the end bearing conditions in the physical models and potential scaling errors in the centrifuge test with respect to mobilization distance to yield. To resolve this uncertainty as well as to improve the understanding of the coupling effects of buried pipelines, there are some recommendations which are listed below.

- 1) Assess the equivalent lateral stress coefficient ( $K_0$ ), value as proposed by Karimian (2006), for axial and oblique pipe–soil interaction events as a function of the pipe diameter, pipe burial depth, soil density and soil strength parameters. The oblique interaction events should be extended to consideration of the axial-lateral and axial-vertical planes.

- 2) Investigate the effects of low confining stress, associated with shallow buried pipe representing practical field conditions, on soil mechanical strength parameters, soil loads and failure mechanisms for oblique pipe–soil interaction events in the axial-lateral, axial-vertical and lateral-vertical planes.
- 3) Evaluate geometric (i.e., pipe diameter,  $H/D$ ) and physical modelling (i.e., mobilization distances in the geotechnical centrifuge) scale effects on the estimate of peak load and mobilization distance to peak load when determining the yield envelope for oblique pipe–soil interaction events. Establish a recommended methodology to determine these parameters when constructing failure surfaces for oblique pipe–soil interaction events.
- 4) Conduct a detailed study, over a range of practical design parameters, using verified continuum finite element methods, or other appropriate numerical simulation method, to establish the yield envelopes and mobilization distances to yield for oblique pipe–soil interaction events in the axial-lateral, axial-vertical and lateral-vertical planes. The key parameters include pipe diameter,  $H/D$ , soil type, and soil strength properties. The outcomes would provide a comprehensive basis to advance current practice for structural based (i.e., beam/spring) pipe–soil interaction models that account for load coupling during oblique load events. The evolution of the failure surface (i.e., strain softening, hardening) on the coupled pipe–soil response and the influence on modelling strategies (i.e., coupled beam-spring versus shell-continuum) should be investigated.

## REFERENCES

ALA (2005) Guidelines for the design of buried steel pipe, American Lifelines Alliance (ALA), 76p.

ASCE (1984) Guidelines for the seismic design of oil and gas pipeline systems, American Society of Civil Engineers, Committee on gas and liquid fuel lifelines, Technical Council on Lifeline Earthquake Engineering, ASCE, New York.

Audibert, J. M. E. and Nyman, K. J. (1977) Soil restraint against horizontal motion of pipes, *Journal of Geotechnical Engineering Division*, ASCE, 103(10): 1119-1142.

Bolton, M. D. (1986) The strength and dilatancy of sands, *Geotechnique*, vol. 36, no. 1, pp. 65-78.

C-CORE (2008) Pipeline Integrity for Ground Movement Hazards, final report prepared for United States Department of Transportation, C-CORE Report R-07-082-459.

Daiyan, N., Kenny, S., Phillips, R., and Popescu, R. (2010) Numerical investigation of oblique pipeline/soil interaction in sand, *Proceedings of the 8th International Pipeline Conference*, American Society of Mechanical Engineers.

Daiyan, N., Kenny, S., Phillips, R., and Popescu, R. (2011) Investigating pipeline-soil interaction under axial-lateral relative movements in sand, *Canadian Geotechnical Journal*, 48:1683-1695.

Daiyan, N. (2013) Investigating soil/pipeline interaction during oblique relative movements, Ph.D Thesis, Memorial University of Newfoundland.

Danish Hydraulic Institute (DHI) and Ramboll and Hannemann (1985), *Danish Submarine Guidelines*, Danish Energy Agency.

Das, B. M., Seeley, G. R. (1975) Load displacement relationship for vertical anchor plates, *Journal of Geotechnical Engineering Division*, 101(GT7), 711-715.

Guo, P. J., and Stolle, D. F. E. (2005) Lateral pipe-soil interaction in sand with reference to scale effect, *Journal of Geotechnical and Geoenvironmental Engineering*, 131(3), 338-349.

Guo, P. J. (2005) Numerical modeling of pipe-soil interaction under oblique loading, *Journal of Geotechnical and Geoenvironmental Engineering*, 131(2), 260-268.

Hansen, B.J. (1961) The ultimate resistance of rigid piles against transversal forces, *Bulletin 12*, Danish Geotechnical Institute, Copenhagen, Denmark.

Hsu, T. W., Chen, Y. J., and Wy, C. Y. (2001) Soil resistant to oblique movement of buried pipes in dense sand, *Journal of Transportation Engineering*, 127(1), 82-87.

Hsu, T-W, Chen, Y-J, and Hung, W-C, (2006) Soil Restraint to Oblique Movement of Buried Pipes in Dense Sand, *Journal of Transportation Engineering*, American Society of Civil Engineers, Vol. 132, No. 2.

Jacky J (1944) The coefficient of earth pressure at rest, *Journal of Society of Hungarian Engineers and Architectures*, 355-358.

Jung, J., O'Rourke, T. & Olson, N. (2013) Lateral Soil-Pipe Interaction in Dry and Partially Saturated Sand, *Journal of Geotechnical and Geoenvironmental Engineering*, vol. 139, no. 12, pp. 2028-2036.

Karimian, S. A. (2006). Response of buried steel pipelines subjected to longitudinal and transverse ground movement. Ph.D. Thesis, The University of British Columbia.

Kennedy R.P., Chow A., W., Williamson R., A. (1977) Fault movement effects on buried oil pipeline, *Transportation Engineering Journal*, ASCE, 617-633.

Kulhawy, F. H. C., Trautmann, C. H., Beech, J. F., O'Rourke, T. D., and McGuire, W.(1983) Transmission line structure foundations for uplift-compression loading, Report No. EL-2870, Electric Power Research Institute.

Lings, M. L., & Dietz, M. S. (2004) An Improved Direct Shear Apparatus for Sand, *Geotechnique*, Vol. 54, No. 4, pp. 245-256.

McAllister, E. W. (2001) Pipeline rules of Thumb handbook, Gulf Professional Publishing, 648p.

Newmark, M., Hall, W. J. (1975) Pipeline design to resist large fault displacement, U.S. National Conference on Earthquake Engineering, Ann Arbor, MI, Paper UILU-ENG-75-2011, 416-425.

Nyman, K. (1984) Soil response against oblique motion of pipes, *J. Transp. Eng.* 110(2):190–202.

O'Rourke T.D., Jerski J. M., Olson N. A., Bonneau A.L., Palmer M.C., Stewart H.E., O'Rourke M. J. (2008) Geotechnics of pipeline system response to earthquakes, *Proceedings of the Geotechnical Earthquake Engineering and Soil Dynamics IV*. GSP(181).

Ovesen N. K. (1964) Anchor slabs, calculation method and model tests, *Bulletin 16*, Danish Geotechnical Institute, Copenhagen, Denmark, Bulletin 16, 40p.

Palmer, A. C., White, D. J., Baumgard, A. J., Bolton, M. D., Barefoot, A. J., Finch, M., Powell, T., Faranski, A. S., and Baldry, J. A. S. (2003) Uplift resistance of buried pipelines: comparison between centrifuge modeling and full-scale tests, *Geotechnique* 53, No. 10, pp. 877-883.

Paulin, M.J., Phillips, R., Clark, J.I., Trigg, A., & Konuk, I., (1998) Full-scale investigation into pipeline/soil interaction, *Proceedings of International Pipeline Conference*, ASME, pp 779-788, Calgary, AB, Canada.

Phillips, R., Nobahar, A., and Zhou, J. (2004) Combined axial and lateral pipe-soil interaction relationships, *Proceedings of International Pipeline Conference*, Calgary, AB, Canada.

Pike, K., Kenny, S., (2011) Advancement of CEL procedures to analyze large deformation pipeline /soil interaction events, *Proceedings of Offshore Technology Conference*, Houston, Texas, USA, May 2011.

Pike, K., Kenny, S., and Hawlader, B., (2013) Advanced analysis of pipe/soil interaction accounting for strain localization, *Proceedings of GeoMontreal*, June 2013.

Pipeline Research Council International, Inc. (PRCI), (2004) *Guidelines for the Seismic Design and Assessment of Natural Gas and Liquid Hydrocarbon Pipelines*, Catalogue No. L51927., Editors: Honegger, D. G., and Nyman D. J.

Pipeline Research Council International, Inc. (PRCI), (2009) Guidelines for Natural Gas and Liquid Hydrocarbon Pipelines in Areas Prone to Landslide and Subsidence Hazards, report prepared by C-CORE, D.G. Honegger Consulting, and SSD, Inc., Catalog No. L52292.

Rowe, R. K., and Davis, E.H. (1982) The behaviour of anchor plates in sand, *Geotechnique*, 32(1), 25-41.

Roy. Kshama.S., Hawlader B.C. & Kenny, S. (2014) Influence of Low Confining Pressure on Lateral Soil/Pipeline Interaction in Dense Sand, *33rd International Conference on Ocean, Offshore and Arctic Engineering (OMAE2014)*, San Francisco, California, USA, June 8-13, 2014.

Roy. Kshama.S., Hawlader B.C., Kenny, S. & Moore I. (2015) Effects of post-peak softening behavior of dense sand on lateral and upward displacement of buried pipelines, *34th International Conference on Ocean, Offshore and Arctic Engineering (OMAE2015)*, St. John's, Newfoundland, Canada, May 31- June 5, 2015.

Schaminee, P. E., Zorn, N. F., and Schotman, G. J. M. (1990) Soil response for pipeline upheaval buckling analyses: full scale laboratory tests and modeling, Proceedings of the 22nd annual Offshore Technology Conference (OTC 6486), Houston, Texas. pp. 563-572.

Sherif, M. A., Fang, Y. S. and Sherif, R. I. (1984)  $K_A$  and  $K_O$  behind rotating and non-yielding walls, ASCE Journal of Geotechnical Engineering, 110, pp. 41-56.

Stroud, M. A. (1971) Sand under low stress levels in simple shear apparatus, PhD thesis, Cambridge University, Cambridge, UK.

Taylor, R. N. (1995). Geotechnical centrifuge technology. Blackie academic & professional, London, 296p.

Trautmann, C. H. (1983) Behavior of pipe in dry sand under lateral and uplift loading, Ph.D. thesis, Cornell University, Ithaca, New York.

Trautmann, C. H. and O'Rourke, T. D. (1985) Lateral force-displacement response of buried pipe. Journal of Geotechnical Engineering, ASCE, 111(9), pp. 1077-1092.

Turner, J. E. (2004) Lateral force displacement behavior of pipes in partially saturated sand, M.A.Sc. Thesis, Cornell University, Ithaca, N.Y.

Wang, J., Ahmed, R., Haigh, S. K., Thusyanthan, N. I. & Mesmar, S. (2010) Uplift resistance of buried pipelines at low cover-diameter ratios, Proceedings of Offshore Technology Conference, Houston, Texas, USA, May 2010.

Wantland, G.P., O'Neil, M.B., Coelogyne, E.H. and Reese, L.C. (1982) Pipeline lateral stability in soft clay. *Journal of petroleum technology*, 34(1), 217-220.

Wijewickreme, D., Karimian, H. and Honegger, D. (2009) Response of buried steel pipelines subjected to relative axial soil movement, *Canadian Geotechnical Journal*, 46, pp. 735-752.

Winkler, E. (1867) *Die Lehre Von Elastizitat und Festigkeit* (Teachings on Elasticity and Stiffness), Prague, Czechoslovakia, 182p.

Yimsiri, S., Soga, K., Yoshizaki, K., Dasari, G. R. and O'Rourke, T. D. (2004) Lateral and upward soil-pipeline interactions in sand for deep embedment conditions. *Journal of Geotechnical and Geoenvironmental Engineering*, 130(8), pp. 830-842.

## **APPENDIX A**

### **Load Cell calibration**

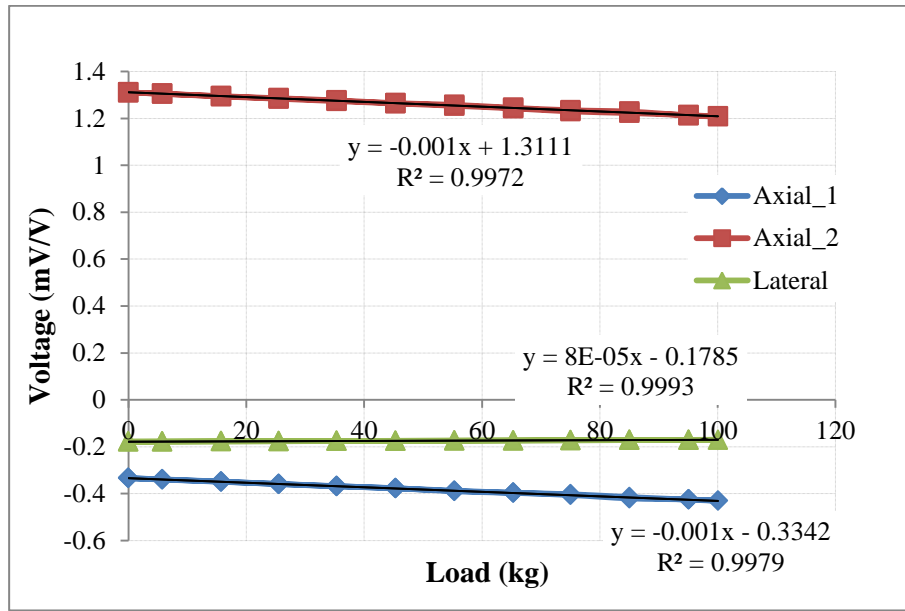


Figure A-1: Axial response during axial load in load cell -1

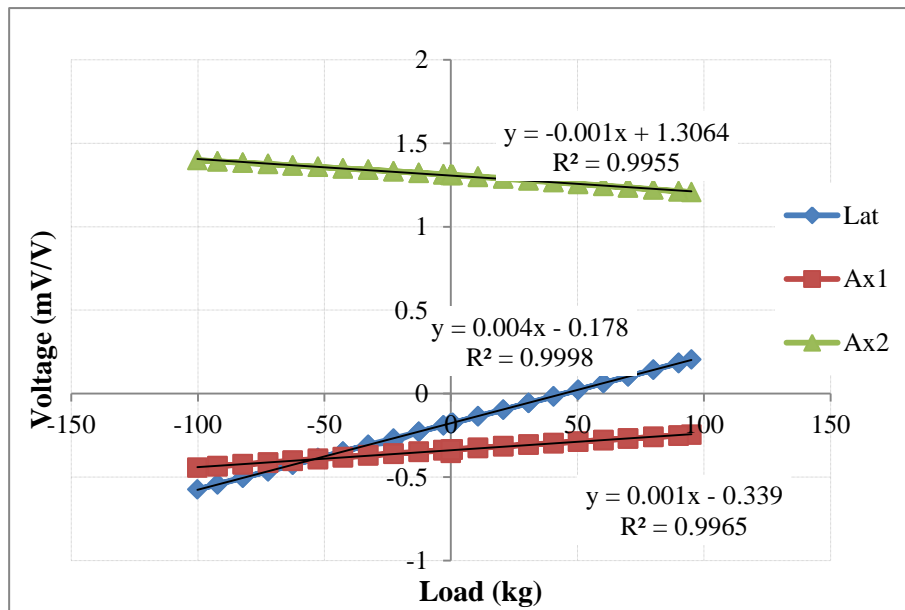
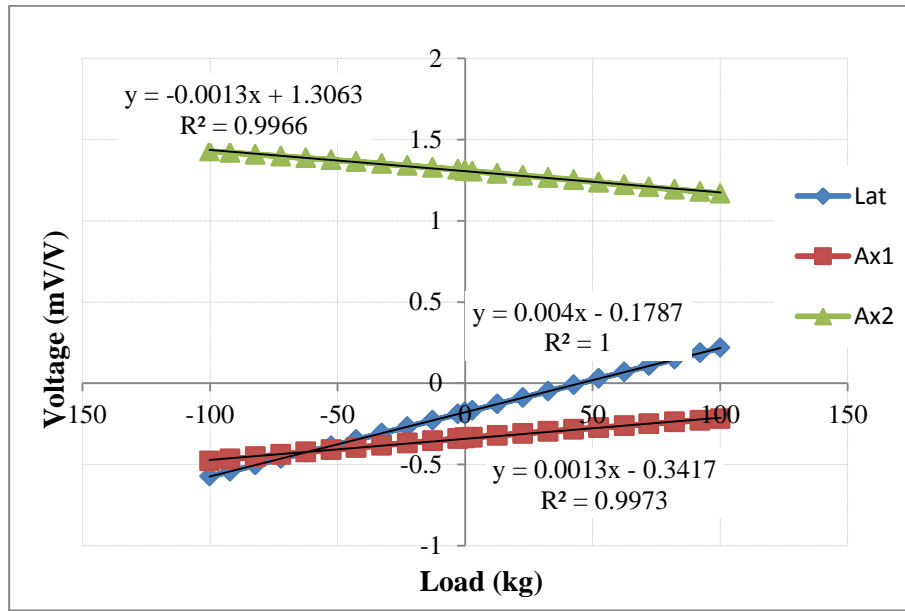
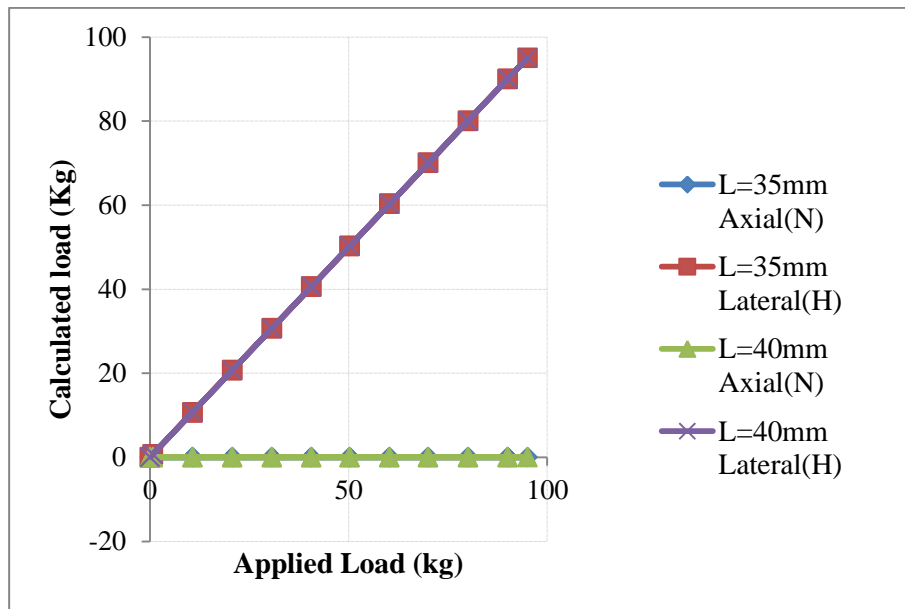


Figure A-2: Load cell response during lateral load applied for the level arm 35 mm in load cell - 1



**Figure A-3: Load cell response during lateral load applied for the level arm 40 mm in load cell -1**



**Figure A-4: Load cell response after calibrating for applying lateral load for 35 mm and 40 mm level arm in load cell -1**

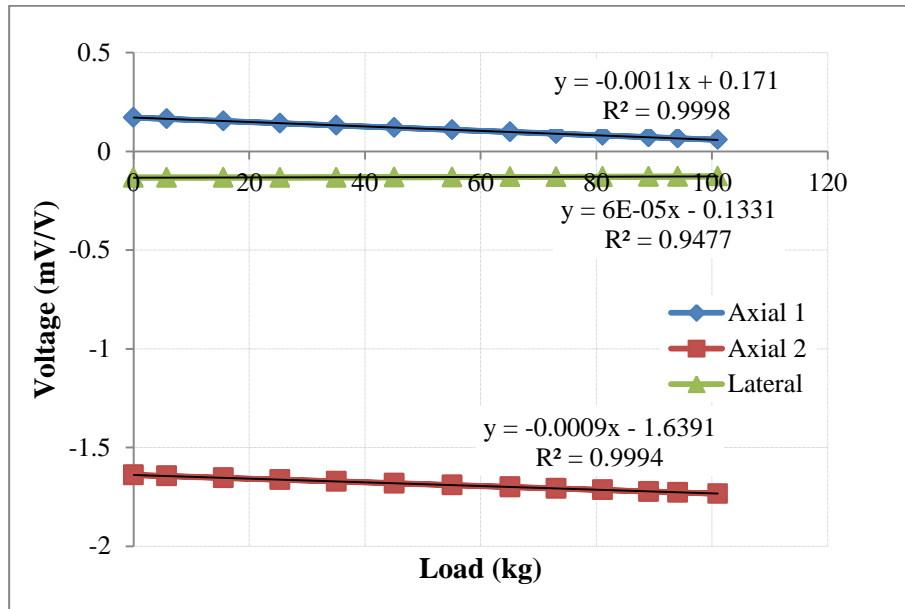


Figure A-5: Load cell response during axial load applied in load cell - 2.

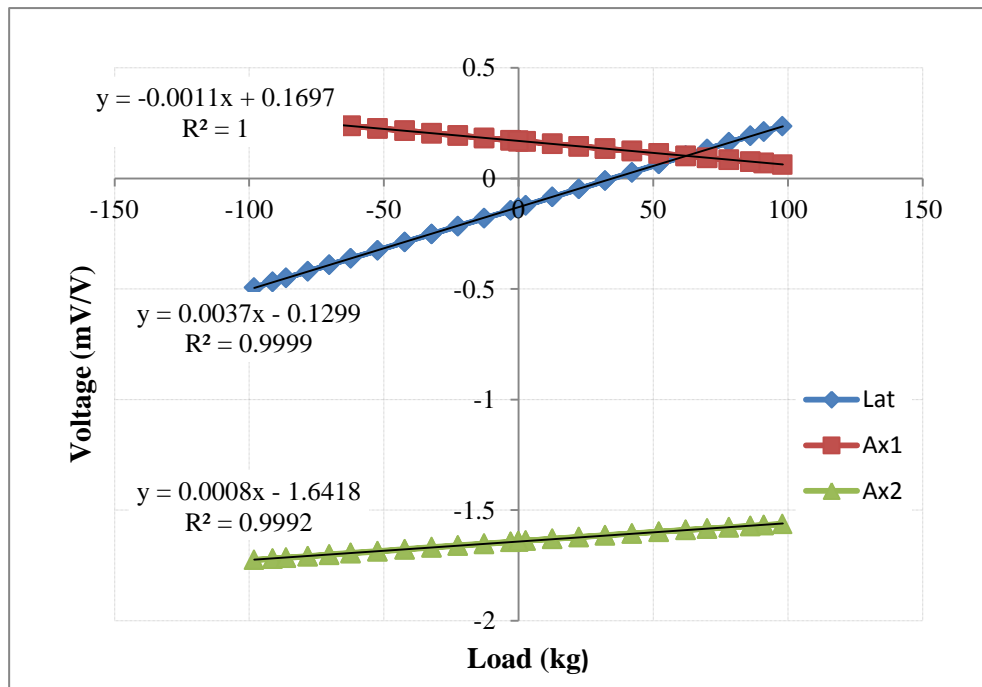
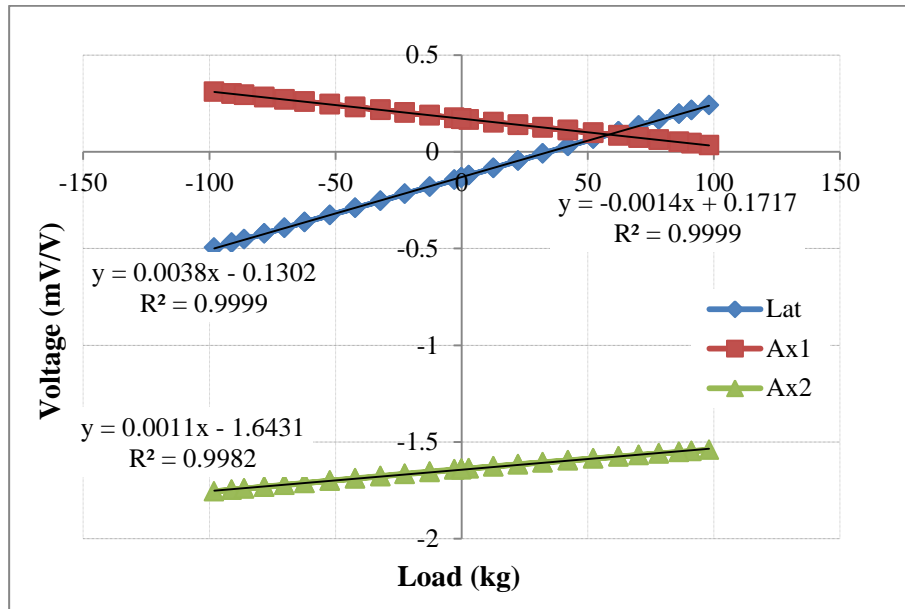
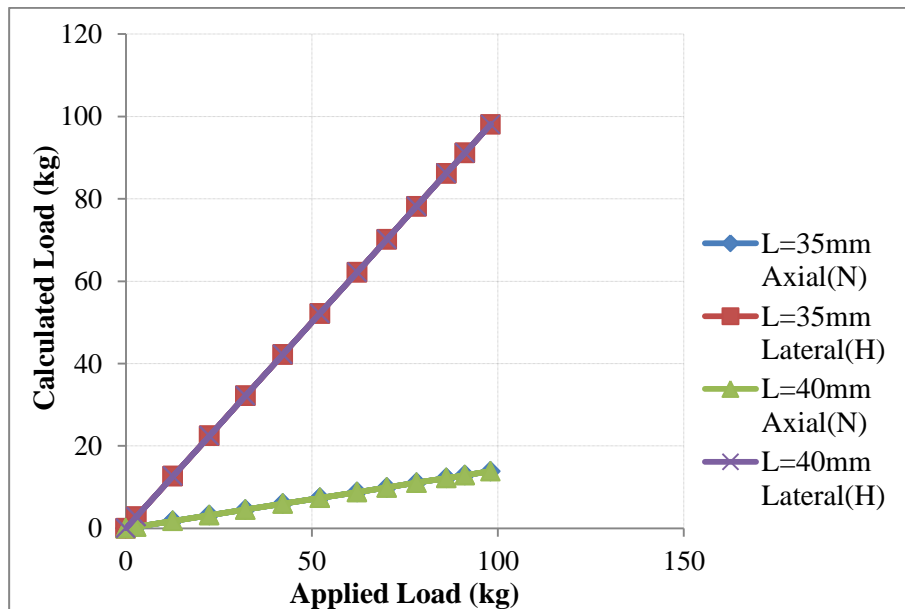


Figure A-6: Load cell response during lateral load applied for the level arm 35 mm in load cell - 2.



**Figure A-7: Load cell response during lateral load applied for the level arm 40 mm in load cell - 2**



**Figure A-8: Load cell response after calibrating for applying lateral load for 35 mm and 40 mm level arm in load cell - 2**

## **APPENDIX B**

### **Direct Shear Test Results on Dense and Loose sand**

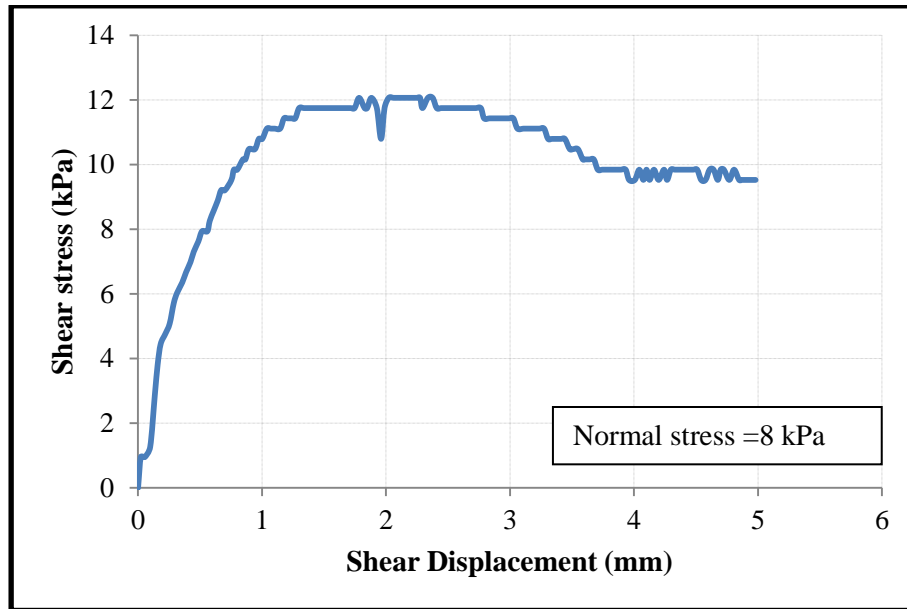


**Figure B-1: Variation of shear stress with displacement for dense sand; Density =  $1578.5 \text{ Kg/m}^3$  ( $D_r = 75.3\%$ ) and normal stress = 8 kPa.**

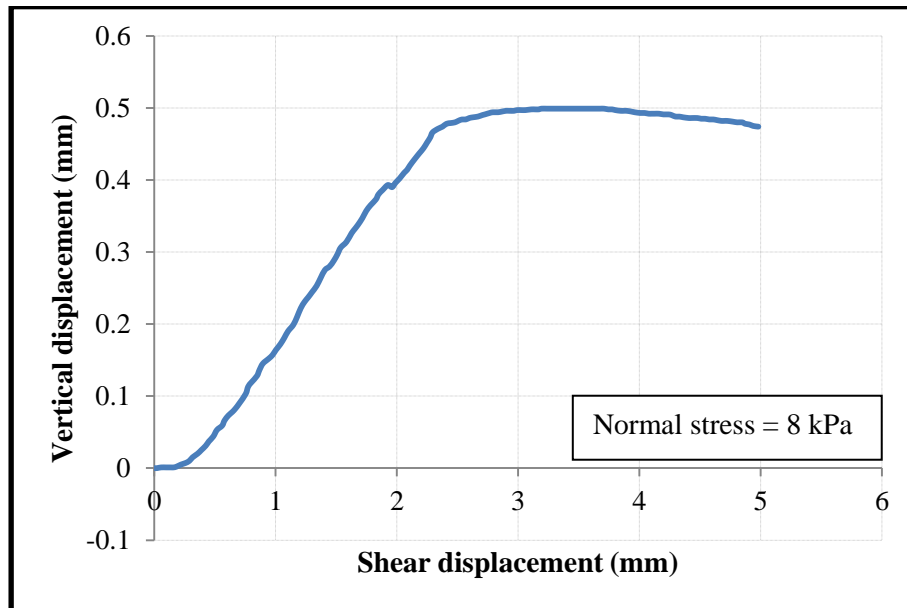


**Figure B-2: Vertical displacement vs shear displacement for dense sand; Density =  $1578.5 \text{ Kg/m}^3$  ( $D_r = 75.3\%$ ) and normal stress = 8 kPa.**

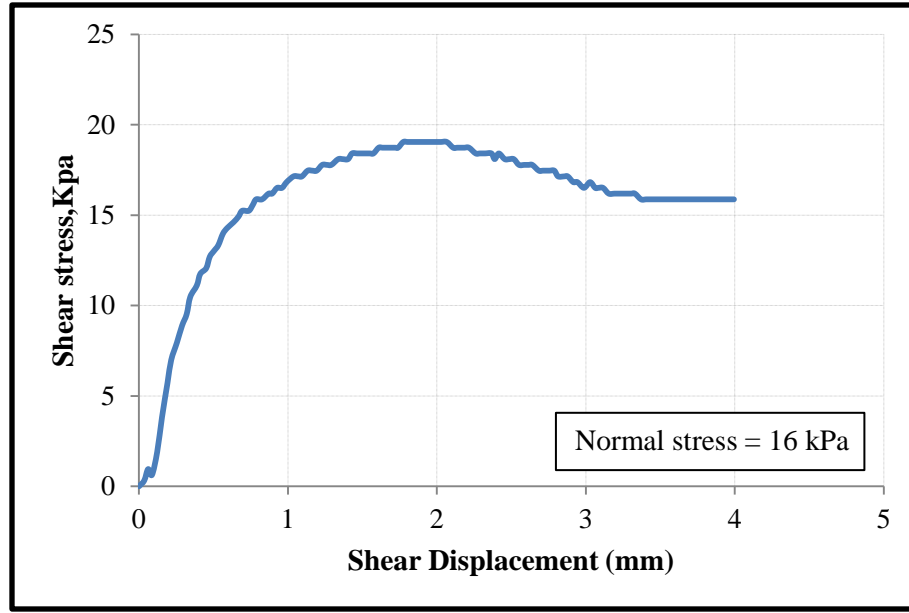


**Figure B-3: Variation of shear stress with displacement for dense sand; Density = 1576.7 Kg/m<sup>3</sup> (Dr = 74.5%) and normal stress = 16 kPa.**

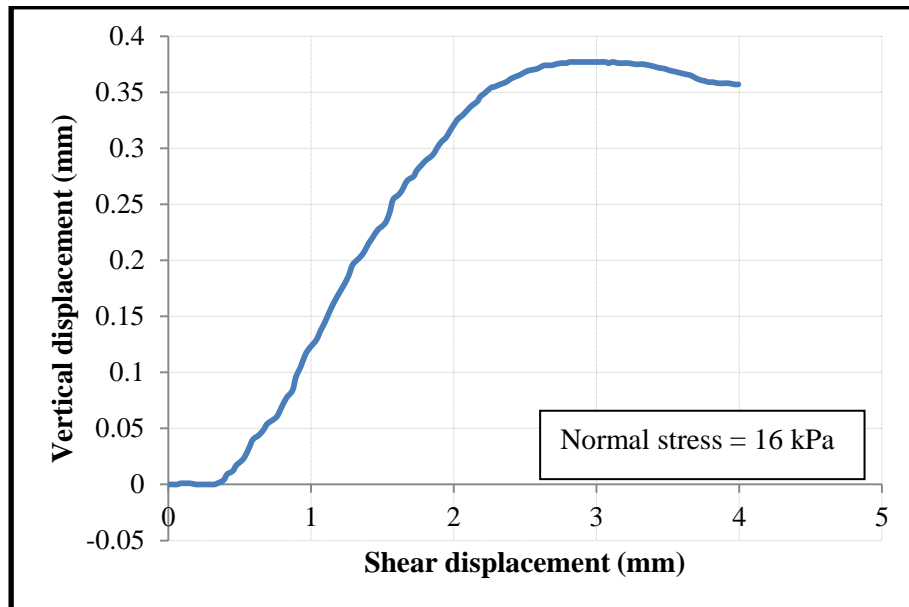


**Figure B-4: Vertical displacement vs shear displacement for dense sand; Density = 1576.7 Kg/m<sup>3</sup> (Dr = 74.5%) and normal stress = 16 kPa.**

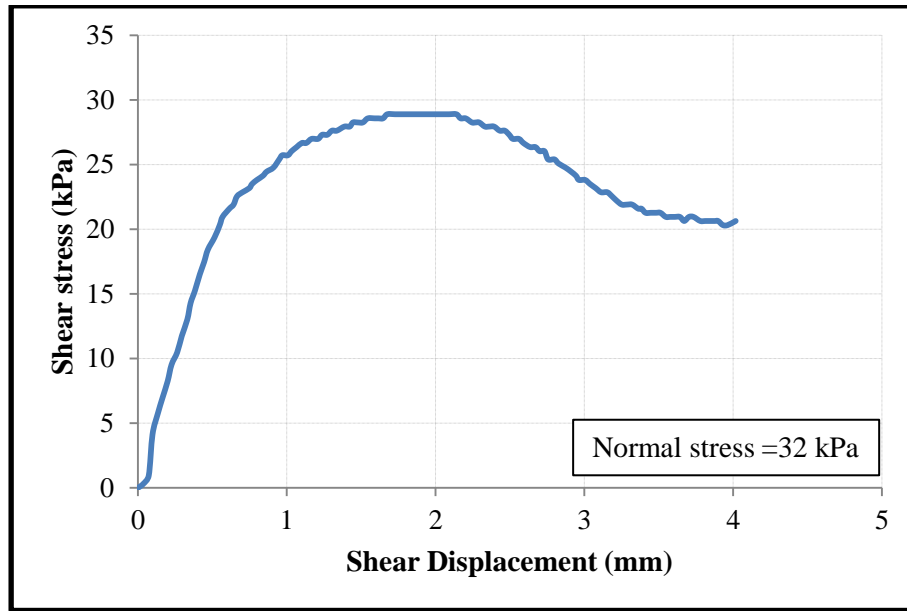


**Figure B-5: Variation of shear stress with displacement for dense sand; Density =  $1576.7 \text{ Kg/m}^3$  ( $D_r = 74.5\%$ ) and normal stress = 32 kPa.**

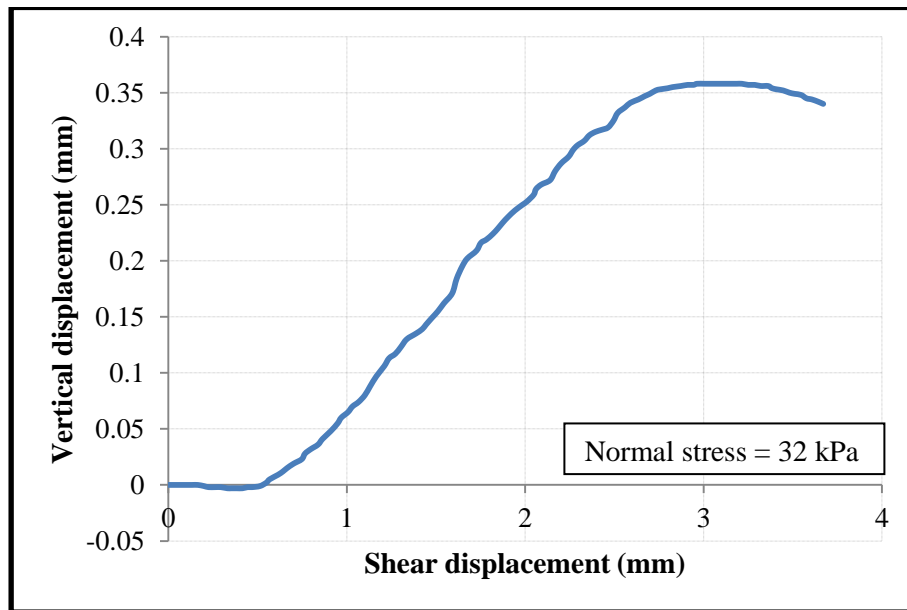


**Figure B-6: Vertical displacement vs shear displacement for dense sand; Density =  $1576.7 \text{ Kg/m}^3$  ( $D_r = 74.5\%$ ) and normal stress = 32 kPa.**

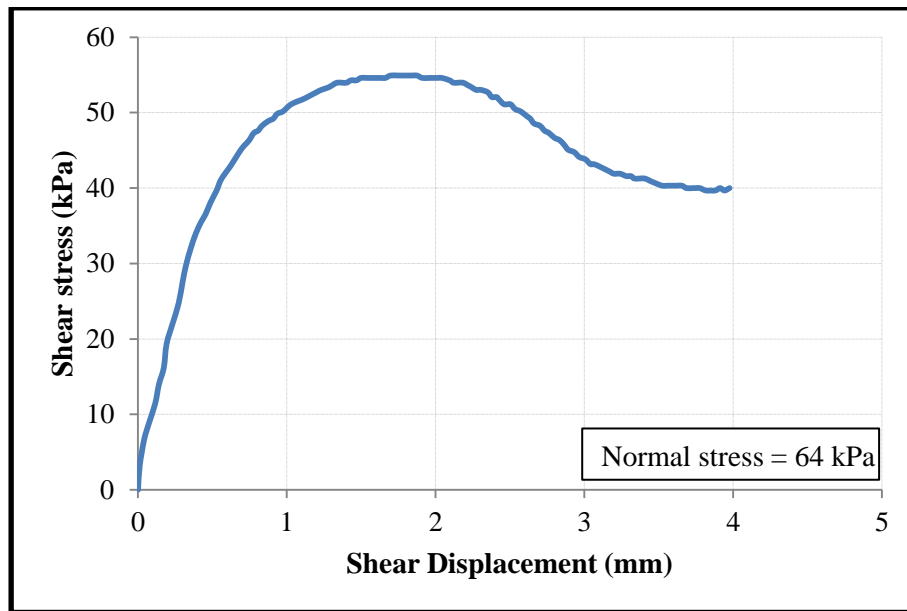


**Figure B-7: Variation of shear stress with displacement for dense sand; Density =  $1578 \text{ Kg/m}^3$  ( $D_r = 75\%$ ) and normal stress = 64 kPa.**

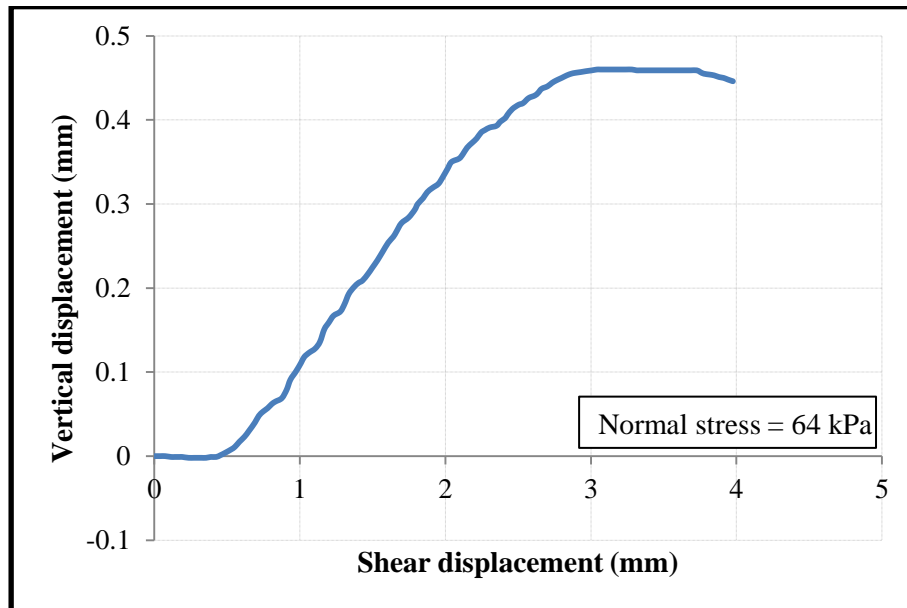


**Figure B-8: Vertical displacement vs shear displacement for dense sand; Density =  $1578 \text{ Kg/m}^3$  ( $D_r = 75\%$ ) and normal stress = 64 kPa.**

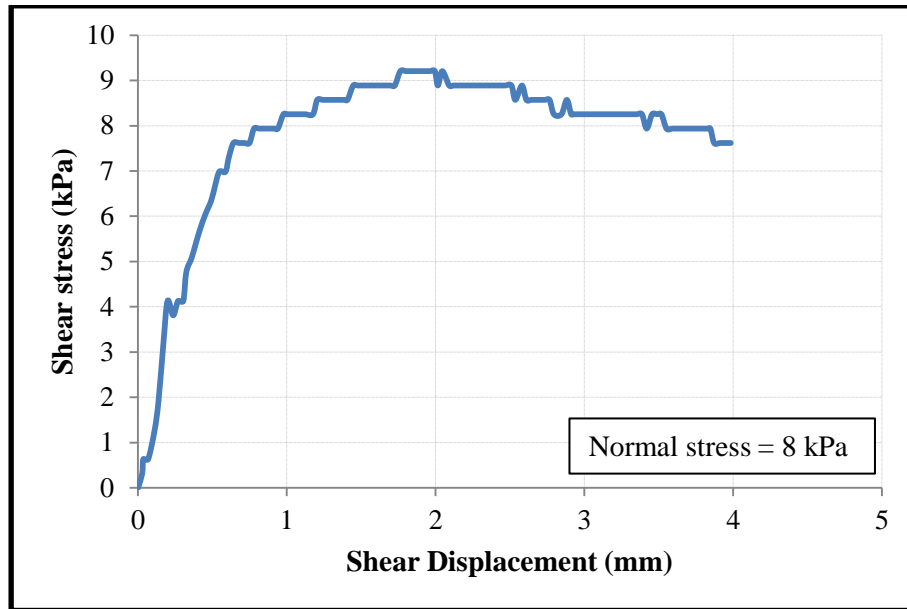


**Figure B-9: Variation of shear stress with displacement for loose sand; Density = 1493.8 Kg/m<sup>3</sup> (Dr = 33.6%) and normal stress = 8 kPa.**

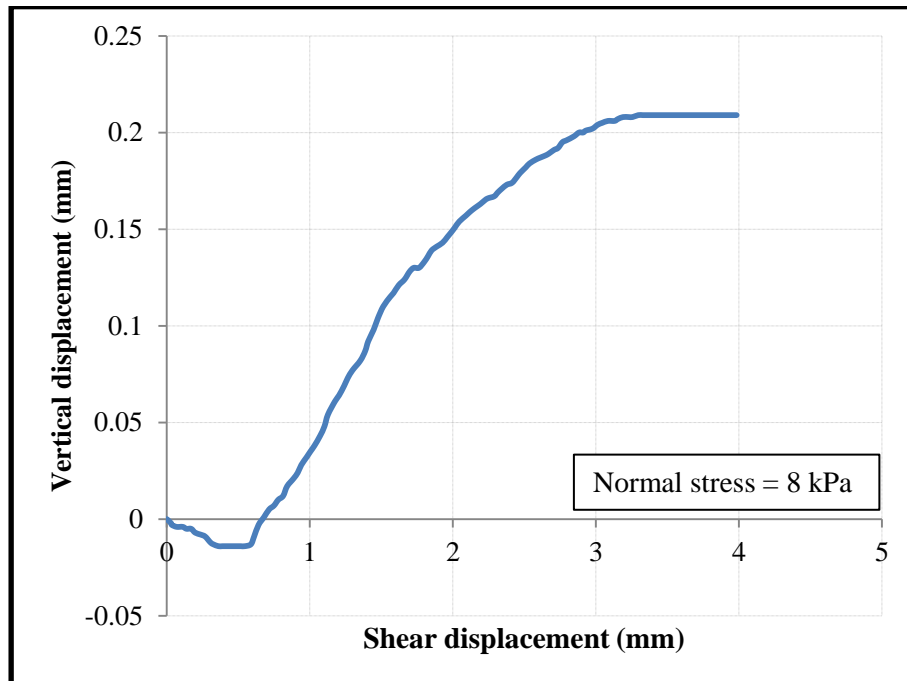


**Figure B-10: Vertical displacement vs shear displacement for loose sand; Density = 1493.8 Kg/m<sup>3</sup> (Dr = 33.6%) and normal stress = 8 kPa.**

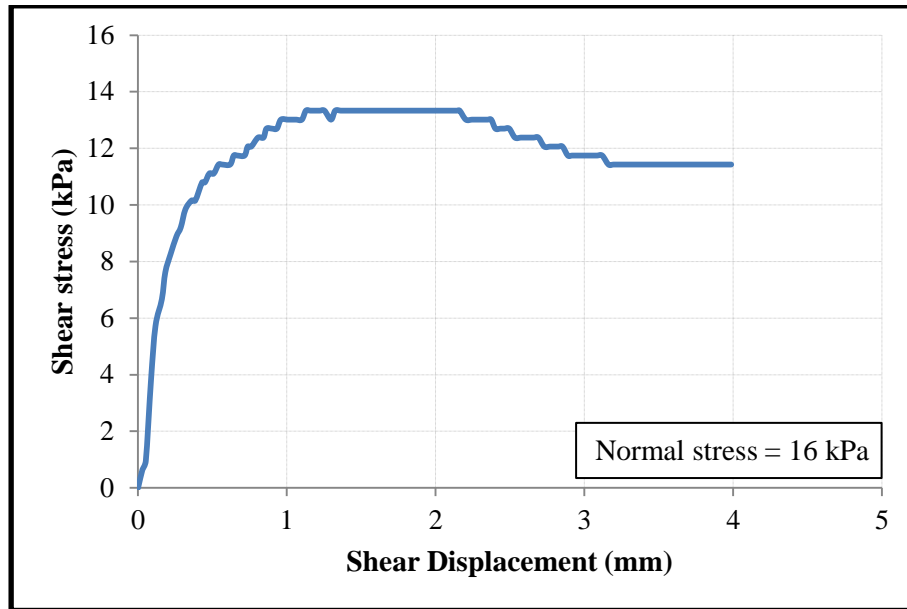


**Figure B-11: Variation of shear stress with displacement for loose sand; Density =  $1491 \text{ Kg/m}^3$  ( $D_r = 32.2\%$ ) and normal stress = 16 kPa.**

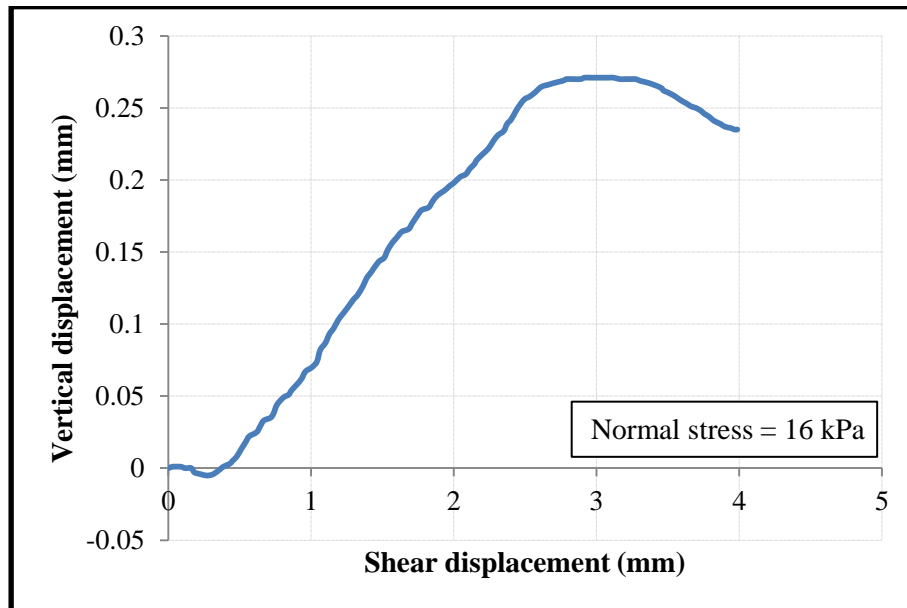


**Figure B-12: Vertical displacement vs shear displacement for loose sand; Density =  $1491 \text{ Kg/m}^3$  ( $D_r = 32\%$ ) and normal stress = 16 kPa.**

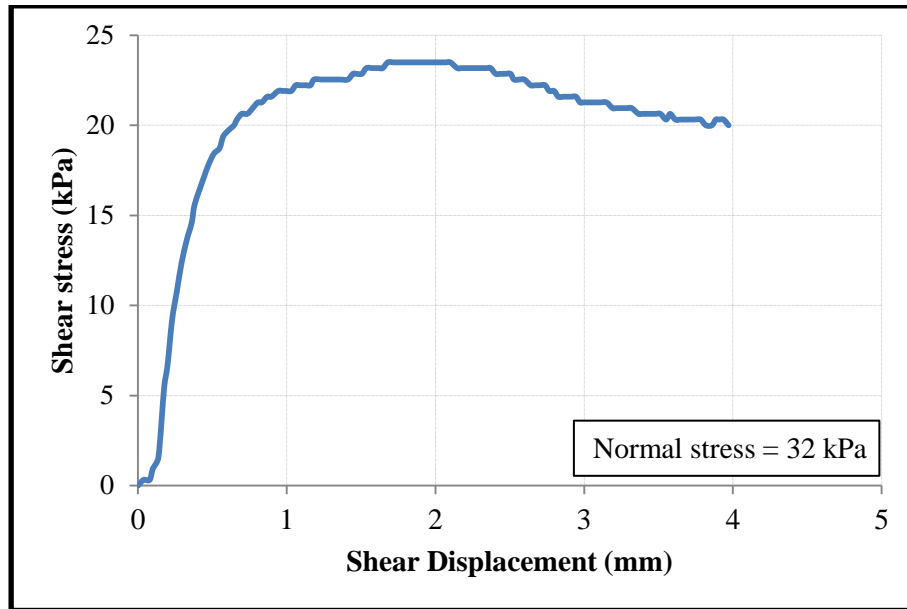


**Figure B-13: Variation of shear stress with displacement for loose sand; Density =  $1493.8 \text{ Kg/m}^3$  ( $D_r = 33.6\%$ ) and normal stress = 32 kPa.**

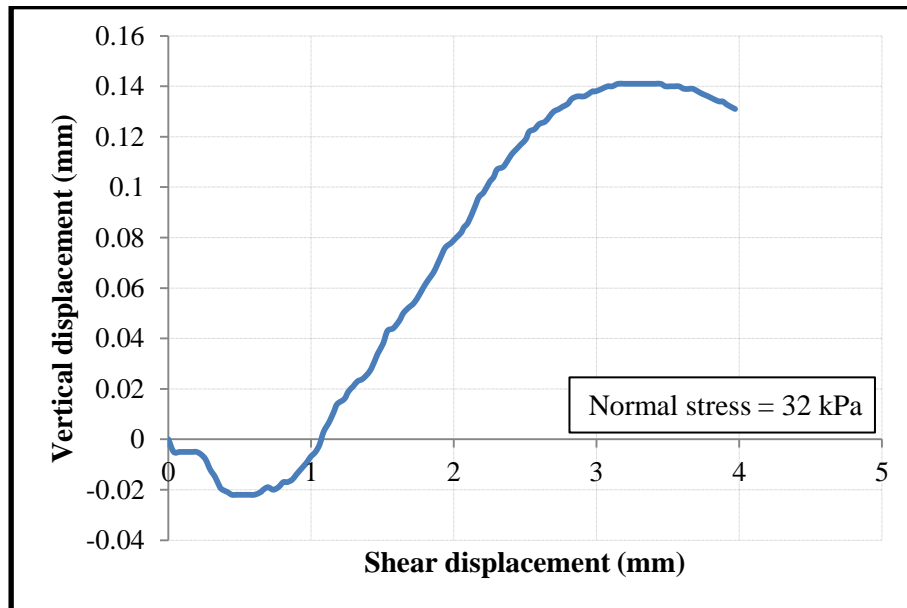


**Figure B-14: Vertical displacement vs shear displacement for loose sand; Density =  $1493.8 \text{ Kg/m}^3$  ( $D_r = 33.6\%$ ) and normal stress = 32 kPa.**

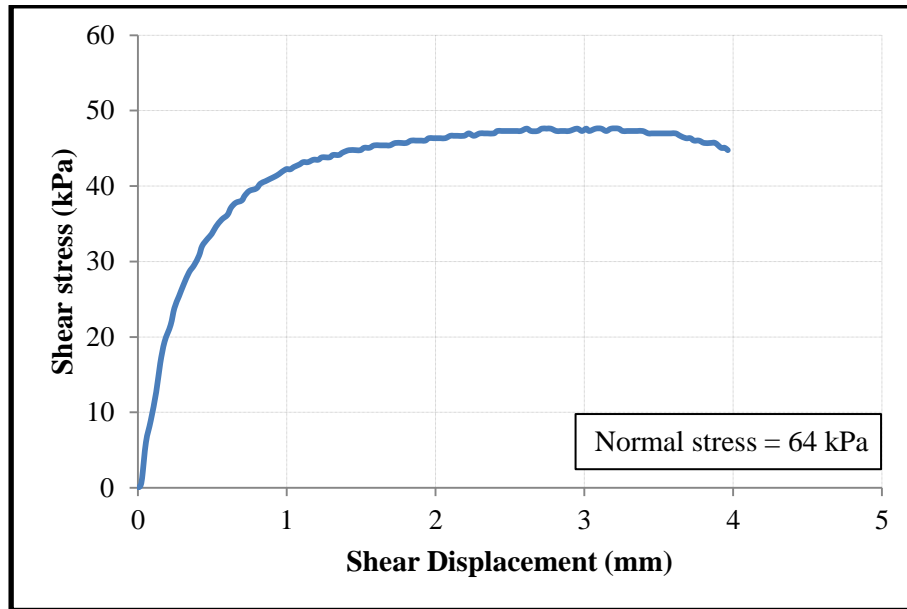


**Figure B-15: Variation of shear stress with displacement for loose sand; Density =  $1493.8 \text{ Kg/m}^3$  ( $D_r = 33.6\%$ ) and normal stress = 64 kPa.**

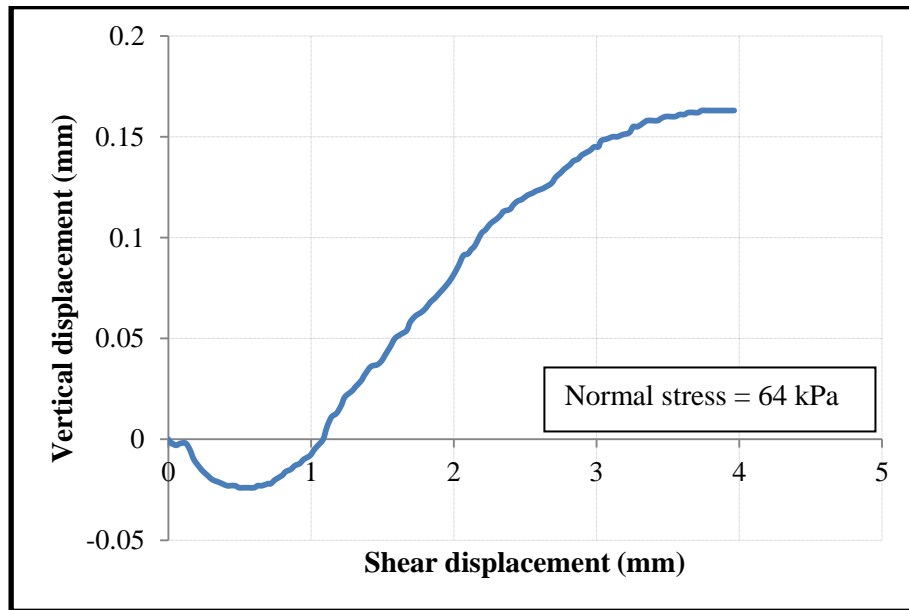


**Figure B-16: Vertical displacement vs shear displacement for loose sand; Density =  $1493.8 \text{ Kg/m}^3$  ( $D_r = 33.6\%$ ) and normal stress = 64 kPa.**

## **APPENDIX C**

### **Integrated Framework in Support of Pipeline Engineering Design for Geohazards**

This paper was presented at the 68<sup>th</sup> Canadian Geotechnical Conference (GeoQuébec 2015). Results from the centrifuge tests conducted and analyzed by the M.Eng. candidate Pijush Debnath were presented. Dr. Kenny prepared linking the physical evidence with the overarching engineering methodology for the design of buried pipelines.

## Integrated Framework in Support of Pipeline Engineering Design for Geohazards

Kenny, S.,

*Department of Civil and Environmental Engineering –  
Carleton University, Ottawa, ON, Canada*

Debnath, P.<sup>1</sup>, Pike, K.<sup>2</sup>, &Hawladar, B.

*Department of Civil Engineering – Memorial University, St. John's, NL, Canada*



**GEOQuébec  
2015**

*Challenges from North to South*

*Des défis du Nord au Sud*

### ABSTRACT

Energy pipelines are critical elements of the national infrastructure for the transportation of oil and gas resource. These pipeline systems may extend hundreds of kilometers in length, traverse across terrain units with varied geotechnical properties and may be impacted by geohazards. The relative ground movement imposes forces on the buried pipeline that may cause local damage and impair the mechanical performance with respect to serviceability or strength limits. The current state-of-practice for the engineering design and integrity assessment of a buried energy pipeline is based on structural pipe/soil interaction models idealized using beam and spring elements. This approach can be deficient when analyzing complex pipeline/soil interaction events that need to account for complex boundary conditions, load transfer processes and failure mechanisms. Continuum finite element methods can address these deficiencies but require an integrated framework including experienced numerical analysts, laboratory tests to define input parameters for soil constitutive models and physical data to verify simulation procedures. In this paper, the framework for integration of these technical approaches in support of pipeline engineering design is discussed with reference to recent studies. The potential for improving current pipeline engineering practice is also explored.

### RÉSUMÉ

Les pipelines d'énergie sont des éléments essentiels de l'infrastructure nationale pour le transport des ressources de pétrole et de gaz. Ces réseaux de canalisations peuvent s'étendre sur des centaines de kilomètres de long, traverse l'ensemble des unités de terrain avec des propriétés géotechniques variées et peuvent être affectées par des risques

géologiques. Le mouvement relatif du sol impose forces sur le pipeline enfoui qui peuvent causer des dommages locale et le rendement mécanique par rapport aux limites de maintenabilité ou résistance. L'état actuel des pratiques pour la conception technique et l'évaluation de l'intégrité d'un pipeline d'énergie enterrée est basée sur le tuyau structurel / modèles d'interaction des sols idéalisés en utilisant des éléments de ressort mécanique. Cette approche peut être déficient lors de l'analyse pipeline / sol événements d'interaction complexes qui doivent tenir compte des conditions aux limites complexes, les processus de transfert de charge et les mécanismes de défaillance. Méthodes d'éléments finis continus peuvent remédier à ces lacunes, mais nécessitent un cadre intégré, y compris les analystes numériques, des tests de laboratoire expérimentés afin de définir les paramètres d'entrée pour les modèles de sol constitutive et les données physiques pour vérifier les procédures de simulation. Dans cet article, le cadre pour l'intégration de ces approches techniques à l'appui de la conception technique du pipeline est discuté en référence à des études récentes. Le potentiel d'amélioration de la pratique de l'ingénierie de pipeline actuel est également exploré.

## 1 INTRODUCTION

Energy pipelines are critical elements of the national infrastructure used to transport oil and gas products that underpin the competitiveness and long-term growth of the Canadian economy, and the quality of life enjoyed by society. In 2013, the energy pipeline industry contributed \$113 billion, representing more than one-quarter of the goods producing value to the national economy (CEPA, 2015).

In Canada, the buried transmission pipeline network exceeds 830,000 km, with greater network lengths in Europe and the US (CEPA, 2015). These pipeline systems extend across terrain with distributed topographical, hydrological, and geotechnical characteristics with varied intensity of anthropogenic activity. These local features may trigger geohazards (e.g., relative ground movement events including subsidence, slope stability, frost heave) that pose loads on the buried pipeline. The load effects may result in local stress or deformation of the pipeline section that may cause damage (e.g., global or local buckling) or failure (e.g., through wall rupture) to occur.

Although the frequency of pipeline rupture incidents due to geohazards is relatively low, typically less than 10% of total incidents (e.g., EGI, 2015; Jeglic, 2004), the consequences can be significant in terms of environmental damage, injury or loss of life. For example, in 2004 a natural gas pipeline, located in Ghislenghien, Belgium, ruptured due to external interference that resulted in the loss of 24 lives, 150 people injured and more than €100 million in property damage. Similar to other industries (e.g., aerospace), ensuing failure events, questions are often raised by the public and industry on the adequacy of current engineering practice, standards, regulations and policies to promote pipeline integrity and safety.

The current state-of-practice for the analysis, design and integrity assessment of buried pipelines subject to geohazards is based on structural pipe/soil interaction models idealized using beam and spring elements (e.g., ALA, 2005). For small deformation loading events, governed by equations of equilibrium, where the pie response is primarily

elastic and specific problems with large deformation (e.g., fault movement), there is sufficient guidance within a sufficiently acceptable technical framework.

This approach can be deficient for the analysis of other pipeline/soil interaction events that may involve complex route alignment (e.g., back-to-back bends), oblique load coupling and large deformation geohazards such slope movement or ice gouging (e.g., Daiyan et al., 2011; Nobahar et al., 2007; Roy et al., 2015). Continuum finite element methods can address these deficiencies but require an integrated framework including experienced numerical modellers, laboratory tests to define input parameters for soil constitutive models and physical data to verify simulation procedures (Pike et al., 2013, 2014; Roy et al., 2014, 2015).

As shown in Figure 1, fully coupled pipeline/soil interaction events involve complex interdependent relationships among the system demand, response and capacity. The system demand (i.e., hazards and loads) includes anthropogenic (e.g., mining, agriculture practices) and natural geohazards. System response directly addresses the geotechnical conditions (e.g., soil type, strength parameters) and pipeline characteristics (e.g., diameter, internal pressure, operating temperature) with respect to the load transfer, load effects and soil failure mechanisms. Performance limits on the pipeline mechanical response are addressed through the system capacity (e.g., stress, ovalization, local buckling, and rupture) and parameters that may have statistically significant interactions.

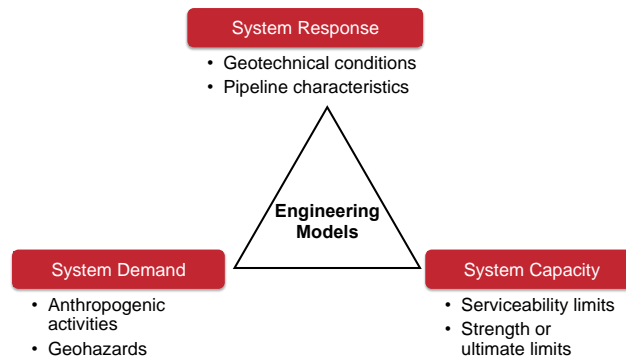


Figure 1. Major elements and parameters for coupled pipeline/soil interaction event

An integrated research framework is needed to establish confidence in practical, reliable, and cost-effective engineering tools that can be used support pipeline design and operations. As part of this framework, laboratory testing can be used to advance constitutive models, while physical modeling can be used to evaluate hypotheses. The results from these studies can be used to verify numerical simulation tools that can assess system demand, response and capacity across a range of practical design and operational conditions. The research outcomes can then be used to advance engineering practice, guidance documents, and governing codes and standards.

In this paper, this integrated research framework is addressed through examination of recent studies that have included laboratory testing, centrifuge and full-scale modelling, and numerical simulation to address pipeline/soil interaction events for energy pipelines. The framework in support of pipeline engineering design is discussed. The potential for improving current pipeline engineering practice is also explored.

## 2 CENTRIFUGE MODELLING STUDIES

A series of reduced scale centrifuge tests examining oblique pipeline/soil interaction (Daiyan, 2013; Daiyan et al., 2011; Debnath, 2015) and full-scale lateral pipeline/soil interaction tests (Burnett, 2015) have been recently conducted. The principal objective for these tests was to support the development and verification of continuum finite element modelling procedures.

A rigid pipeline was pulled through a prepared dry, cohesionless soil test bed, in the loose and dense conditions, to examine the load-displacement response, pipe/soil interaction response, soil failure mechanisms and strain localization. The instrumentation included load cells to measure soil forces, potentiometers, LVDT's and lasers to measure displacement and, for the full-scale tests, Digital Image Correlation (DIC) technique was used to measure soil deformations and strain localization.

Further discussion on the reduced-scale centrifuge test apparatus and procedures is presented in the following subsections

### 2.1 Apparatus and Instrumentation

Centrifuge modelling provides a basis to simulate soil/structure interaction problems where the prototype soil stress field, due to the effects of gravitational acceleration, can be simulated at reduced scale through the laws of similitude (e.g., Craig, 1995; Garnier et al., 2007; Gaudin et al., 2016).

A series of tests were conducted using the C-CORE geotechnical centrifuge located on the campus of Memorial University (Daiyan, 2013; Debnath, 2015). As shown in Figure 2, a rigid pipeline [1] was pulled through a dry, cohesionless test bed to examine the coupled axial-lateral pipeline/soil interaction response for oblique loading events. The axial and lateral loads were measured through two bi-axial load cells [2, 3], and the pipeline was pulled through the soil via a supporting structure consisting of two stanchions [4,5] that was braced by a dogbone [6].

As shown in Figure 3, each stanchion was connected to a ball race [7, 8], which allowed for vertical motion. The ball races were connected to a guiding plate [9] that was connected to a motorized carriage [11] providing the means to move the pipe through the soil. The guiding plate was also used to orientate and fix the longitudinal axis of the buried pipeline relative to the direction of motion (e.g., pure axial, pure bearing, oblique motion) in the soil test bed. Two linear variable differential transformers (LVDT), with one shown as [10] in Figure 3, were used to measure the pipe vertical movement. Two lasers, with one shown as [12] in Figure 3, were used to measure the pipe lateral or horizontal displacement.

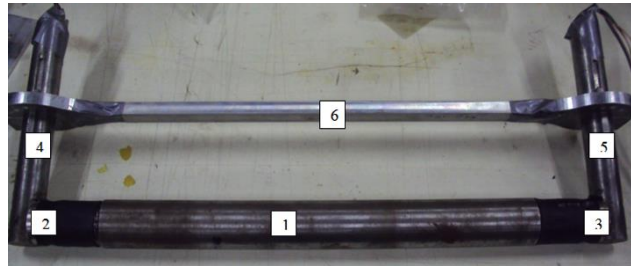


Figure 2. Pipe assembly [1] with biaxial load cells [2,3] stanchions [4,5] and dogbone [6] (Debnath, 2015)

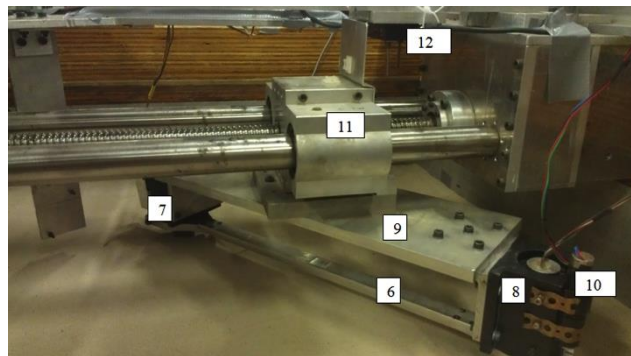


Figure 3. Major elements of the centrifuge test apparatus including the dogbone [6], ball race [7, 8], guiding plate [9], LVDT [10], motorized carriage [11] and laser [12](Debnath, 2015)

## 2.2 Pipe/Soil Interaction Test Parameters

The centrifuge test bed was a dry, cohesionless soil using dry fine silica sand in the loose (Debnath, 2015) and dense (Daiyan, 2013; Debnath, 2015) condition. A summary of the soil properties is presented in Table 1. The acceleration field for the tests conducted by Daiyan (2015) and Debnath (2013) was 12.3g and 13.25g, respectively. A summary of the test parameters for the centrifuge strong box and rigid pipeline are summarized in Table 2.

The friction angles were measured using triaxial cell (Daiyan, 2013) and direct shear box (Debnath, 2015) apparatus. Magnitudes of the peak and critical state friction angle for loose sand may be considered on the higher end of the range.

In terms of the relative angle of attack between the pipeline and soil, Daiyan (2013) conducted 4 experiments that examined axial ( $0^\circ$ ), lateral bearing ( $90^\circ$ ) and 2 oblique loading conditions ( $40^\circ$  &  $70^\circ$ ). In the study conducted by Debnath (2015), for the dense test bed condition there were 6 experiments conducted, which examined relative angle of attack between the pipeline and soil for axial ( $0^\circ$ ), lateral bearing ( $90^\circ$ ) and 4 oblique ( $20^\circ$ ,  $40^\circ$ ,  $50^\circ$  &  $70^\circ$ ) loading conditions. In the loose test bed condition, 4 tests were conducted that examined axial ( $0^\circ$ ), lateral bearing ( $90^\circ$ ) and 2 oblique ( $40^\circ$  &  $70^\circ$ ) loading conditions.

Table 1. Soil test bed parameters

Parameter	Value	
	Daiyan (2013)	Debnath (2015)
Average particle size, $d_{50}$ (mm)	–	0.22 mm
Coefficient of uniformity (#)	–	1.92
Average dry density, loose ( $\text{kg/m}^3$ )	N/A	1467
Relative density, loose (%)	N/A	33
Peak friction angle, loose ( $^\circ$ )	N/A	40
Constant volume friction angle, loose ( $^\circ$ )	N/A	36
Average dry density, dense ( $\text{kg/m}^3$ )	1598	1567
Relative density, dense (%)	82	72
Peak friction angle, dense ( $^\circ$ )	43	47
Constant volume friction angle, dense ( $^\circ$ )	33	40

Table 2. Centrifuge strongbox and model pipeline parameters

Parameter	Value	
	Daiyan (2013)	Debnath (2015)
Acceleration field, g	12.3	13.25
Pipe diameter (mm)	41	46
Pipe/soil interface friction coefficient (#)	0.44	N/A
Centrifuge strong box (mm $\times$ mm $\times$ mm)	1180 $\times$ 940 $\times$ 400	
Pipe length to diameter ratio, L/D (#)	8	
Pipe burial depth at springline to diameter ratio, H/D (#)	2	

### 2.3 Axial Pipe/Soil Interaction

In this section, test data for axial ( $0^\circ$ ) pipeline/soil interaction (Daiyan, 2013; Debnath, 2015), obtained using the geotechnical centrifuge, were analysed and compared with public domain data sets from full-scale tests (Hsu et al., 2001, 2006; Karimian, 2006). The physical test data is presented in Figure 4 where the normalized axial force is presented as a function of the normalized axial displacement. The measured normalised axial force was also compared with guidance from other studies (Schaminee et al., 1990) and current engineering practice (ALA, 2005).

The normalized axial force was defined as the real axial force per unit length divided by the dry soil unit weight ( $\gamma$ ), the burial depth to the pipe spring line ( $H_s$ ), and pipe diameter ( $D$ ). The normalized axial yield displacement was defined by the mobilized soil displacement at the axial yield force divided by the pipe diameter ( $D$ ). The ALA (2005) guidelines define the yield displacement as 3 mm and 5 mm for dense and loose sand, respectively. The study by Schaminee et al., (1990) did not define an axial yield displacement criterion.

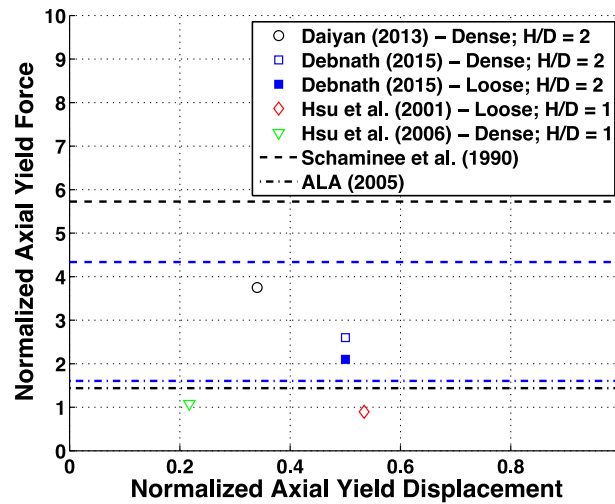


Figure 4. Normalized axial force and yield displacement for axial pipe/soil interaction

As shown in Figure 4, for an  $H/D$  of 2, the measured normalized axial yield force was greater than the ALA (2005) guidelines by a factor of 2.6 and 1.6 for the centrifuge tests conducted by Daiyan (2013) and Debnath (2015), respectively. In the full-scale tests, Hsu et al. (2006) observed normalized axial yield forces less than 1 for dense sand (peak friction angle of  $42^\circ$ ) across the range of  $H/D$  ( $H/D = 1, 2, 3$ ) examined, which was less than the ALA (2005) guidelines.

For cohesionless soil, the ALA (2005) guidelines define the axial force as

$$t_u = \rho g H_s D_c \frac{1 + K_o}{2} \frac{\bar{\sigma}}{\theta} \tan \delta \quad [1]$$

where  $\gamma$  is the effective unit weight,  $K_o$  is the coefficient of earth pressure at rest and  $\delta$  pipe/soil interface friction angle. A coating dependent friction factor of 0.7 was used to represent smooth steel. In the study by Hsu et al. (2001), direct shear test results indicated a friction coefficient of 0.67 the soil friction angle. For dense sand, the  $K_o$  value was estimated using the expression presented by Sherif et al. (1984).

The experimental apparatus, instrumentation and procedure for the centrifuge (Daiyan, 2013; Debnath, 2015) and full-scale (Hsu et al., 2006) tests were similar. Differences in the test results may be attributed to the boundary conditions, pipe self-weight and local failure mechanisms.

Due to the pipe and soil placement processes, there may be local variation and gradient in soil properties (e.g., relative density) in comparison with the far-field conditions. This could influence soil mechanical behavior (e.g., strength, dilation). The expectation would be a reduced peak friction angle and lower relative density that tends to decrease the yield axial force.

The centrifuge tests placed high-density, compliant foam blocks on the leading face of the stanchions, to promote local failure during the movement of the test frame through the soil, and thereby reduce end-bearing loads effects being transmitted onto the pipe assembly (Figure 2). The stanchions would impose bearing load on the foam to mitigate soil deformations and failure processes on the leading face. The tests conducted by Hsu et al. (2001, 2006) used a rigid blanking plate on the end pipe segment. The difference in compliance and boundary conditions may account for the discrepancy between the physical models.

To maintain rigid condition, the model pipelines used in the centrifuge studies were thick-walled pipe with a diameter-to-thickness (D/t) ratio of 6 (Daiyan, 2013) and 12 (Debnath, 2015). Conventional onshore energy pipelines would have a D/t ratio between 50 and 80, whereas offshore pipelines would have a typical D/t range of 30 to 45. The thicker wall increased the pipe self-weight, which increased the average local stress at the pipe spring line. Accounting for this stress component, the axial resistance can be expressed as (Schaminee et al., 1990)

$$t_u = \frac{\rho}{4} g H_c D_c^2 + 2K_o + b + K_o \frac{D}{H_c} \tan \delta \quad [2]$$

Where  $H_c$  is the cover depth to the pipe crown, and  $\beta$  is the pipe weight normalized by  $gH_c D$ . Accounting for the effect of the pipe self-weight, estimates of the soil axial force, using Equation [2], were greater than the centrifuge results by a factor of 1.5 and 1.7 for the tests conducted by Daiyan (2013) and Debnath (2015), respectively.

In a recent study conducted by Karimian (2006), for well-defined and controlled axial pull-out tests, the axial soil resistance for loose sand test bed conditions was consistent with estimates using the ALA (2005) guidelines, as defined in Equation [1]. For dense sand conditions, however, Karimian (2006) concluded the measured peak soil forces were 2 to 3 times greater than the ALA guidelines. The difference was attributed to increased resistance due to localized failure during shear deformation associated with constrained dilation around the pipe circumference. The shear zone was focused across a small

annular layer with a thickness of 1 m to 3 mm or approximately  $10 d_{50}$ . An equivalent lateral earth pressure coefficient was defined that was a function of the pipe diameter, soil elastic modulus and internal friction angle.

For the centrifuge tests parameters, the equivalent lateral earth pressure coefficient as defined by Karimian (2006) would range from approximately 1.0 to 2.25. Using Equation [1] with equivalent lateral earth pressure coefficients of 2.6 and 1.6 would match the centrifuge tests conducted by Daiyan (2013) and Debnath (2015), respectively. These observations would hold true for the tests in loose sand conducted by Debnath (2015).

In the tests conducted by Debnath (2015), the peak axial force for dense sand was 1.2 times greater than the loose sand test bed condition. In large scale axial pipe/soil interaction tests, Paulin et al. (1998) found that post-peak axial loads in dense sand were on average approximately 1.6 times greater than tests on loose sand.

The mobilization of yield displacement for the physical tests, ranging from 0.2D to 0.5D, were significantly greater than the estimates using ALA (2005) guidelines and results of Karimian (2006), which are on the order of millimetres (i.e., 0.005 D to 0.01 D). This may be due to the test setup, end bearing effects and boundary conditions for the centrifuge (Daiyan, 2013; Debnath, 2015) and full-scale (Hsu et al., 2001,2006) studies.

In addition, as presented by Daiyan et al., (2011) through numerical simulation, the axial load-displacement response becomes moderated at low oblique attack angles, which can be associated with misalignment of the test frame, where the peak load occurs at greater mobilization distances. In a physical test, the existence of any bifurcation, at low mobilization distances (e.g.,  $< 0.1D$ ), may not be discernable and thus account for the higher peak forces and mobilization distances to yield being reported.

## 2.4 Oblique Loading

Early studies on the effects of oblique pipeline/soil interaction events were based on analytical solutions (e.g., limit load analysis) that were complemented by analogue events such as inclined plate anchor tests (Meyerhof and Hanna 1978; Nyman, 1984). More recently, an increasing number of studies have investigated the load coupling effects during oblique pipeline/soil interaction events (e.g., Daiyan, 2013).

Based on the centrifuge tests conducted by Daiyan (2013) and Debnath (2015), as shown in Figure 5, the normalized axial ( $0^\circ$ ) and lateral ( $90^\circ$ ) interaction forces are coupled and dependent on the pipeline/soil attack angle. For these centrifuge tests, the coupled interaction was associated with two mechanisms characterized by the bounding surfaces of two yield envelopes. At low interaction angles (i.e., oblique attack angles) the soil failure was controlled by shear strength and friction along the pipeline/soil interface. This failure mechanism was associated with increased effective axial force with increasing attack angle. This has been observed in numerical studies on oblique pipeline/soil interaction in cohesive (Phillips et al., 2004a; Pike and Kenny, 2012a, b) and non-cohesive soil conditions (Daiyan, 2013; Daiyan et al., 2011,2010). The axial loads can increase by a factor as high as 2.5 for oblique attack angles less than  $40^\circ$ . The continuum finite element models on dense sand by Dayian (2013) were in good

agreement with the centrifuge data with the greatest discrepancy between the physical and numerical model observed for the axial loading condition.

As the attack angle increases, the axial-lateral load coupling effects are moderated where the failure mechanism is governed by shear failure through the soil mass. For the lateral ( $90^\circ$ ) normalized bearing force, the centrifuge data is consistent with some public domain data (e.g., Audibert and Nyman, 1977; Calvetti et al., 2004) but is greater than current practice (e.g., ALA, 2005) by a factor of 1.35 and 1.6 for loose and dense sand, respectively. The full-scale test by Hsu (2001, 2006) under predicts the normalized bearing load by a factor of 0.57 and 0.81 for loose and dense sand, respectively.

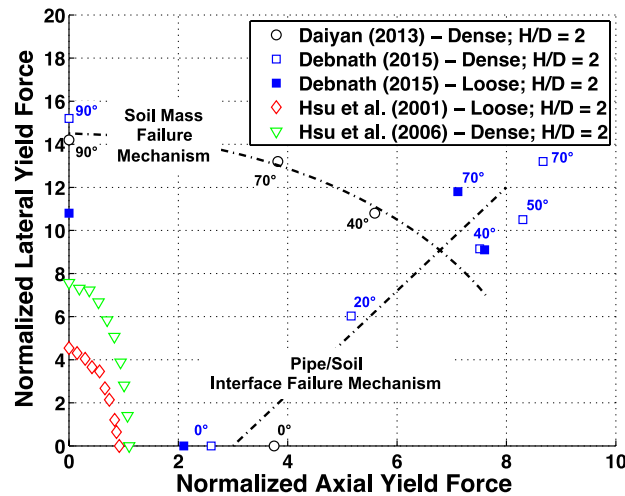


Figure 5. Normalized lateral-axial interaction

Through a parameter analysis, Daiyan (2013) has shown a family of yield envelopes (as shown by the dash-dot lines in Figure 5) exist that is a function of the soil peak friction angle, pipe/soil interface friction angle, and burial depth ( $H_s/D$ ). Using Design of Experiments (DoE) techniques, empirical relationships defining the yield envelope were established. There was agreement between the numerical simulations and centrifuge data.

The greatest uncertainty lies with the differences between the geotechnical centrifuge and full-scale physical model results, particularly for the oblique loading cases. The centrifuge tests (Daiyan, 2013; Debnath, 2015) exhibited greater coupling between axial-lateral forces with attack angle than the full-scale tests (Hsu et al., 2001, 2006). This degree of coupling is supported by results from continuum finite element simulations (e.g., Daiyan, 2013; Daiyan et al., 2011; Phillips et al., 2004a; Pike and Kenny, 2012a, b). There may be two reasons for this discrepancy between the physical modelling approaches related to the boundary condition and geotechnical centrifuge scaling laws.

As discussed in the Section 2.3, although the physical models had similar test conditions and procedures, one of the differences was treatment of the end bearing boundary condition. Differences in end compliance may influence the bearing loads and soil failure mechanisms on the leading face of the pipe during the interaction event that may influence the measured axial load response and be a moderating factor that accounts for differences between the two datasets.

A study conducted by Palmer et al. (2003) on the upheaval buckling response of pipelines observed the mobilization distance did not scale, between reduced-scale centrifuge and full-scale physical modelling tests, with respect to soil particle size. The comparative uplift resistance, however, was consistent. The mobilization error was related to soil kinematics and failure mechanisms associated with strain localization and formation of shear zones. The centrifuge mobilization distance was a fraction of the pipe diameter, which is similar to the observations in this study, and moderated the characteristic shape of the load-displacement relationship. This effect was related to the relative displacement and the evolution of shear stress.

For the oblique pipe/soil interaction tests, these scaling effects may, in part, influence the mobilization distance (Figure 4) and relative displacement that affects soil kinematics and formation of shear zones. This would, in turn, influence the determination of the peak loads that may influence the shape of the coupled yield envelope (dash-dot lines) as shown in Figure 5. For shallow buried pipelines, the lateral interaction factor is governed by a passive failure wedge and dependent on the soil weight (e.g., Daiyan, 2013; Phillips et al, 2004b; Rossiter and Kenny, 2012).

The potential influence of centrifuge scale effects, with respect to the vertical mobilization distance as observed by Palmer et al. (2003), on the yield load and displacement to peak load for lateral pipe/soil interaction events is shown in Figure 6. The centrifuge test results exhibit higher normalized mobilization distances to yield force that may be related to kinematics, soil failure mechanisms, and formation of shear zones. This would moderate the load-displacement response and interpretation of the peak load as shown by Method 1 and Method 2 in Figure 6. The peak load using Method 1 was based on the intersection of two tangents to the load-displacement relationship as proposed by Wantland et al. (1982). Using Method 2, based on the work of Terzaghi's, defines the peak load at the point of tangency for the nonlinear plastic deformation. There exists confidence in the centrifuge results, however, where the finite element simulations conducted by Daiyan (2013) are consistent with the physical test data. Other factors that may influence this response include the soil particle shape, gradation, and relative density. This issue requires further detailed investigation.

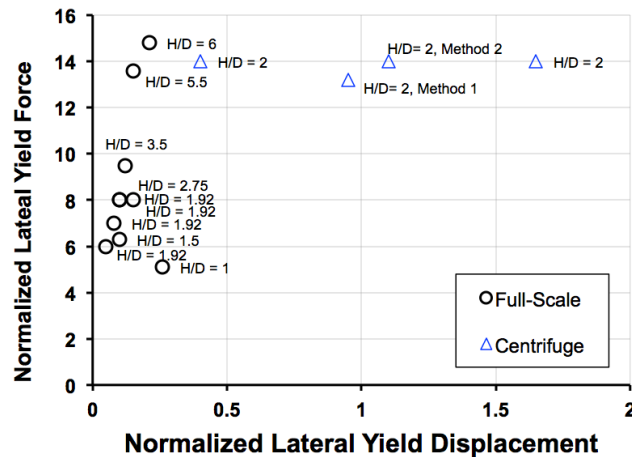


Figure 6. Normalized lateral-axial interaction

### 3 Advancing Practice and Standards

#### 3.1 Overview

Current engineering practice (e.g., ALA, 2005) recommends the use of numerical modelling procedures employing decoupled, structural beam/spring (i.e., structural) system for the analysis of pipeline/soil interaction events. This methodology provides a relatively simple, cost-effective strategy to support pipeline engineering design across a range of practical considerations (e.g., conventional stress based problem, above ground transitions).

There is a need to advance these computational models in support of pipeline design and integrity management for more complex scenarios. As the energy industry ventures into frontier regions, the operational requirements (e.g., high pressure, temperature) and environmental loads (e.g., frost heave, ice gouging) are becoming more challenging that imposes demands on the development of effective engineering solutions.

#### 3.2 Enhanced Structural Models

For stress-based design, pipeline/soil interaction events subject to multi-directional loading (e.g., upheaval buckling, ice gouging, slope failure) requires an enhanced structural model (e.g., Kettle, 1984) due to the coupled load response and failure envelope (e.g., Figure 5).

Improved numerical tools to address this coupled interaction include macro-elements (e.g., Cochetti et al., 2009a,b) and finite element structural modelling procedures (e.g., Daiyan, 2013). These enhanced structural models account for the effects of mechanical load and displacement coupling. The soil yield envelope is defined in terms of the peak load and yield displacement along three orthogonal planes for specific design parameters (e.g., pipe diameter, pipe burial depth, soil type and strength properties and attack angle).

Physical models, which may be integrated with numerical simulations to extend the parameter database, provide the basis to define the nonlinear soil response due to soil deformations, material behaviour and load coupling.

#### 3.3 Continuum Computational Models

For complex pipeline/soil interaction events, there is a need for more complex, computational modelling procedures (e.g., continuum finite element methods) to address strength evolution with deformation (e.g., change in peak stress, residual stress, dilation due to strain softening), load and stress path dependency, and deformation mechanisms (e.g., strain localization, shear bands).

The primary constraints on using these tools are requisite skills and expertise of the analyst, laboratory test data used to refine constitutive models, physical test data to verify the computational modelling procedures, and software and hardware requirements to conduct the simulation. Recent studies, using verified continuum finite element modelling

procedures (e.g., Daiyan, 2013; Pike et al., 2012a, b, 2013, 2014; Rossiter and Kenny, 2012; Roy et al., 2014, 2015) have supported these observations but have also shown the future potential of these tools to address complex problems, support engineering design and operations, and enhance engineering standards (e.g., Phillips et al., 2014a,b; Pike et al., 2014).

#### 4 Conclusions

Physical modelling and numerical simulations have demonstrated the significance of load coupling effects during oblique pipeline/soil interaction events. There is observed agreement between reduced scale-centrifuge and continuum finite element modelling procedures on the load coupling effects for lateral-axial pipeline/soil interaction in cohesive and cohesionless soil. There exists uncertainty on the characteristics of the yield envelope for oblique lateral-axial interaction events when these observations are compared with available full-scale data. This may be related to differences in the end boundary conditions used in the physical models and potential scaling errors in the centrifuge tests with respect to mobilization distance to yield. Future tests should conduct direct comparison (i.e., equivalent pipe and soil parameters) at reduced-scale and full-scale to resolve this uncertainty. Although there are some constraints, the use of continuum finite element modelling procedures will become more common place in supporting engineering design and can be used to advanced current engineering practice.

#### ACKNOWLEDGEMENTS

The authors would like to acknowledge the financial investment from the Wood Group and NSERC Discovery Grant in supporting these research activities.

#### REFERENCES

- ALA 2005. Guidelines for the design of buried steel pipes. American Lifelines Alliance, 76p.
- Audibert, J. M. E., and Nyman, K. J. 1977. Soil restraint against horizontal motion of pipes. *J. Geo. Eng. Div. ASCE*, 103(NGT10) :1119-1142.
- Burnett, A. 2015. Investigation of full scale horizontal pipe-soil interaction and large strain behaviour of sand. M.A.Sc. Thesis, Queen's University, 118p.
- CEPA 2015. [www.cepa.com](http://www.cepa.com), February 2015.
- Calvetti, F., di Prisco, C., and Nova, R. 2004. Experimental and numerical analysis of soil-pipe interaction. *J. Geo. Geoenv. Engg.*, 130(12):1292-1299.
- Cocchetti, G., Prisco, C., Galli, A. and Nova, R. 2009a. Soil-pipeline interaction along unstable slopes: a coupled three-dimensional approach. Part 1: Theoretical formulation. *Can. Geo. J.*, 46(11):1289-1304.

- Cocchetti, G., Prisco, C., and Galli, A. 2009b. Soil-pipeline interaction along unstable slopes: a coupled three-dimensional approach. Part 2: Numerical analysis. *Can. Geo. J.*, 46(11):1305-1321.
- Craig, W.H. 1995. Geotechnical centrifuge: Past, present and future. *Geotechnical Centrifuge Technology*, pp.1-18.
- Daiyan, N. 2013. Investigating Soil/Pipeline Interaction During Oblique Relative Movements. Ph.D. Thesis, Memorial University of Newfoundland, 204p.
- Daiyan, N., Kenny, S., Phillips, R. and Popescu, R. 2011. Investigating pipeline/soil interaction under axial/lateral relative movements in sand. *Can. Geotech. J.*, 48(11): 1683-1695.
- Daiyan, N., Kenny, S., Phillips, R. and Popescu, R. 2010. Numerical investigation of oblique pipeline/soil interaction in sand. *Proc., IPC2010-31644*:6p
- Debnath, P. 2015. Centrifuge modeling of oblique pipe/soil interaction in dense and loose sand. M.Eng. (Thesis), Memorial University of Newfoundland, 120p. (in preparation)
- diPrisco, C., and Galli, A. 2006. Soil-pipe interaction under monotonic and cyclic loads: Experimental and numerical modelling. *Advances in Geomaterials and Structures* :755-760.
- EGIG 2015. Gas Pipeline Incidents. Report EGIG 14.R.0403, February 2015, 61p.
- Garnier, J., Gaudin, C., Springman, S.M., et al. 2007. Catalogue of scaling laws and similitude questions in geotechnical centrifuge modelling. *Int. J. Phy. Mod. Geo.*, 7(3):1-23.
- Gaudin, C., Randolph, M. and White, D. 2016. *Centrifuge Modelling in Geotechnics*. CRC Press, ISBN 9780415522243, 544p.
- Hsu, T.W., Chen, Y.J. and Hung, W.C. 2006. Soil restraint to oblique movement of buried pipes in dense sand." *J. Transp. Eng.* 132(2):175-181.
- Hsu, T.W., Chen, Y.J. and Hung, W.C. 2001. Soil friction restraint of oblique pipelines in loose sand. *J. Transp. Eng.* 127(1):82-87.
- Jeglic, F. 2004. Analysis of ruptures and trends on major Canadian pipeline systems. *Proc., IPC2004-0272* :9p.
- Karimian, S.A. 2006. Response of Buried Steel Pipelines Subjected to Longitudinal and Transverse Ground Movement. Ph.D. Thesis, University of British Columbia, 329p.
- Kettle, R.J. 1984. Soil-pipeline interaction: A review of the problem. *Proc., Pipelines and Frost Heave*. Caen, France:pp.35-37.
- Meyerhof, G. G., and Hanna, A. M. 1978. Ultimate bearing capacity of foundation on layered soil under inclined load. *Can. Geotech. J.*, 15(4):565-572.
- Nobahar, A., Kenny, S. and Phillips, R. 2007. "Buried pipelines subject to subgrade deformations." *Int. J. Geomechanics* 7(3), pp.206-216.
- Nyman, K. 1984. Soil response against oblique motion of pipes. *J. Transp. Eng.*, 110(2):190-202.
- Palmer, A. C. et al. 2003. Uplift resistance of buried submarine pipelines: Comparison between centrifuge modelling and full-scale tests. *Géotechnique*, 53(10):877-883.
- Paulin, M. J., Phillips, R., Clark, J. I., Trigg, A., & Konuk, I. 1998. Full-scale investigation into pipeline/soil interaction. *Proc., CGS*:241-248.

- Phillips, R., Nobahar, A., and Zhou, J. 2004a. Combined axial and lateral pipe-soil interaction relationships. Proc., IPC-0144:5p.
- Phillips, R., Nobahar, A., and Zhou, J. 2004b. trench effects on pipe-soil interaction. Proc., IPC-0141:7p.
- Pike, K.P. and Kenny, S.P. 2012a. Lateral-axial pipe/soil interaction events: Numerical modeling trends and technical issues. Proc., IPC-90055:6p.
- Pike, K. and Kenny, S. 2012b. Numerical pipe/soil interaction modelling: Sensitivity study and extension to ice gouging. Proc., OTC-23731:8p.
- Pike, K. Kenny, S. and Hawlader, B. 2013. Advanced analysis of pipe/soil interaction accounting for strain localization. Proc., CSCE GeoMontreal-305:6p.
- Pike, K., Kenny, S., and Hawlader, B. 2014. Numerical and constitutive model development to aid design against pipeline geohazards. J. Pipeline Eng., 13(3):201-209.
- Rossiter, C. and Kenny, S. 2012. Evaluation of lateral-vertical pipe/soil interaction in clay. Proc., OTC-23735:13p.
- Roy, K., Hawlader, B., Kenny, S. and Moore, I. 2015. Finite element modeling of lateral pipeline-soil interactions in dense sand. Can. Geo. J. (in press).
- Roy, K.S., Hawlader B.C., Kenny, S. and Moore, I. 2014. Finite element modeling of uplift pipeline/soil interaction in sand. Proc., Geohazards 6:8p.
- Schaminee, P. E. L., Zorn, N. F., & Schotman, G. J. M. 1990. Soil response for pipeline upheaval buckling analyses: Full-scale laboratory tests and modelling. Proc., OTC-6486:563-572.

